Univerzita Karlova v Praze

Matematicko-fyzikální fakulta

Fyzikální ústav

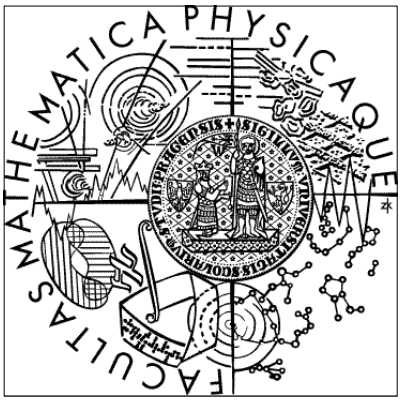

Optical properties of $Cd_{1-x}Zn_xTe$

Doctoral thesis

Petr Horodyský

Supervisor: **Doc. RNDr. Pavel Hlídek, CSc.**

Section: **F6 – Quantum optics and optoelectronics**

Acknowledgement

I thank my supervisor Pavel Hlídek for his great aid to me, especially in the experimental domain. I also thank Roman Grill for his critical comments and contributions to the non-experimental part of this work and I thank Eduard Belas for characterization of electrical properties of samples.

List of important symbols and abbreviations

A^0	neutral acceptor
A^0D^0	acceptor to donor transition
A^0e	neutral acceptor to band transition
A^0X	exciton bound to neutral acceptor
a_B	Bohr radius
BX	bound exciton
c	speed of light in vacuum
c_{st}	concentration of *st*
d	thickness
D^0	neutral donor
D^0X	exciton bound to neutral donor
DAP	donor-acceptor pair
E	photon energy; energy
e; e	electron; electron charge
E_B, E_A, E_D	binding energy, acceptor binding energy, donor binding energy
E_g, E_0	fundamental energy gap
FIR	far infrared region
FX	free exciton
h	hole
h	Planck constant
k	index of extinction (imaginary part of the complex refraction index)
k_B	Boltzman constant
k_{st}	segregation coefficient of *st*
LO	longitudinal optical phonon
m_e	effective electron mass
m_h	effective hole mass
MIR	middle infrared region
m_r	reduced mass
n	index of refraction
NBEL	near band energy luminescence
NIR	near infrared region
PL	photoluminescence
PLE	excitation photoluminescence
R	reflectance
RT	room temperature
R_X	binding energy of free exciton
S	Huang-Rhys factor
T	transmittance; temperature
TET	two-electron transition
x	zinc fraction in $Cd_{1-x}Zn_xTe$
y	cadmium fraction in $Hg_{1-y}Cd_yTe$
ZPL	zero phonon line
a	absorption coefficient
e_r	relative permittivity
e_0	permittivity of vacuum
m	mobility
t	lifetime

1 Introduction

This work is intended to review the knowledge of characterization of CdTe crystals and CdZnTe alloys by optical means. The first chapter's purpose is to establish a general feeling about importance and possible use of CdTe as semiconductor material. In the second part of this introduction, the sample preparation and the experimental setup will be briefly described. The meaning of this work is explained in the section 1.2.4.

1.1 Interest of CdTe and CdZnTe

Cadmium telluride (CdTe) is a direct band gap group II-VI semiconductor of 1.5 eV band gap energy at room temperature. Very often, it is replaced by a ternary alloy cadmium zinc telluride ($Cd_{1-x}Zn_xTe$), with zinc concentration x typically from 4 to 12%. Addition of zinc improves the mechanical properties, growth of the alloy is easier and the band gap energy is shifted towards higher energies.

This section is meant to describe the use and interest in CdTe-based materials. It is sorted by the degree of the quantum electronic confinement.

1.1.1 Bulk CdTe

The direct band gap of about 1.5 eV (≅830 nm) places CdTe both among wide and narrow semiconductors. The absorption coefficient at the band gap energy is superior to 20 000 cm^{-1}. These two properties designate CdTe for fabrication of infrared filters. The absorption edge energy is typically 1.45 eV for thick samples; addition of 1% of zinc increases the band gap by about 5 meV.

CdTe's band gap energy is nearly the ideal one for the single junction solar cell; the theoretical efficiency is nearly 30%, the one of commercial solar cells is about 10% [Bon92]. In Fig. 1.1, a scheme of typical CdTe/CdS solar cell is presented. Several micrometer thin polycrystalline CdTe layer's function is to absorb the light. The p-n junction is formed by p-type CdTe and n-type CdS layers. CdTe solar cells are commercially available; the investment return is quite fast, but probably they will never take over the silicon solar cells.

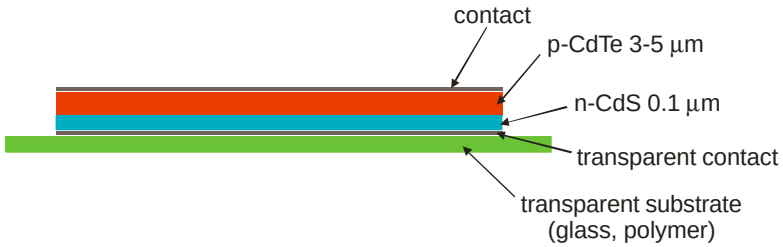

Fig. 1.1. *An example of CdTe/CdS solar cell illuminated from down side.*

The high atomic numbers of cadmium (48) and tellurium (52) make CdTe a perspective material for detection of γ and X radiation. For this purpose, semi-insulating semiconductor with high mt (mobility-lifetime) product is required. The deep levels needed to fix the Fermi level in the middle of the band gap seem to have often high cross sections for capture of free carriers, so their lifetime is insufficient for good detector performance. A schematic picture of detector is plotted in Fig. 1.2. Counting of generated carriers provides energy spectrum of detected radiation. The space resolution can be better than for classical LN_2 cooled Si and Ge detectors. Another advantage of CdTe is that it does not require cooling. Further details can be found for example in [Fie99]. The commercial production of high-quality crystals is limited by relatively difficult growth technology.

CdTe has high Pockels coefficients that made it suitable for use in electro-optical and opto-optical modulators for fast 1.5 μm communications [Pie01].

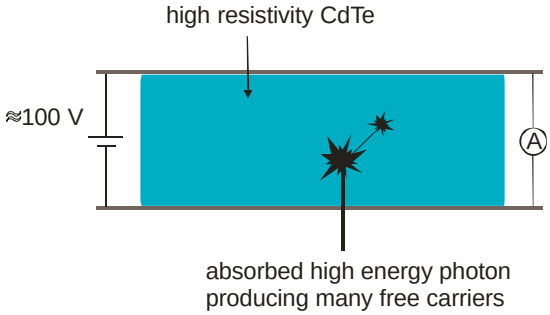

Fig. 1.2. *X and* gama-*ray detector.*

Finally, $Cd_{1-x}Zn_xTe$, $x \cong 0.04$, is an important substrate material for growth of infrared detectors $Hg_{1-y}Cd_yTe$ by MBE epitaxy. This application requires large monocrystalline wafers of the highest quality [Mor06]. The basic persistent problem is the general low quality of substrates (mainly high dislocation density and wide rocking curves).

1.1.2 2D CdTe

Quantum wells combining CdTe and related materials (CdMgTe, CdMnTe, CdZnTe and others) are prepared to study the relaxation and tunneling of charge carriers, exciton and trions. In recent time, majority of these studies are devoted to the investigation of magnetic properties and spin dynamics [Naw04].

Combination of electronic and photonic confinements is exploited in microcavities, which use the strong electron-photon coupling of II-VI materials [Obe02]. The visionary applications of these structures are laser without threshold, one photon source and quantum computing.

1.1.3 1D CdTe

CdTe quantum wires [Zha03] and quantum rings [Kim04] were recently prepared. However, it is not obvious for what purpose except pure research they could be used.

A lot of attention has attracted the discovery of CdTe tetrapods [Man03]. These nanoparticles combine 0D and 1D quantum confinement in tetrahedral symmetry. They are formed by four arms of wurtzite structure grown on a zinc-blend core. The arm length and diameter can be tuned independently. Due to the tetrahedral symmetry, they can be easily oriented in one direction on a planar substrate. This configuration is a promising field for investigation of electrical transport like the single electron transistors [Cui05] or possibly as solar cells.

1.1.4 0D CdTe

Quantum dots or nanocrystals are nowadays widely used as multiplex biological markers. Another use would be coding of information by several distinct emission bands with distinct emission intensities. The energy of the ground electronic level can be tuned in a wide range by the nanocrystal diameter. Although the chemical nature is not so important as for bulk material application, also CdTe nanocrystals (usually with CdS shell but also without it) are commonly used [www1].

1.2 This work, its context and its meaning

1.2.1 Samples

Most of investigated CdTe and CdZnTe crystals were grown at the Institute of Physics of the Faculty of Mathematics and Physics of the Charles University in Prague. Kristallographisches Institut of the Albert-Ludwig Universität in Freiburg, Chernivtsi State University, Centro Nacional de Microelectrónica in Madrid, and Istituto dei Materiali per l' Elettronica ed il Magnetismo in Parma provided further samples. Several samples are of commercial origin. List of samples is found in Tab. 1.1. The beginning of the sample name is usually the crystal name; the possible extension gives further sample information.

Sample	Doping	Origin	*c*		Sample	Doping	Origin	*c*
1072	CdTe	commercial	p=2x10^{16}		PU1	CdTe	unknown	-
1076	CdTe	commercial	p=0.8x10^{15}		S81	CdTe:Cl	commercial	n=1x10^{10}
1077	CdTe	commercial	p=10^{15}		SR20	CdTe	Prague	p=3x10^{13}
2003	CdTe:Ge	Freiburg	-		SR21	CdTe:In	Prague	p=10^{9}-10^{10}
AF13	CdTe:Sn	Freiburg	-		SR317	CdTe	Prague	-
AF15	CdTe:Sn	Freiburg	-		SU910	CdTe	commercial	-
E239	CdTe	Prague	p=10^{14}-10^{16}		TF29	CdTe:Cl	commercial	-
E3314	CdTe:In	Prague	-		U17	CdTe	Chernivtsi	-
F2504	CdTe:Sn	Prague	-					
F2652	CdTe	Prague	p=10^{12}		19572	CdZnTe	commercial	-
F35	CdTe:Sn	Prague	p=5x10^{11}		E5	CdZnTe	Prague	p=5x10^{10}
F36	CdTe	Prague	p=5x10^{15}		E10	CdZnTe	Prague	-
F37	CdTe:Sn	Prague	-		F13	CdZnTe	Prague	-
F38	CdTe:In	Prague	p=5x10^{10}		RC2	CdZnTe:In	commercial	p=1x10^{11}
H81	CdTe	Prague	-		RITEC	CdZnTe:Cl	commercial	-
NUK45	CdTe	Prague	p=5x10^{15}		WJ	CdZnTe:V	Freiburg	-
PD38	CdTe:Cl	unknown	-		Zap05	CdZnTe	Parma	p=5x10^{13}

Tab. 1.1. *Samples, doping, provenience and RT carrier concentrations (c) if known.*

The characterized samples were low, standard and high quality single crystals grown from 5N to 7N purity starting elements. They were grown mostly by the vertical gradient freezing method. More details about the growth of the Prague crystals can be found in [Tur04]. CdZnTe crystals were prepared rather undoped, whereas some of the CdTe crystals were doped with In, Ge, Sn or Cl.

CdTe crystals are grown usually as unintentional p-types with small resistivity (typical concentrations at RT are 10^{14}-10^{16} cm^{-3}; Fermi level energy is then found about 100-200 meV above the valence band). Doping by In, Cl, Ge or Sn, for example, usually results in high-resistivity material. Tab. 1.2 shows concentrations of tested elements present in the crystals. CdTe F36E5 and CdZnTe F13G3 were grown as undoped; CdTe F38 and SR21A23 were doped by indium; CdTe SR37A32 was doped by tin.

Element	F36E5	F38C3	SR21A23	SR37A32	F13G3
Li	<2	<2	<1.5	<1.5	<2
B	7	30	60	20	20
Na	160	260	84	130	10
Mg	20	60	30	15	120
Al	5	30	12	2	150
Si	<5	20	60	<5	8
P	2	14	0,8	1,2	20
S	50	64	130	30	110
K	<8	<5	<5	<6	<7
Ca	<25	80	73	<20	<20
V	<0.2	<0.1	<0.1	<0.1	<0.5

Cr	7	30	120	23	23
Mn	<18	<20	<15	<18	<15
Fe	<30	40	320	<20	300
Co	0,7	0,6	3	0,5	<0.2
Ni	8	25	26	25	120
Cu	120	160	86	160	<20
Zn	5	55	90	7	4.5%
Ge	<7	<8	<8	<8	50
As	<100	<60	<140	<100	<50
Se	<8	<5	<5	<6	<15
Br	<7	<6	<7	<8	<7
Ag	<30	<25	<20	<20	<80
In	<20	83000	5800	<20	<25
Sn	<20	<20	<20	260	<25
Sb	<20	<12	<11	<30	<20
Hg	<1	<1	<0.8	<1	<2
TI	<0.2	0.9	0.6	<0.2	<0.2
Pb	<0.4	0.7	8	<0.4	<0.4
Bi	<0.1	<0.1	0,3	<0.1	<0.1

Tab. 1.2. *GDMS analysis of chosen elements. Units are ppb atomic. The sign < shows the detection limits. Concentration of 1 ppb corresponds to* $3x10^{13}$ cm^{-3}.

1.2.2 Experimental details

Optical spectra (photoluminescence, transmittance and reflectance) were recorded with FTIR spectrometer Bruker IFS/66 operating in NIR and MIR spectral regions. In NIR, mostly silicon diode is used as detector and the beamsplitter material is quartz. In MIR, a thermal photodetector (DTGS) is frequently used together with the KBr beamsplitter. The maximal possible spectral range of the spectrometer setup is from 60 meV to 1.8 eV (for RT transmittance). The maximal spectral resolution is 20 μeV. Flow helium cryostat Leybold-Hereaus provided temperature control of the sample in the 4-300 K range. A heated vacuum chamber was used for temperatures up to 500 K. Optical mapping measurements were performed with Cryovac Konti cryostat equipped with an automated x-y stage. PL spectra were excited with a semiconductor laser (635 nm≈1.95 eV) of optical power of 20 mW. The laser was focused into a spot of diameter of less than 100 μm. The excitation intensity was of about 10 Wcm^{-2} (in PL mapping experiment, due to use of another focusing mirror, the excitation intensity is 50 Wcm^{-2}). The optical setup is schematically depicted in Fig. 1.3.

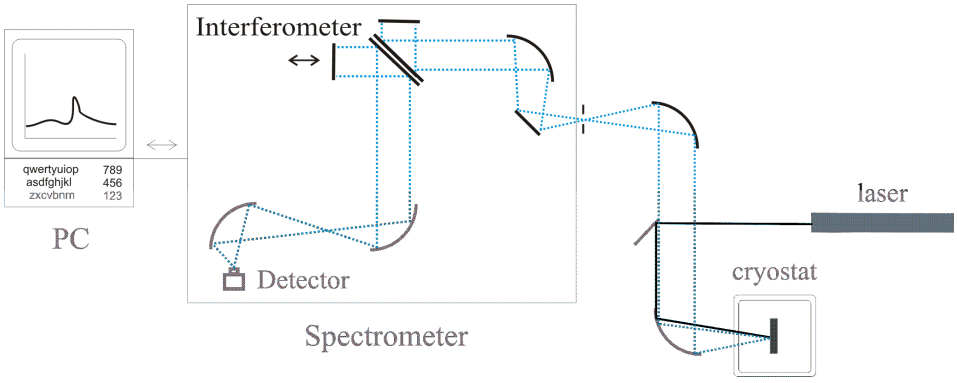

Fig. 1.3. *The classical PL setup.*

For measurements of transmittance the samples were polished into a planparallel shape. Prior to photoluminescence experiments, samples were etched in 2% bromine solution in methanol. The same treatment was applied before reflectance measurements. Thickness of about 10 μm removed during etching was found sufficient to remove the damaged surface layer

influenced by the polishing. In some cases, to remove the oxidized surface of an “old” surface, mechano-chemical polishing in solution of bromine in ethylenglycol was used.

Experimental details of photoluminescence mapping can be found in section 4.2.

1.2.3 Spectral response of the setup

PL spectra were corrected with respect to the spectral response of the spectrometer system. The measured response to the NIR light source (bulb whose filament temperature is estimated to 2400 K) was compared to a black body spectrum multiplied by spectrum of emissivity of wolfram, see Fig. 1.4. Spectral responses of all detectors that can be used for PL are depicted in Fig. 1.5.

However, in practice, the spectral correction is of importance only for GeD and InSb detectors – e.g. consider the spike of the GeD detector at 0.8 eV. For example, the Huang-Rhys factors of shallow defects (SiD detector) obtained from fitting a spectrally corrected spectrum and the as-measured one do not differ substantially.

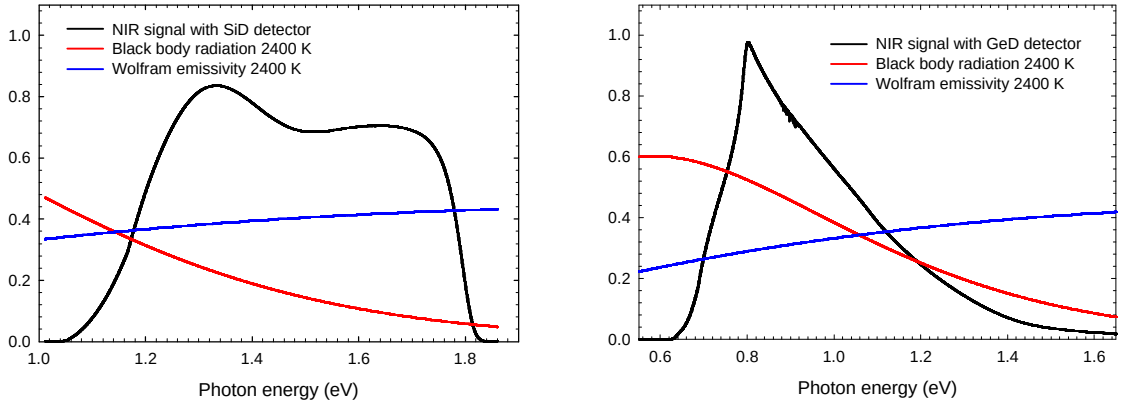

Fig. 1.4. *Bulb spectrum as recorded by the spectrometer setup with Si and Ge detectors (and quartz beamsplitter). Theoretical radiation spectrum of a bulb filament is a black body spectrum multiplied by the material emissivity.*

Few words will now be spent concerning the absolute values of the PL radiation power. The PL signal is collected from a spatial angle corresponding to q=10°. Rough estimation of PL efficiency was done comparing signal of a bulb and the PL radiation. Based on consideration of the black body radiation and wolfram emissivity spectra we conclude, that spectrally about 20% of the bulb radiation power is detected by the spectrometer when the silicon detector is used. During the experiment, the optical paths for PL radiation and bulb emission were exactly the same. The spatial angle inside the semiconductor from which the PL radiation is collected is approximately by a factor of n^2, ($n \approx 3$), smaller. Bulb radiation had to be attenuated by a 0.1% neutral filter. Then, from a comparison of integrated spectral intensities (signal from the 50 W bulb filament, and PL excited by about 10 mW absorbed laser power), we calculate the power efficiency of PL processes to be about 1% for the most efficient samples. For other samples, the efficiency is usually several times lower. In rare cases (e.g. high Ge doping in 2003), the PL signal is found even two orders lower. Highest power efficiency of PL is shown by samples with strong A-center bands (fast and dominant capture mechanism). Generally, the CdZnTe samples produce more intense emission.

The dominant non-radiative recombination channels are probably the surface, dislocations and precipitates. E.g., if the surface is only polished (not chemically etched), excitonic PL is several orders smaller, but the one-electron emissions are much less decreased. This can be explained by capture of excitons on dislocations created by the polishing.

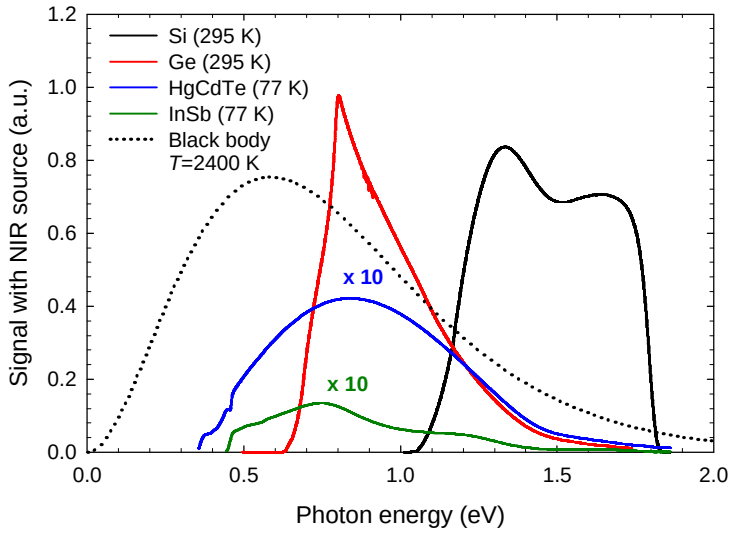

Fig. 1.5. *Spectral response of used detectors to the NIR source (with quartz beamsplitter), without additional amplification of signal. For photoluminescence measurement, with maximum hardware amplification, the sensitivity of the InSb detector is slightly better than that of the HgCdTe detector. The InSb detector is equipped with a thermal-shielding window for noise reduction, which is responsible for the shift of its spectral range to higher energies. The sensitivity of the HgCdTe detector extends to wider range at low energies, but the NIR source (a bulb) does not emit in the spectral range 0-0.35 eV due to absorption of SiO_2.*

1.2.4 Original results of this work

Although, a great part of this work is dealing with photoluminescence of defects in CdTe, almost no experiments were carried out in order to clarify the origin of these. The general aim of this doctoral work was characterization of crystals produced in the Institute of Physics. The most interesting results are found probably in the last chapter dealing with optical mapping of wafers. To our best knowledge, our PL mapping of CdTe and CdZnTe crystals at liquid helium temperature is first of its kind that was published. First, we have performed a series of experiments of PL line-scanning on short-time annealed samples. We investigated the dynamics of the annealing process by visualizing profiles of PL intensities of various defects. Possibility of measuring by PL the changes of relative concentrations were demonstrated in [Hor05].
Secondly, a new setup for 2D PL mapping was built and used. High space and composition resolution imaging of $Cd_{1-x}Zn_xTe$ wafers was demonstrated. The resolution as good as 0.0005 in x is easily achieved by PL mapping. Using this method, the time evolution of solidification of the crystal is visualized with high resolution. This can reveal e.g. local zinc minima, which tell about the convection currents in the melt during solidification [Hor06c], (see section 4.3.2). The possibility of determination of segregation coefficients of PL intensities and of corresponding concentrations is presented in [Hor06b] and in section 4.4.2.1.

Some interesting results were obtained in another field. While studying absorption of extra-thin CdTe samples (about 2μm thick, selfstanding), we have obtained a new insight into the interpretation of some effects in PL spectroscopy. We have removed uncertainty in interpretation of the origin of two band-edge PL peaks at higher temperatures. The new result is that the dip between them is just a reabsorption effect by the FX peak (section 3.2.4.1), [Hor1]. This is directly connected to the uncertainty about position of the energy gap at high temperatures. Thus, as major achievement can be considered the establishment of a new temperature dependence of the fundamental energy gap in CdTe (section 3.3.5), [Hor06a]. Furthermore, in the view of the new value of the RT energy gap, we have proposed a new interpretation of the band edge RT photoluminescence emission, which is present only for some specific samples [Hor1] (section 3.2.4.2).

2 General properties of CdTe crystals

This chapter is intended to briefly review the values of parameters of CdTe and CdZnTe crystals, which are of relevancy for the investigation of optical properties of these crystals. An extended review of properties of CdTe and related compounds can be found in [Cap94].

2.1 Material properties

2.1.1 Crystal structure

CdTe is composed of tellurium and cadmium face centered sublattices shifted by quarter of body cell diagonal. Each cadmium atom has 4 tellurium atom in its closest neighborhood and vice versa. A picture of such a structure is given in Fig. 2.1. Tab. 2.1 resumes other important physical properties that may be generally useful. Values are taken from [Cap94] and [Tur04]. However the dispersion of values found elsewhere is not negligible. The temperature dependence of the thermal conductivity in more details was subject of study in [Sla64]. [Cap94] also describes thermal expansion in the range 0-300 K, as well as other mechanical and thermal properties.

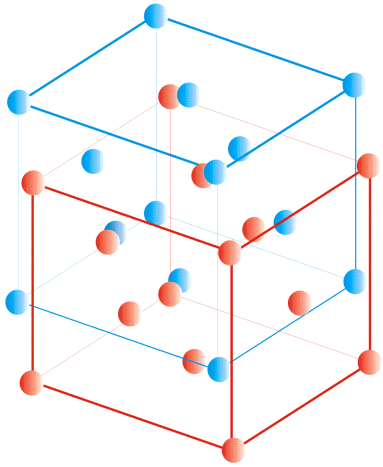

Fig. 2.1. *Representation of the zinc-blend structure of CdTe.*

Lattice parameter (295 K)	0.648 nm
Density (295 K)	5.85 gcm^{-3}
Thermal expansion coeff. (295 K)	4.6 10^{-6} K^{-1}
Thermal expansion coeff. (75 K)	2.2 10^{-6} K^{-1}
Specific heat (295 K)	0.21 $Jg^{-1}K^{-1}$
Thermal conductivity (295 K)	0.06 $Wcm^{-1}K^{-1}$
Thermal conductivity (8 K)	8 $Wcm^{-1}K^{-1}$

Tab. 2.1. *Values of chosen parameters of CdTe.*

2.1.2 Electronic structure, phonons

For the investigation of optical properties of CdTe in the infrared region, it is sufficient to describe the electronic structure near the Γ point by Fig. 2.2. Temperature dependence of the fundamental energy gap will be studied in detail in 3.3.5. Values of effective masses of quasiparticles are resumed in Tab. 2.2.

The phonon dispersion was studied for example in [Row74]. The most interacting with electrons is the longitudinal optical phonon (LO). Its energy is only slightly depending on k-space direction and has value of about 21 meV. LO phonons and the LO phonon-electron

interaction are background for many of high temperature properties like electron and hole mobility, heat transfer or band gap energy.

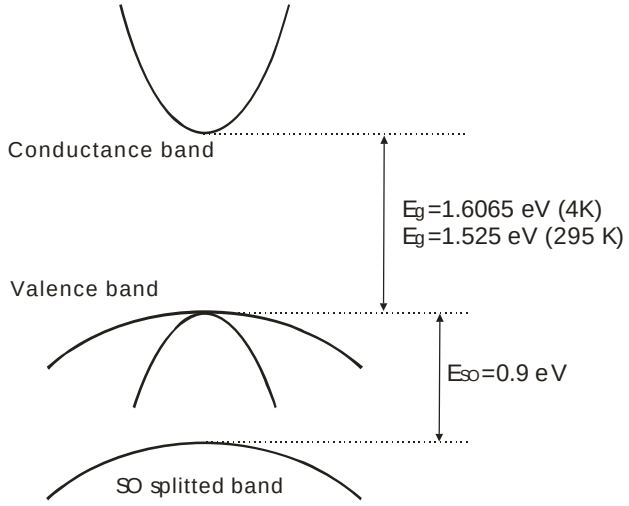

Fig. 2.2. *Band structure scheme of CdTe.*

m_e	0.1
m_{lh}	0.12
m_{hh}	0.7

Tab. 2.2. *Effective masses in m_0 units [Cap94].*

2.2 Defect structure

Good knowledge of defect levels is extremely important for semiconductor technology. In the particular case of CdTe, this knowledge is in a very simplified way depicted in Fig. 2.3. Optical spectroscopy provides information mainly about shallow levels (effective mass acceptor E_B≈57 meV, effective mass donor E_B≈14 meV). Cadmium (zinc) vacancy has been for a long time supposed to be the dominant electrically active defect in CdTe (ZnTe). This interpretation is no longer so widely used today. Unfortunately, the energy levels of cadmium vacancy are not known until nowadays. Cadmium vacancy acts as a double acceptor. A defect complex consisting of the metal vacancy and a donor in the closest position is called A-center (see Fig. 2.4). The character ‘A’ in the expression ‘A-centre’ should not be mistaken with ‘A’ as general symbol for acceptor. Deep levels can be detected by specific techniques like deep level transient spectroscopy (DLTS), thermally stimulated currents (TSC) or photo-induced current transient spectroscopy (PICTS) (an extended review of traps obtained from PICTS was published recently [Mat03]). A review of defect levels in CdTe and ZnTe was recently given in [Cap94, p. 546-554]. From this review are taken the defect binding energies in Tab. 2.3-Tab. 2.6. The conflicting values in Tab. 2.5 and Tab. 2.6 are reproduced in order to give a feeling about the uncertain nature of defect assignment.

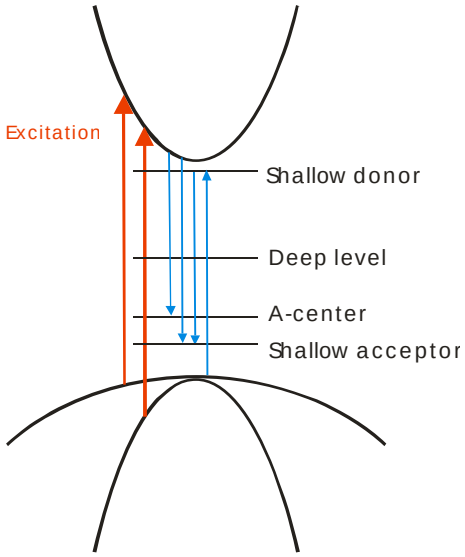

Fig. 2.3. *Scheme of defect levels in typical intentionally undoped CdTe. Some of important one-electron transitions occurring in PL experiment are depicted (in color).*

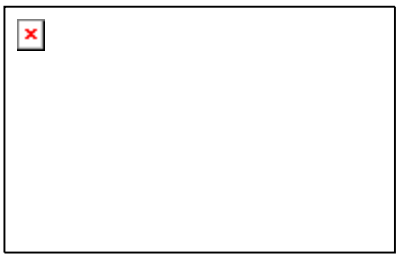

Fig. 2.4. *Scheme of A-centre defect in CdTe. Tellurium atoms (red), cadmium (blue), cadmium vacancy (empty blue circle) and cadmium-substitutional donor (black). The donor can be also substituting a tellurium position.*

Impurity	E_A (meV)	A_1 (eV)
Li	58.0	1.58293
Na	58.7	1.58916
Cu	146.0	1.58956
Ag	107.5	1.58848
Au	263	1.57606
N	56.0	1.5892
P	68.2	1.58897
As	92.0	1.58970

Tab. 2.3. *Acceptors in CdTe [Cap94]. Ionization energies (E_A) and excitonic lines energies (A_1) from PL spectra.*

Impurity	E_D (meV)	D_1 (eV)
Ga	13.88	1.59309
Al	14.05	1.59305
In	14.15	1.59302
F	13.67	1.59314
Cl	14.48	1.59296

Tab. 2.4. *Donors in CdTe. Ionization energies (E_D) and excitonic line energies (D_1) [Cap94].*

Impurity	Energy (eV)
Ge	E_c-0.95
	E_v+0.73
Sn	E_c-0.85
	E_c-0.9
	E_c-0.89, E_c-0.43
Pb	E_c-1.28

Tab. 2.5. *Deep levels of group IV elements in CdTe from various methods and works [Cap94].*

Impurity	Energy (eV)
Sc	E_c-0.01
Ti	E_c-0.73
V	E_v+0.74
Cr	E_v+1.34
Fe	E_v+0.35
	1.1, 1.475
	1.03, 1.13
	E_v+0.15
	E_v+0.2
Co	E_v+1.25
Ni	E_v+0.92
	E_c-0.76

Tab. 2.6. *Levels of transition metal impurities in CdTe and their assignment [Cap94].*

3 Optical properties of CdTe and CdZnTe

3.1 Theory of optical transitions

This chapter contains a brief summary of concepts and descriptions of particular optical transitions that are used in characterization of properties of a direct semiconductor.

3.1.1 Radiative and non-radiative recombination

Radiative processes in semiconductors are represented directly by emission spectra, whereas the non-radiative ones have only indirect influence on optical properties. Radiative centers can differ a lot by the capture cross-section for free particles and thus the PL manifestation of a given defect is not granted. The non-radiative recombination is usually classified into three types: 1) Auger processes, 2) capture through excited states and 3) recombination via emission of phonons. The Auger recombination is probably negligible in experiments where rather low concentration of free particles is generated (cw PL). An example of cascade capture through closely lying excited states could be the states at the surface of a semiconductor (surface recombination). This kind of recombination via many close states could be in principle also radiative, but there are probably no ways to measure it. Of course, all the non-radiated energy must be dissipated via phonon emission. The direct manifestation of phonon emission are LO phonon replicas, which carry the most of radiated energy in emission spectra of CdTe compounds. This will be briefly described in the following section.

3.1.2 LO phonon coupling

In II-VI materials, electron-phonon interaction is very strong. In absorption as well in photoluminescence spectroscopy, this is manifested by strong intensity of so-called LO phonon replicas. If the electron-phonon interaction is taken in the first order approximation (so-called linear modes) [Kei65], than the probability of electron recombination accompanied by emission of n phonons is given by

$$p_n = e^{-S}\frac{S^n}{n!}, \qquad \textit{Eq. 3.1}$$

where S is the so-called Huang-Rhys factor. Its value describes the strength of the electron-phonon interaction. Also, the S is the ratio of intensities of the first LO replica to the zero phonon line (ZPL). In CdTe, the LO phonon can couple with Huang-Rhys factor up to $S\approx$3-4. Since the distribution of replica intensities is not monotonous for S>1, the maximum PL intensity is not found for the zero phonon line for strong electron-phonon coupling constant. The parameter S is also the average number of emitted phonons.

If the defect complex symmetry has center of inversion, then the distribution of so-called quadratic modes will be given by

$$I_n \approx \frac{2n!}{2^{2n}(l!)^2}S'^{2n}, \qquad \textit{Eq. 3.2}$$

where I_n is intensity of n-th phonon replica, S' is a parameter expressing the interaction strength [Kei65]. The parameter S' is always less than one; the distribution of replica intensities is always monotonously decreasing.

Generally, the complex process of deexcitation can be described by an appropriate configuration coordinate model [Neu83]. An example of such a diagram with equal displaced parabolas is depicted in Fig. 3.1. The situation for quadratic modes is described by non-displaced

parabolas with different parabolicity. The energy that was not radiatively dissipated can be emitted through several LO phonons.

In CdTe, the individual LO phonon replicas are separated by energy of about 21 meV.

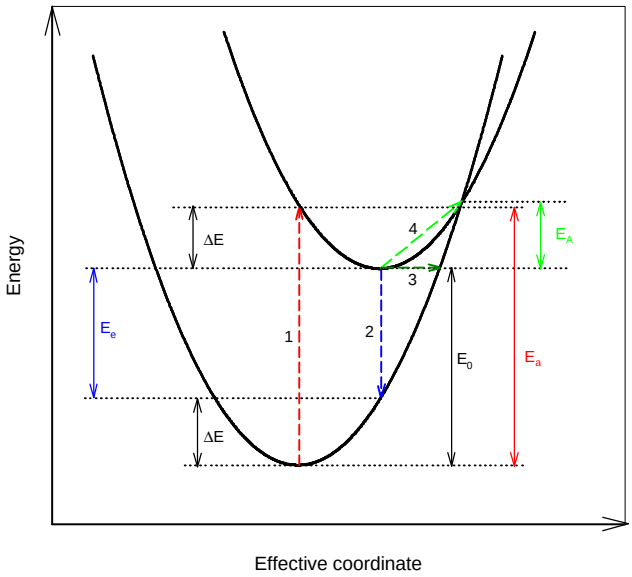

Fig. 3.1. *The configuration coordinate model for two equal, displaced parabolas. Various transition energies are defined. Photon absorption (red, 1). Return to the electronic ground state is possible by three basic ways: direct transition from the upper minimum (blue, 2), tunneling (dark green, 3) and thermally activated transition (light green, 4).*

3.1.3 Intrinsic transitions

For clarity, basic relation between optical constants will be briefly resumed. The constants describing optical properties (imaginary and real parts of complex dielectric function e_i and e_r, imaginary and real parts of complex refraction index n and k, absorption and normal reflection coefficients a and R, respectively) are connected via following relations:

$$n(E)=\sqrt{\frac{1}{2}\left(e_i(E)+\sqrt{e_i^{\,2}(E)+e_r^{\,2}(E)}\right)}, \qquad \textbf{Eq. 3.3}$$

$$k(E)=\frac{e_i(E)}{2n(E)}, \qquad \textbf{Eq. 3.4}$$

$$a(E)=\frac{E}{c\eta n(E)}e_i(E), \qquad \textbf{Eq. 3.5}$$

$$R(E)=\frac{(n(E)-1)^2+k(E)^2}{(n(E)+1)^2+k(E)^2}, \qquad \textbf{Eq. 3.6}$$

E is the photon energy.

The spectra of the real and imaginary parts of the optical functions are interdependent via the Kramers-Krönig relations.

Band-to-band transitions

In this work, our interest is limited to transitions within the fundamental energy gap E_g. For a direct band gap, the optical density of states expressed by the imaginary part of the dielectric function e_i, yielded by the one-electron approximation [Yu96], is in form of:

$$e_i(E) \approx \frac{2e^2(2m_r)^{3/2}}{m^2\eta E^2}|P_{CV}|^2(E-E_g)^{1/2}. \qquad \textit{Eq. 3.7}$$

m_r is the effective reduced mass ($1/m_r=1/m_e+1/m_h$), P_{CV} is the electric dipole transition matrix element.

Unfortunately, the simple expression 3.7 is nearly without any relevancy for a direct semiconductor, since excitonic effects really dominate in the vicinity of E_g. Excitonic interaction produces discrete lines

$$e_i(E) \approx \frac{8p\eta m_r^3}{3e_0^3E^2}|P|^2\sum_{n=1}^{\infty}\frac{1}{n^3}d\left(E-E_g+\frac{R_X}{n^2}\right) \qquad \textit{Eq. 3.8}$$

and enhances the continuum absorption into

$$e_i(E) = \frac{2p\eta^2|P|^2(2m_r)^{3/2}R_X^{1/2}e^Z}{3E^2\sinh Z} \qquad \textit{Eq. 3.9}$$

with

$$R_X = \frac{m_r e^4}{3\eta^2 e_0^2 e_r^2} \text{ as exciton binding energy and} \qquad \textit{Eq. 3.10}$$

$$Z = p\sqrt{\frac{R_X}{E-E_g}}. \qquad \textit{Eq. 3.11}$$

[Yu96] shows that expressions 3.8 and 3.9 smoothly meet at E_g.

3.1.4 Extrinsic transitions

Very little will be written about extrinsic transitions, more details can be found in any textbook. These transitions can be divided into excitonic and one-electronic.

Bound excitons

Exciton can exist as bound state on a potential generated by a defect. Usually, such a complex exists on a neutral defect. Since the bound exciton has no degree of freedom, the line-widths of these transitions are very small. Complexes of more than two electron involved (trions, biexcitons) also exist, but they are not observed in our experimental conditions (low density of generated particles, relatively high temperatures). Typical binding energies of donor bound excitons (D^0X) are 4 meV, whereas for excitons bound on neutral acceptors (A^0X) it is from 6 to 16 meV.

Bound-to-free

are called transition between acceptor and donors and valence or conductance bands. The energy balance must account with the kinetic energy of the free electron/hole.

DAP transitions

correspond to transfer of electron between bound states of a donor and acceptor pair. The energy difference is

$$\Delta E = E_g - E_D - E_A + \frac{e^2}{4per_{DA}}.$$

The distance between donor and acceptor r_{DA} can take discrete values only. In principle the corresponding transitions carry information about distribution of r_{DA}. With assumption of random distribution of donor-acceptor pairs, for typical dopant concentrations ($\approx 10^{16}$ cm^{-3}), the Coulomb term has value of several meV.

3.2 Photoluminescence spectroscopy

At the beginning of this subchapter, interpretation of PL lines of various defects is reviewed. Typical examples of emission of different defects are plotted. Temperature evolution of spectra as well as temperature quenching of PL is discussed. No excitation intensity dependence experiments are presented in this work. At the chapter end, effects of reabsorption occurring in the PL experiment are treated with particular attention. Also, a new interpretation of the room temperature emission band is proposed.

3.2.1 Comments on photoluminescence spectroscopy

PL characterization of solids has begun in the 40's [Neu97]. Probably, first measurements of low temperature PL of CdTe date back to the end of the 50's. Many fundamental problems of defects and PL in CdTe have been solved during the 60's, 70's and 80's. Since the 90's, the number of works focusing on the subject seems to still grow. A lot of old problems are tracking until now and from the point of view of a rather realistic view, they are not going to be resolved soon. The nature of electronic and excitonic PL transitions was recognized since the beginning, however many (rather majority) of these optical transitions cannot be ascribed with certainty until now.

To our best knowledge, one of the first optical measurements on CdTe were performed by [Nob59] (at least [Nob59] does not refer to earlier works). The absorption and photoluminescence spectra were recorded only at liquid nitrogen temperature. [Hal61] in the early 60's published probably first measurements of photoluminescence (often called fluorescence) emission spectra at liquid helium temperature. These spectra included most of optical transitions known today including excitonic radiation. PL spectra show that some of the "old" crystals were of very good quality. However, almost no correlation was found between doping and PL defect bands [Hal61].

The topic of assignment of PL lines and bands to specific chemical defects in CdTe includes more than 1000 works only since 1980 [www2]. Many of these works concern rather low quality CdTe (polycrystalline CdTe, CdZnTe of imprecise composition, epitaxial growth on not lattice-matched substrates). These are the reasons why we will refer to rather a small number of papers that seem to us relevant. Running unambiguous assignment experiments is rather complicated and expensive for following reasons. Two compound semiconductor CdTe is difficult to be grown in a repetitive quality and purity. Many intrinsic defects (mainly Cd vacancy, Cd interstitial, Te precipitates and inclusions, dislocations) often form complexes with extrinsic defects. Furthermore, electrical properties in some cases seem unstable (sensibility e.g. to humidity or to low temperature annealing). This reflects fast diffusion of some dopants (e.g. silver at room temperature); these properties may be connected to the large lattice constant of CdTe.

The basic extended works assigning principal shallow acceptors and donors are [Mol82a], [Mol84], [Pau85] and [Fra90]. From these papers originate most values of shallow defect levels (e.g. Na_{Cd}, Li_{Cd}, Ag_{Cd}, Cu_{Cd}, Na_{Cd}, P_{Cd}, In_{Cd}, Cl_{Te}) in section 2.2.

Many elements show PL emission on several energies, which can correspond to distinct defects. Some of these lines, which are observed in our samples too, give often rise to tentative ascriptions. Our insight on the interpretation of these PL lines is given in the following. Important dopants are commented in separate paragraphs, whereas the other PL transitions are grouped by similar properties.

Silver

Ascription of silver related PL transitions (acceptor to band E_A=108 meV, bound exciton at 1.5885 eV [Mol82]) was unambiguously confirmed recently via experiments using implantation of short-decay radioactive Ag [Ham98] and [Ham00]. These two transitions are often observed in our samples. However, there are more PL lines showing correlation with silver

doping. The 1.5815 eV line was tentatively attributed to Ag_{Cd}-Ag_i complex by [Mon86]. Furthermore, interstitial silver atom would act as a donor; this is observed non-optically by conversion into n-type material by RT diffusion of silver.

Indium

Probably, the first extended paper on PL properties of indium doping was [Bar75]. The band with many LO phonon replicas with binding energy of about 150 meV was assigned to a cadmium vacancy-indium donor complex (nowadays called A-center). Sharp bound excitonic line was observed near 1.584 eV, which is attributed to a center involving an indium atom too. [Wor95] has shown, using magnetophotoluminescence, the 1.5842 eV bound exciton to correspond to an isoelectronic complex defect involving cadmium vacancy, two indium donors and another displaced cadmium atom. Our measurements show that some In doped samples emit weak PL radiation near 0.7-0.8 eV (the high-resitivity level). (However, the 0.7-0.8 eV emission correlates with strong PL signal of A-centers; in a detector-grade material the 0.7-0.8 eV band is not observed.)

Chlorine

Many spectral lines are correlated with chlorine doping. [Fra90] describes Cl donor via observation of bound exciton and its two electron transitions (TET). (The TET transition is the process when the electron of the donor remains in an excited state.) The exciton localization energy would be 3.5 meV (1.593 eV is the BX PL energy). From energy positions of the TET lines, donor binding energy is calculated as 14.5 meV. But the donor-free hole transition is not observed. [Set92] observes in Cl-doped CdTe 1.5903 eV bound exciton (tentative assignment to cadmium vacancy-chlorine complex), 1.586 eV line is observed in highly doped CdTe:Cl. [Shi98] assigns the peak at 1.590 eV to Cd vacancy and two Te-substituting chlorine donors, the 1.586 eV line is attributed to complex of a cadmium vacancy and a single chlorine donor. Deep level emission is usually not observed in CdTe:Cl, however [Kru91] reports on a PL band near 0.8 eV for co-doped CdTe:Cl:Cu. Many other works dealing with effects of annealing of CdTe:Cl on the PL spectra have been published.

A-centers

A broader study of A-center binding energies and Huang-Rhys factors was presented in [Sta95]. Those values are reproduced in Tab. 3.1. The values were derived with an assumption of a DAP transition; the value of 14 meV for the donor energy was used, the Coulomb energy ($e^2/4\pi\varepsilon_0\varepsilon_r r_{DA}$) contribution was neglected. However, our investigations show that at least for all our samples, the coulomb term is approximately 6-8 meV. Then the energy peak difference is not 14 meV, but 8-6meV. This effect could have influence on the binding energies in Tab. 3.1.

Donor	E_B (meV)	S
F	116	3.2
Cl	125	2.2
Br	119	2.6
I	128	1.5
Ga	131	1.7
In	142	1.8

Tab. 3.1. *Binding energies and Huang-Rhys factors of PL bands of A-center defects [Sta95].*

Y band

So-called Y PL band near 1.475 eV was shown to be related with dislocations by microscopic cathodoluminescence in [Hil97]. The authors calculated the Huang-Rhys factor of 0.2. [Kuh92] showed, using magnetoluminescence, that the 1.475 eV PL band stems from D^0h transition (E_B=131 meV). From our experience, the maximum position as well as the relative intensities of its replicas differ a lot from sample to sample. We think, that this PL come from a

defect bound to the dislocation. In summary, this PL band is sensitive to particular sample preparation and it should not be used as a measure of dislocation density.

Deep levels

Deep levels were investigated by several authors (see for e.g. [Sta95] and references therein), but the knowledge about these emission bands is really insufficient and interpretations are very contradicting. For example, [Bry68] attributes the 1.1 eV emission to an intrinsic defect connected to Te (V_{Te} or Te_i). [Lis85] observes and correlates 1.03 eV and 1.13 eV levels with iron doping. [Kru96] distinguishes in the 1.1 eV band two components at 1.08 and 1.17 eV and interprets it as DAP recombination of the closest and next-closest pairs of unknown origin. Some of the deepest levels emitting near 0.6-0.8 eV are recognized to originate from e.g. Sn, Ge, V.

PL of other impurites

Works on optical properties of CdTe crystals doped by Si, Co, P, Fe, O, I, As, Sb, V, Ge, N, H, Hg, Au, Cu, Ga, Al, Tl, Ti or Sn exist also, but most of them do not seem to us to be of such interest for the present study to be mentioned in this short review.

3.2.2 Examples of defect photoluminescence

Defect photoluminescence in CdTe can be classified into four very characteristic spectral regions. First, sharp lines of PL originating from free and bound excitons are found at energies 10-20 meV below the gap energy. It is very sensitive to material purity and, of course, from experimental point of view, sensitive to excitation intensity. Second category is occupied by shallow acceptor transitions (free-to-bound as well as donor-acceptor transitions) with binding energies ranging from 50 to 70 meV. Third spectral region is reserved for PL from so-called A-centers. Typical binding energies are 140-170 meV. The fourth category includes deep level's photoluminescence whose maxima are found near the middle of the band gap. Intensity of these broad bands is often very weak.

PL of these four types is partially superposing mainly due to the omnipresent LO phonon replicas. Thus, good understanding of the overlying PL transitions requires numerical fitting. Majority of spectra can be fitted using only several elementary transitions. Each group of luminescence transitions is completely characterized by PL intensity of the ZPL line, line width and Huang-Rhys factor. The LO phonon energy is more or less constant. Usually, one A-center, one shallow acceptor and several bound exciton transitions are sufficient to a good reproduction of the PL spectrum by fitting. Examples are given in Fig. 3.2. Several weak transitions can be now better discerned. E.g. another shallow acceptor transition in CdTe E239 at 1.55 eV, or the so-called Y band in CdTe U17 in the proximity of 1.475 eV. The Y band is typical by its irregular and unusual line-shape (see Fig. 4.17).

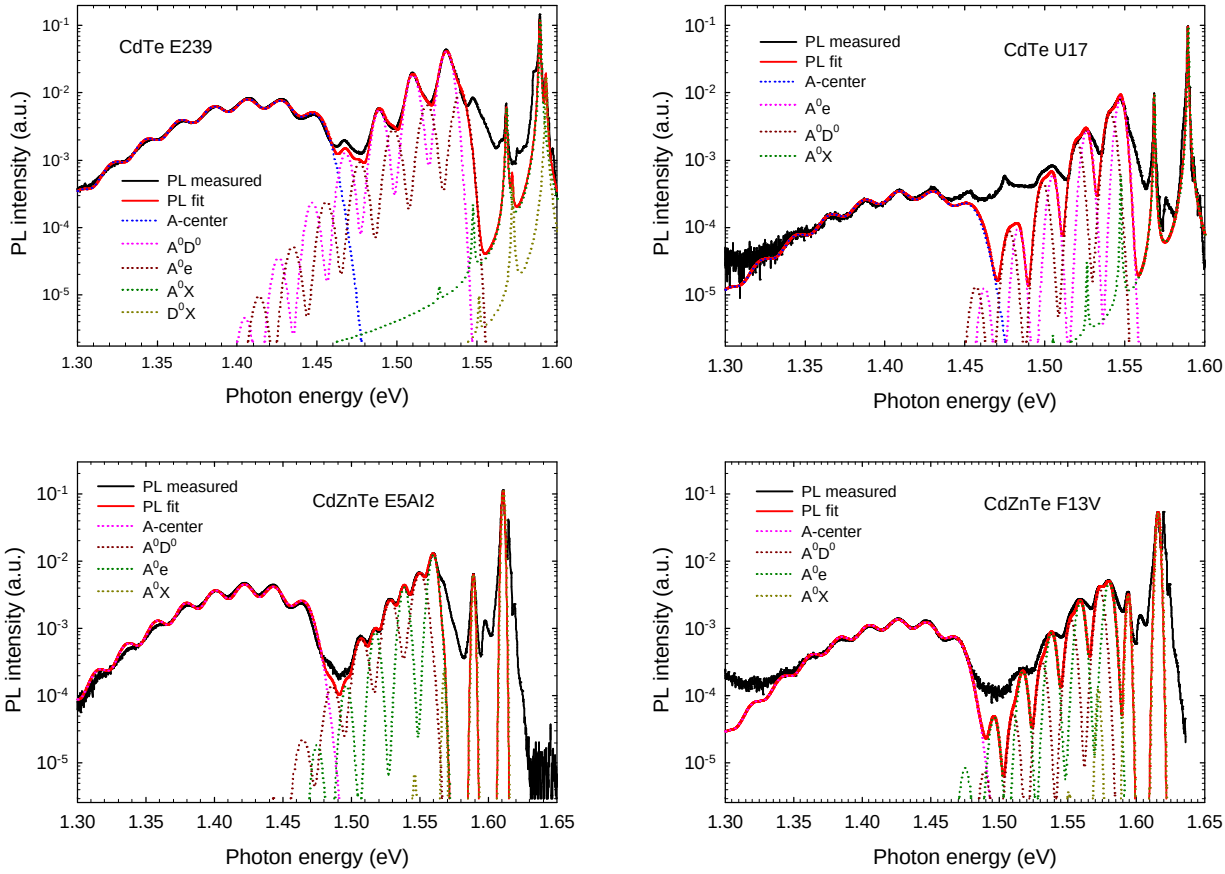

Fig. 3.2. *Typical PL spectra of undoped CdTe and CdZnTe crystals. The spectra are decomposed into deep and shallow acceptor transitions and bound-excitonic transitions near the band gap energy. The most of the PL intensity is due to only several characteristic defect transitions. The peaks are simulated by Gauss function except for excitonic transitions where Lorentzian functions were used.*

3.2.2.1 Excitonic photoluminescence

Usually, in highly pure semiconductor materials, low temperature photoluminescence spectra are dominated by excitonic emissions. Photoluminescence of excitons can be divided into intrinsic radiative recombination of free excitons and extrinsic emission of excitons bound on potential of defects (mainly neutral acceptors and donors). The free exciton's photoluminescence is typical by manifestation of distribution of kinetic energy corresponding to a certain effective temperature (superior to the lattice temperature), whereas bound excitons, having no degree of freedom, posses the narrowest lines observed for electronic states in solids.

Free-excitonic PL is manifested almost uniquely by LO phonon replicas and its intensity is a reasonable criterion of material purity and quality. For doping concentrations above 10^{16} cm^{-3}, usually, free-exciton LO replicas cannot be observed at all.

Photoluminescence emission of bound excitons can be divided into subgroups formed by excitons bound to neutral donors (binding energies 3-4 meV) and excitons bound to neutral acceptors with larger a more spread binding energies (6-20 meV). Excitons bound on ionized impurities are not well known. Donor bound excitons show very weak electron-phonon coupling, the first LO phonon replica is hardly detectable. In most cases, the acceptor bound exciton intensity is very strong since CdTe grows naturally mostly as p-type. Up to 3-4 replicas of acceptor bound excitons can be discerned in PL spectra of high quality samples.

In CdZnTe, broader bound exciton bands are usually only two, corresponding to acceptor and donor bound excitons with no possibility to discern chemical different defects.

Fig. 3.3 and Fig. 3.4 show that the classical Poisson distribution which is valid for the so-called linear modes cannot be applied with success to experimental data. Much better agreement is obtain when replicas of excitons are modeled by distribution for quadratic modes by Eq. 3.2 (compare Fig. 3.3 and Fig. 3.4 and consider the logarithmic scale). The coupling constants are gathered in Tab. 3.2.

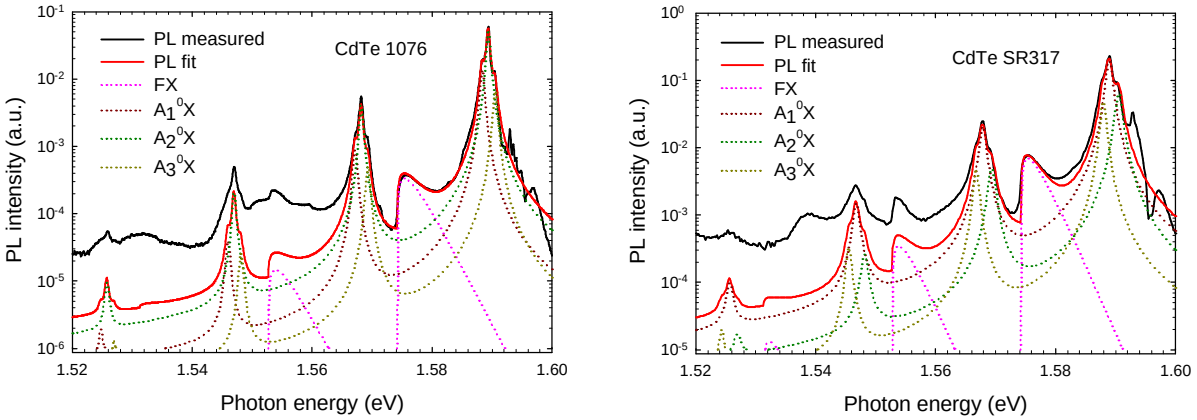

Fig. 3.3. *LO phonon replicas of bound excitons fitted by the Poisson distribution (Eq. 3.1).*

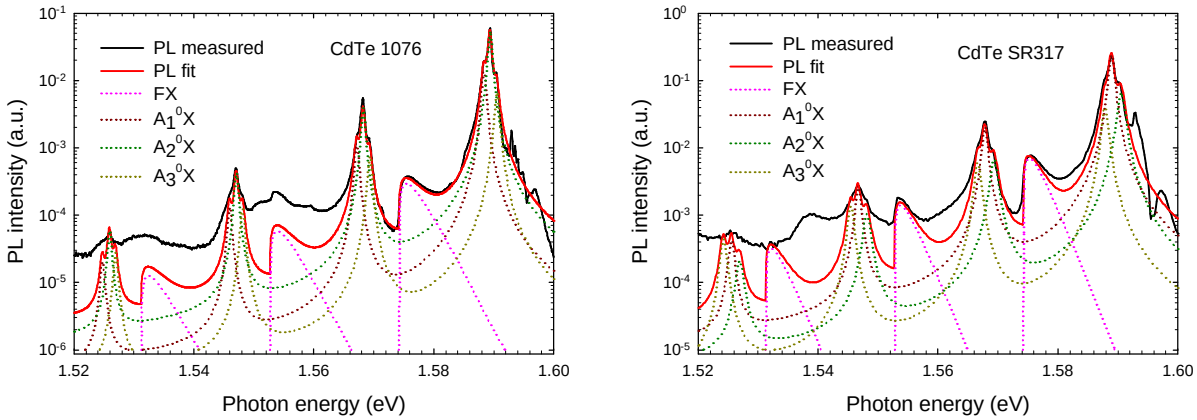

Fig. 3.4. *LO phonon replicas of bound excitons fitted by the intensity distribution by Eq. 3.2.*

Material	Sample	Transition	E_{ZPL} (eV)	S'	*FWHM* (meV)
CdTe	1076	A^0X	1.5883	0.4	0.8
CdTe	1076	A^0X	1.5893	0.4	0.7
CdTe	1076	A^0X	1.5905	0.5	0.8
CdTe	1076	FX	1.596	0.5	-
CdTe	AF15	A^0X	1.5891	0.3	0.15
CdTe	AF15	A^0X	1.5894	0.3	0.15
CdTe	AF15	A^0X	1.5896	0.3	0.15
CdTe	AF15	FX	1.596	0.65	-
CdTe	F36E4	A^0X	1.5896	0.35	0.8
CdTe	SR317	A^0X	1.5878	0.55	0.5
CdTe	SR317	A^0X	1.5889	0.41	0.5
CdTe	SR317	A^0X	1.5905	0.5	0.6
CdTe	SR317	FX	1.596	0.5	-

Tab. 3.2. *ZPL energies and coupling constant S' values of acceptor bound and free excitons in CdTe. Donor bound exciton lines show very small LO phonon coupling.*

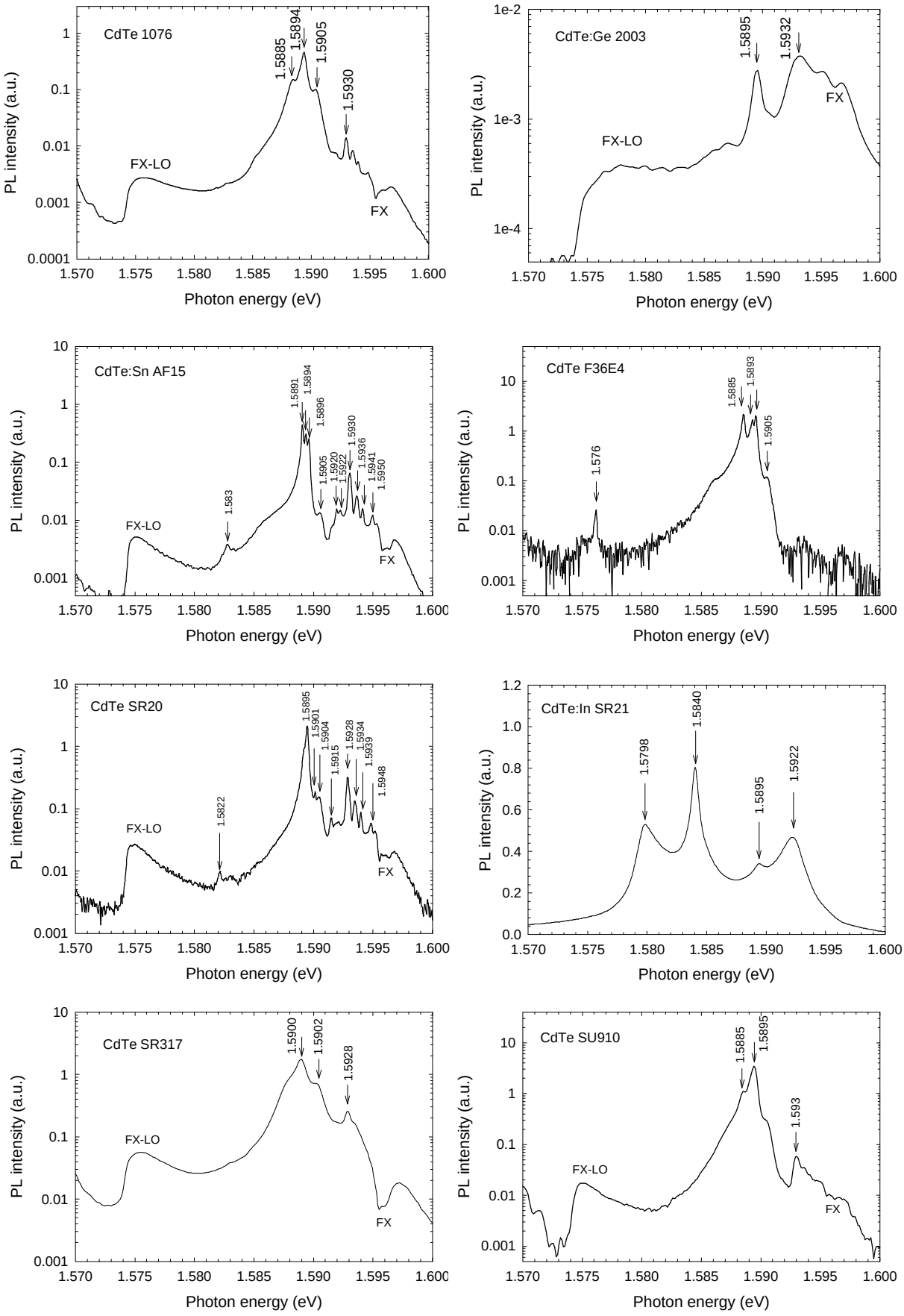

Fig. 3.5. *Excitonic PL spectra of CdTe samples.*

Fig. 3.5 depicts 8 spectra of good quality CdTe crystals in the excitonic region. Comparing the marked energies with Tab. 2.3 and Tab. 2.4, we can find that most intense emission comes from excitons bound on neutral acceptors. Donor bound excitons are sometimes badly detectable. An intense PL of free exciton replicas is sometimes observed.

Majority of samples exhibit strong BX lines near energy of 1.5895 eV. Several acceptor defects are reported to manifest in the close vicinity of this energy (Li, Na, Cu, see Tab. 2.3) so it is extremely difficult to tell which of these common acceptors is polluting the particular sample. Donor bound excitons usually show weak lines. As their binding energy is small and very similar, the chemical identification is even more impossible. Some crystals (mainly doped ones) exhibit BX emission at lower energies compared to standard shallow acceptors and donors. Lines of BX found at energies 1.580 eV, 1.581 eV, 1. 584 eV and others are supposed to correspond to complexes of defects.

3.2.2.2 Photoluminescence of shallow acceptors

PL emission of several undoped crystals produced in the Institute of physics is depicted in Fig. 3.6. Even though these crystals were grown from similarly pure starting elements, shallow acceptors have quite different binding energies (50-80 meV) and thus different chemical origin. Small fluctuations of the ZPL lines are also due to mixing of A^0e and A^0D^0 transitions. These two bands are rather wide and they superpose strongly. Numerical fitting cannot be used to separate their respective contributions because of their very non-trivial line shape. Depending on the particular concentration of donors and acceptors, the maximum of the A^0e and A^0D^0 composed band shift to higher or lower energy. Generally, most donors in CdTe have 14 meV as binding energy; this energy is expected to separate maxima of A^0e and A^0D^0 transitions. The Coulomb energy decreases this difference by 10-4 meV. To identify whether a given band is an A^0e or A^0D^0 transition, the temperature dependence must be known (see 3.2.3). The purest samples do not show any PL connected with transfer of single electron from the acceptor states.

Binding energies, Huang-Rhys factors of PL band connected to shallow acceptors in CdTe and CdZnTe samples are written in Tab. 3.3. Based on the comparison with Tab. 2.3, the chemical nature of acceptors is given, but should be considered with precaution. Most of transitions can be correlated with substitutional Li or Na, which have too much close binding energy to be distinguished one from each other. Some deeper transitions can be attributed to P. However, we observe further unidentified acceptor defect transitions.

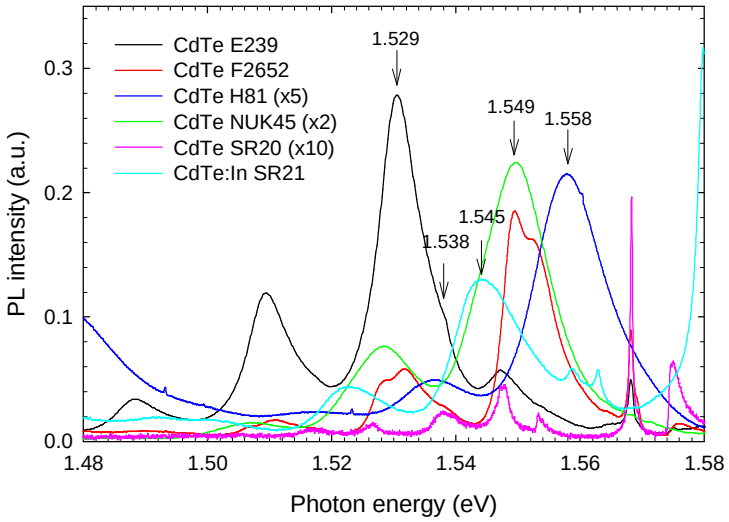

Fig. 3.6. *PL spectra of shallow acceptors is undoped CdTe samples. Arrows indicate positions of the ZPL lines. Mixing of A^0e and A^0D^0 transitions is observed for chemically different acceptors.*

Material	Sample	Transition	E_B (meV)	S	*FWHM* (meV)	Defect
CdTe	E239	A^0D^0	76	0.9	8.3	P?
	E239	A^0e	66	1.3	5.2	P?
CdTe	F2652	A^0e	53	0.8	7.0	?
CdTe	F36E4	A^0D^0	66	0.65	5.8	Li, Na?
	F36E4	A^0e	60	0.65	6.6	Li, Na?
CdTe:In	F38C8	A^0e	57	0.8	9.9	Li, Na?
CdTe	H81	?	48	0.5	9.0	?
CdTe	NUK45	A^0e	57	0.7	13.2	Li, Na?
CdTe	SR20	A^0D^0	68	0.8	3.3	P? or Li, Na?
	SR20	A^0e	59	0.6	3.2	Li, Na?
CdTe	SR21	A^0D^0	61	0.65	8.0	Li, Na?
CdZnTe	E5AI2	A^0D^0	87	0.8	9.9	?
	E5AI2	A^0e	77	0.65	6.6	?
CdZnTe	F13V	A^0D^0	61	0.9	6.6	Li, Na?
	F13V	A^0e	54	1.05	6.6	Li, Na?
CdZnTe:In	RC2	?	68	0.65	9.1	?
CdZnTe:Cl	RITEC	?	68	0.6	9.9	?

Tab. 3.3. *Binding energies, Huang-Rhys factors and probable chemical nature of shallow acceptor transitions in CdTe and CdZnTe. (Binding energy in this table is taken as the difference between E_g and the peak maximum.)*

3.2.2.3 Photoluminescence of A-centers

Transitions related with A-center defects are described via Tab. 3.4, Fig. 3.7 and Fig. 3.8. The mixing of A^0e and A^0D^0 transitions is very similar to shallow acceptors. Again, binding energies are quite spread, within the 120-170 meV interval. The Huang-Rhys factor ranges from 2.75 to 3.6. Its magnitude is so high because of natural strong dipole of the A-center defect. The specific defect identification using Tab. 3.1 is not very successful since our binding energies are rather greater. However, the strong A-center bands in Cl and In doped crystals very probably correspond to the doping by these elements in most cases. We have no idea about the chemical origin of the deep A-centers (150-170 meV). Also, it seems that binding energies for CdZnTe are generally greater. This may be due to possibly higher concentration of zinc atoms near the A-center defect (binding energies in ZnTe are slightly greater then for CdTe).

Material	Sample	E_B (meV)	S	E_{LO} (meV)	*FWHM* (meV)
CdTe	1076	155	3.2	21.0	6.9
CdTe	1076	161	2.9	21.0	18.6
CdTe:Sn	AF13	151	3.1	21.0	18.2
CdTe	E239	159	3.0	20.6	17.2
CdTe:In	F38C8	144	2.95	20.8	23.1
CdTe:Cl	H81	130	3.0	21.0	23.1
CdTe:Cl	PD38	132	3.0	21.2	18.2
CdTe	PU1	121	3.1	21.4	23.1
CdTe:	S81	132	2.75	21.2	18.5
CdTe:In	SR21	152	3.0	20.7	18.6
CdTe:Cl	TF29	151	3.0	20.7	20.6
CdZnTe	E5AI2	172	3.25	21.2	17.0
CdZnTe	F13V	167	3.3	20.8	18.0
CdZnTe:In	RC2	160	3.0	21.4	23.1
CdZnTe	RITEC	167	3.6	20.8	23.1

Tab. 3.4. *Binding energies and Huang-Rhys factors of A-center defects in CdTe and CdZnTe.*

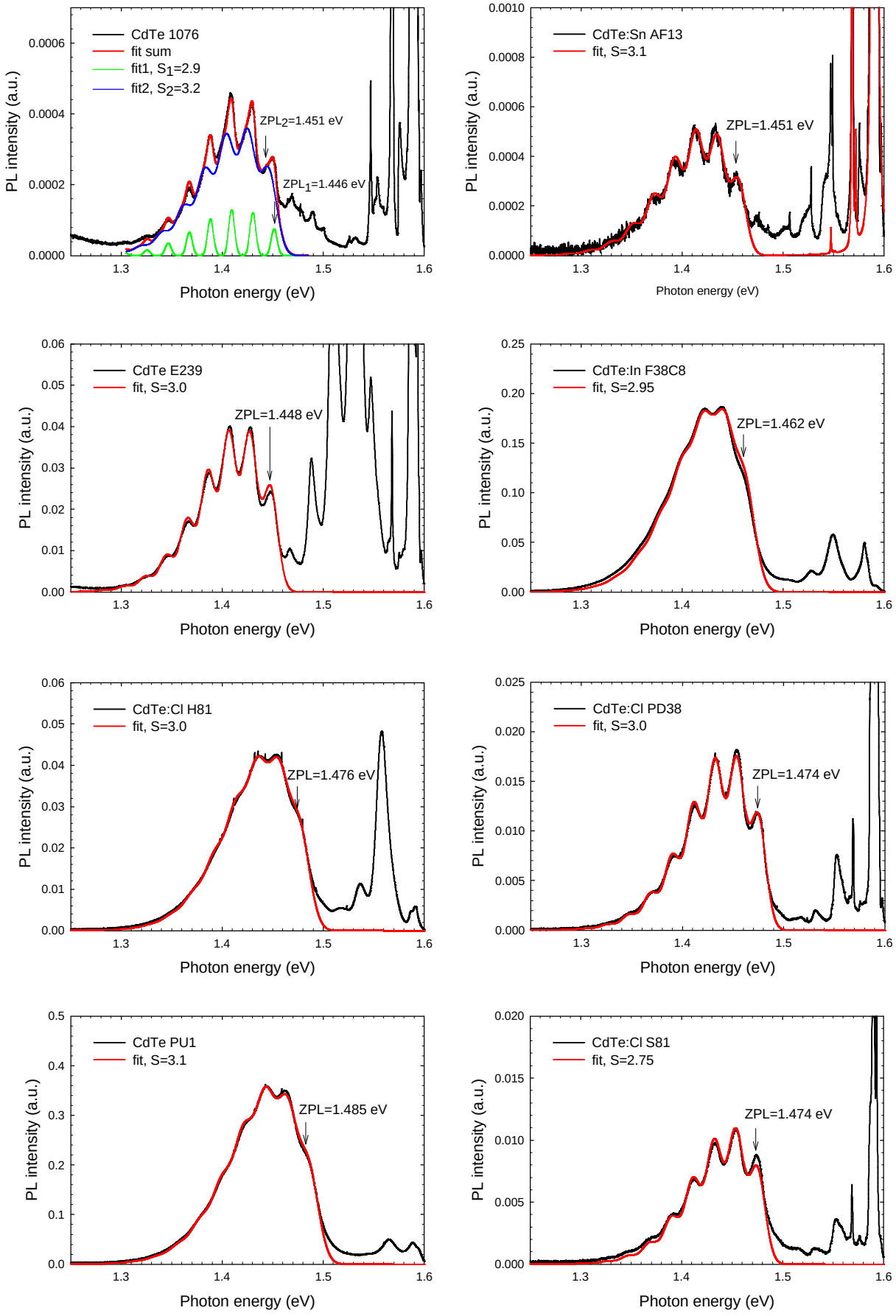

Fig. 3.7. *Shapes of phonon replicas in CdTe samples for A-center acceptors.*

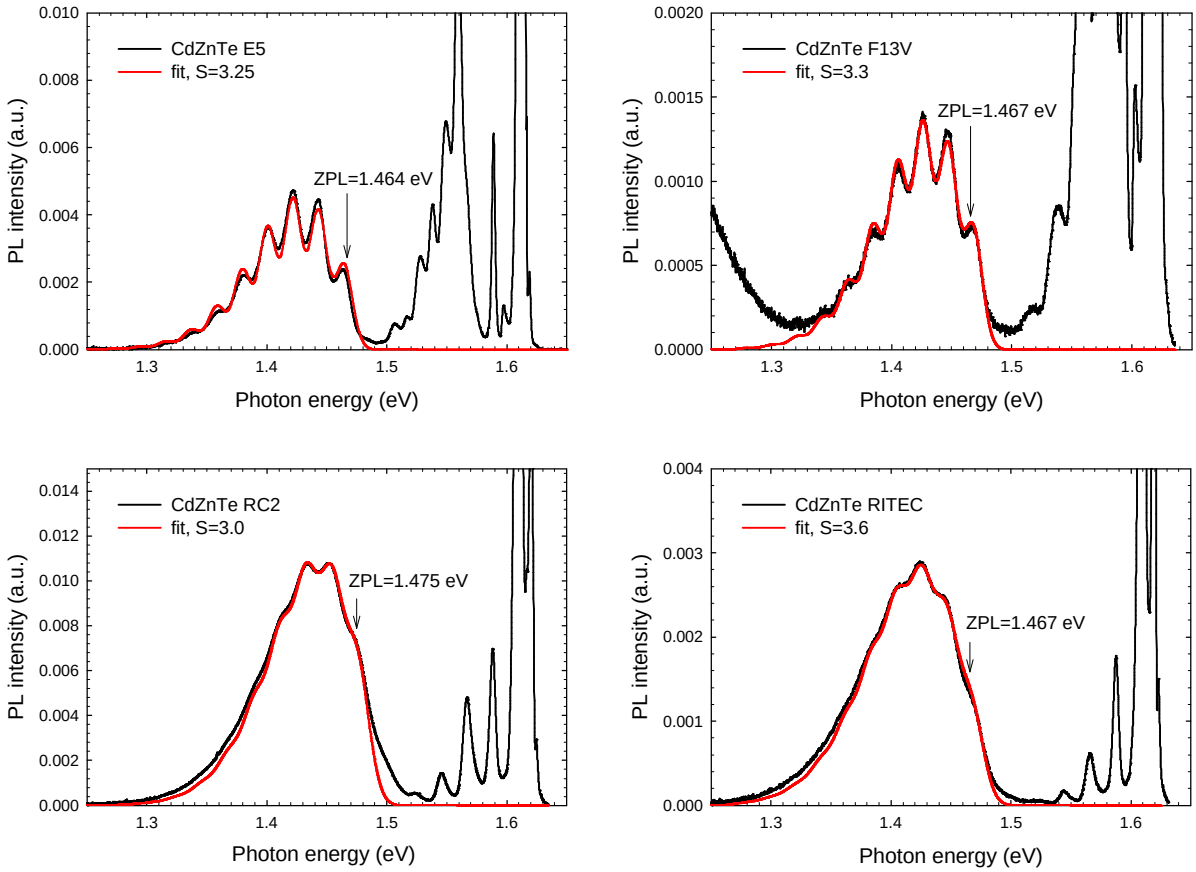

Fig. 3.8. *Shapes of phonon replicas in chosen CdZnTe samples.*

3.2.2.4 Photoluminescence of deep levels

Any information on deep levels is very appreciated when trying to understand the defect structure of high-resistivity CdTe. Also, information in literature on very deep levels is not rich. The so-called deep levels PL bands can be divided into two rather separated spectral regions (see Fig. 3.11). The first one is situated in the proximity of 1.1-1.2 eV and is present in majority of samples (thus could be tentatively ascribed to an intrinsic vacancy or vacancy complex). The second region is situated in the middle of the energy gap, between 0.6-0.8 eV. This emission is usually not present in undoped samples. Whereas the PL originating from the 1.1-1.2 eV can be recorded and analyzed using the silicon detector and applying spectral corrections to the line shape, the latter one requires to be measured either using Ge or InSb detector (see spectral spectromer response in the first chapter). PL recorded with InSb detector ranges from 0.45 eV up to higher energies. Most of samples do not posses deep levels between 0.45-0.8 eV. Only 4 spectra of doped material, which are plotted in Fig. 3.9 and Fig. 3.10 show measurable PL signal in this region.

Detailed information on deep energy levels in characterized samples is found in Tab. 3.5. Fig. 3.11 resumes positions of deep levels in CdTe samples. Despite the scattering of values, it is possible to track several discrete energy levels. Levels in the 0.7-0.8 eV interval obviously correspond to intentional doping, whereas the other ones are found more or less in each crystal.

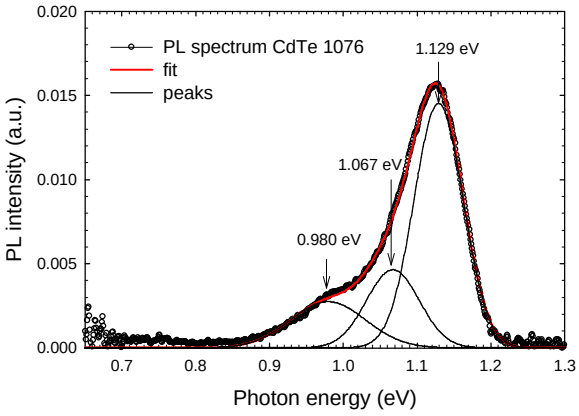
PL spectrum CdTe 1076
fit
peaks
1.129 eV
1.067 eV
0.980 eV
PL intensity (a.u.)
Photon energy (eV)

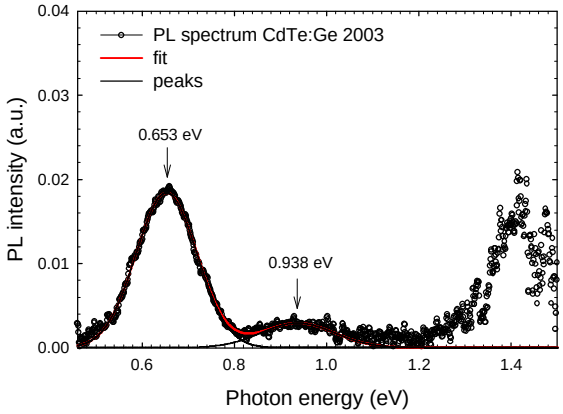
PL spectrum CdTe:Ge 2003
fit
peaks
0.653 eV
0.938 eV
PL intensity (a.u.)
Photon energy (eV)

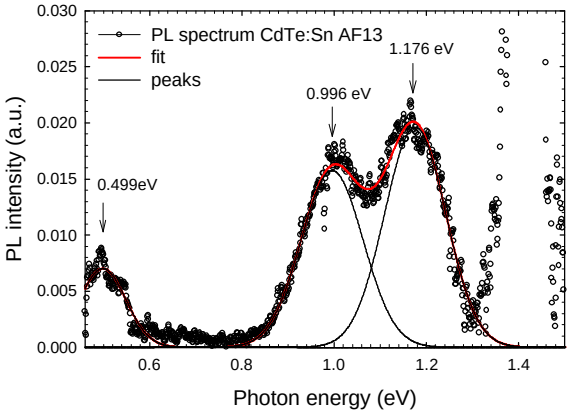
PL spectrum CdTe:Sn AF13
fit
peaks
1.176 eV
0.996 eV
0.499eV
PL intensity (a.u.)
Photon energy (eV)

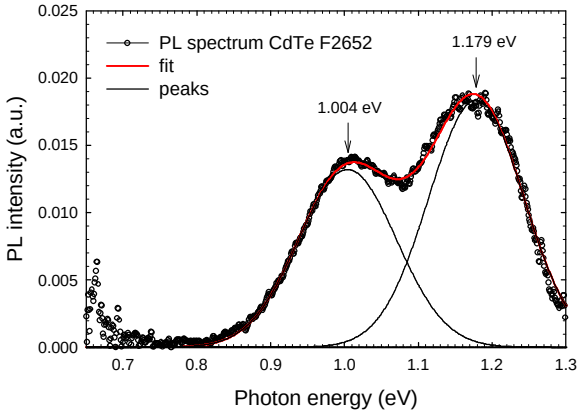
PL spectrum CdTe F2652
fit
peaks
1.179 eV
1.004 eV
PL intensity (a.u.)
Photon energy (eV)

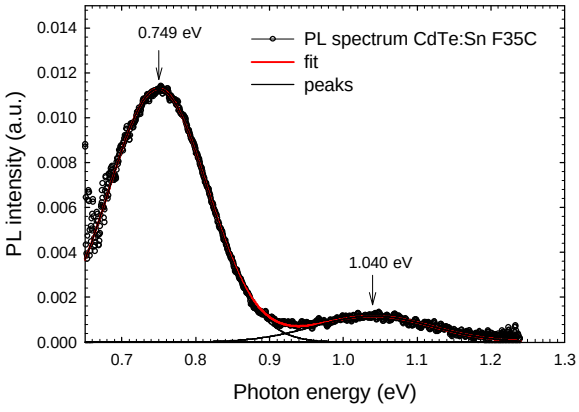
PL spectrum CdTe:Sn F35C
fit
peaks
0.749 eV
1.040 eV
PL intensity (a.u.)
Photon energy (eV)

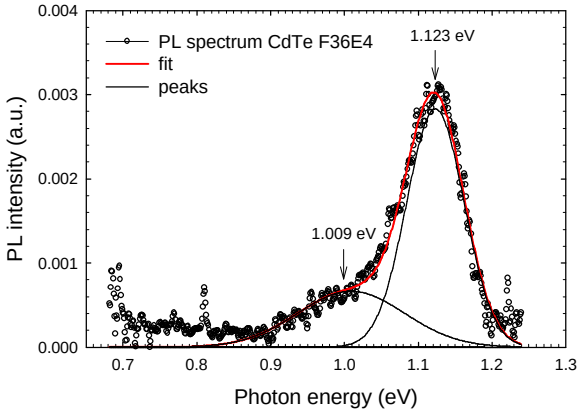
PL spectrum CdTe F36E4
fit
peaks
1.123 eV
1.009 eV
PL intensity (a.u.)
Photon energy (eV)

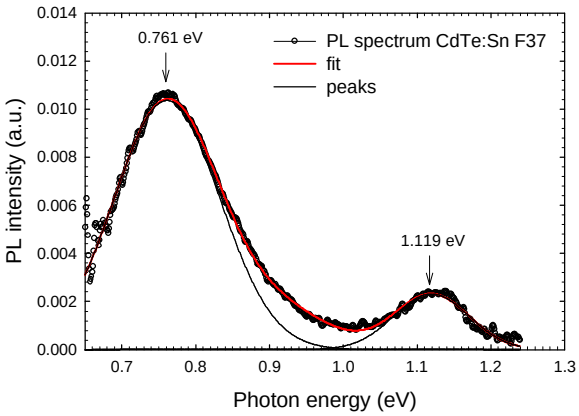
PL spectrum CdTe:Sn F37
fit
peaks
0.761 eV
1.119 eV
PL intensity (a.u.)
Photon energy (eV)

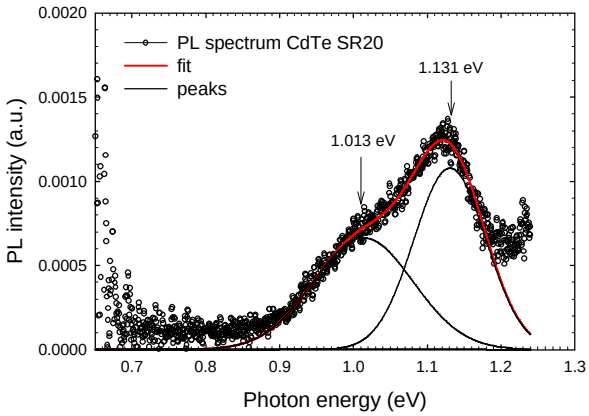
PL spectrum CdTe SR20
fit
peaks
1.131 eV
1.013 eV
PL intensity (a.u.)
Photon energy (eV)

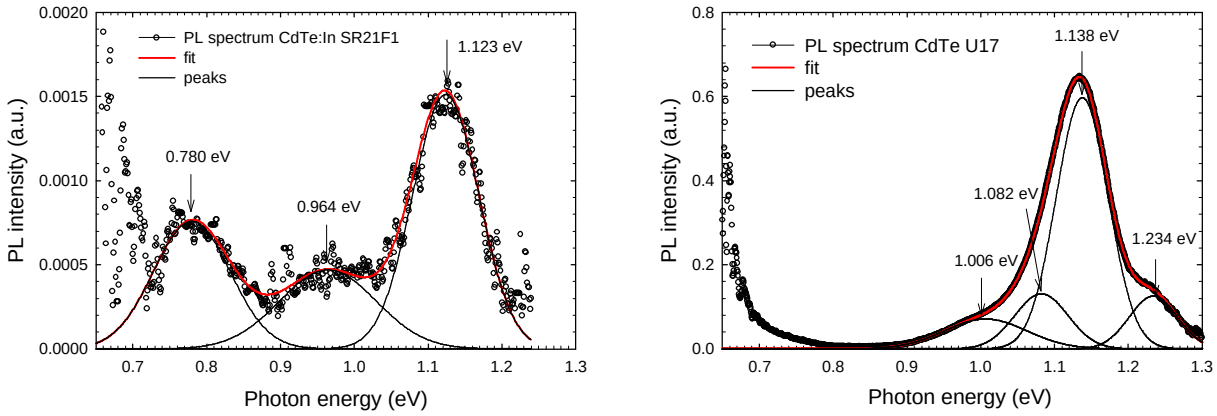

Fig. 3.9. *Photoluminescence spectra of deep levels in CdTe crystals (10 graphs). Spectra 2003 and AF13 were recorded using InSb detector, the others using Ge detector. The detectivity of the InSb detector starts at 0.45 eV. Samples characterized by the Ge detector do not show deeper emission than 0.65 eV.*

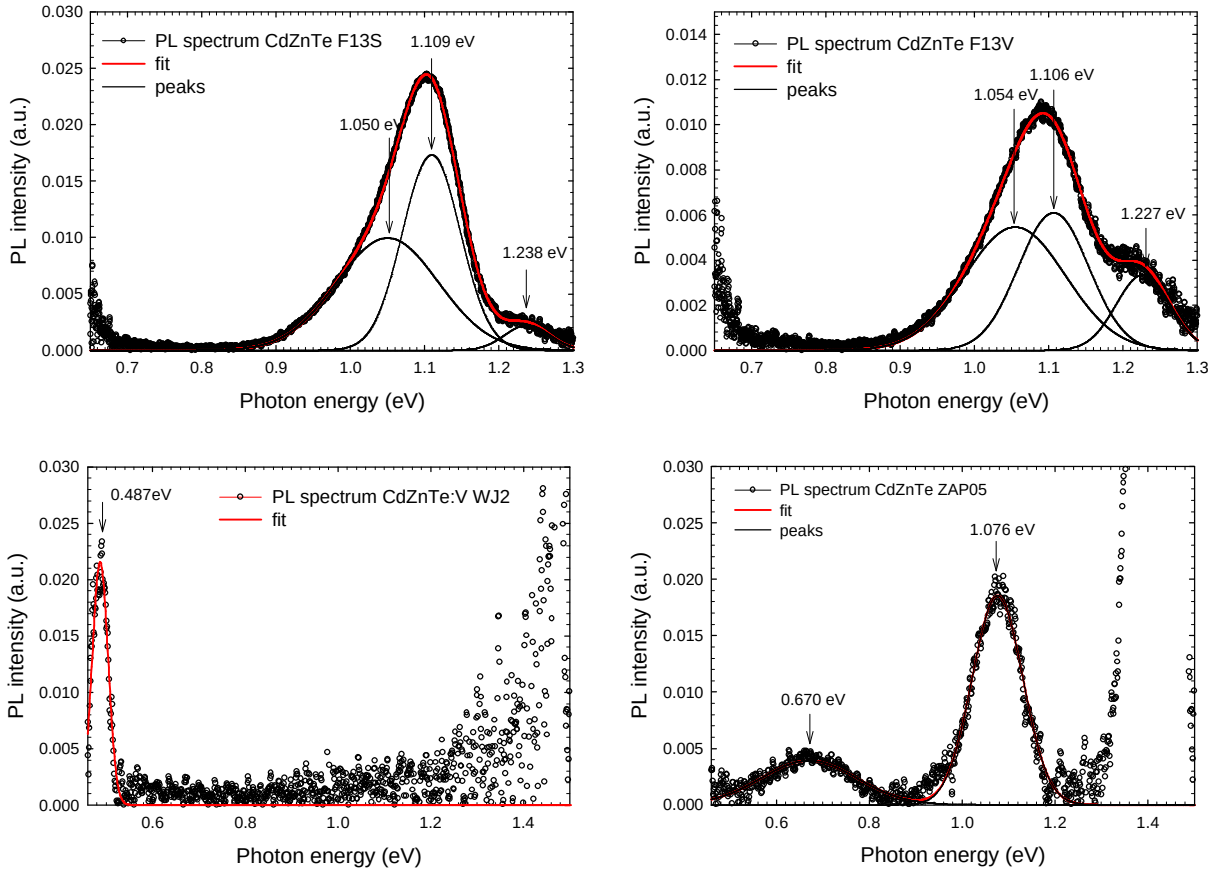

Fig. 3.10. *PL spectra of CdZnTe samples. Photoluminescence of F13S and F13V was recorded with the Ge detector, while emission of WJ2 and ZAP05 with the InSb detector as the latter samples showed deeper PL signal.*

Material	Sample	Sample number	Energy (eV)	FWHM (meV)
CdTe	1076	1	0.980	72
			1.067	51
			1.129	47
CdTe:Ge	2003	2	0.655	82
			0.924	116
CdTe:Sn	AF13	3	0.738	104
			1.080	174
CdTe:Sn	AF15	4	0.765	80
			1.035	155
CdTe	E239	5	1.131	59
CdTe	F2652	6	1.005	95
			1.179	90
CdTe:In	E3314	7	0.874	111
			1.129	70
CdTe:Sn	F35C	8	0.749	93
			1.04	113
CdTe	F36E4	9	1.009	102
			1.123	55
CdTe:Sn	F37A	10	0.761	101
			0.921	92
			1.119	72
CdTe:In	F38C8	-	no emission	low quality
CdTe	H8	-	no emission	low quality
CdTe	NUK45	11	1.029	110
			1.126	51
CdTe:Cl	PD38	-	no emission	high quality?
CdTe	PU1	-	no emission	low quality
CdTe:Cl	S81	-	no emission	high quality
CdTe	SR20	12	1.013	96
			1.131	69
CdTe:In	SR21	13	0.780	74
			0.964	93
			1.123	63
CdTe	SR317	14	1.030	115
			1.127	52
CdTe	SU910	-	no emission	high quality
CdTe:Cl	TF29	-	no emission	high quality??
CdTe	U17	15	1.006	78
			1.082	51
			1.138	50
			1.234	46
CdZnTe	19572	-	no emission	high quality
CdZnTe	F13S	-	1.050	97
			1.109	55
			1.238	42
CdZnTe	F13V	-	1.054	96
			1.106	67
			1.227	51
CdZnTe	RC2	-	no emission	high quality??
CdZnTe	RITEC	-	1.062	93
CdZnTe	WJ1	-	no emission	low quality

Tab. 3.5. *Deep level's peak energies and line-widths.*

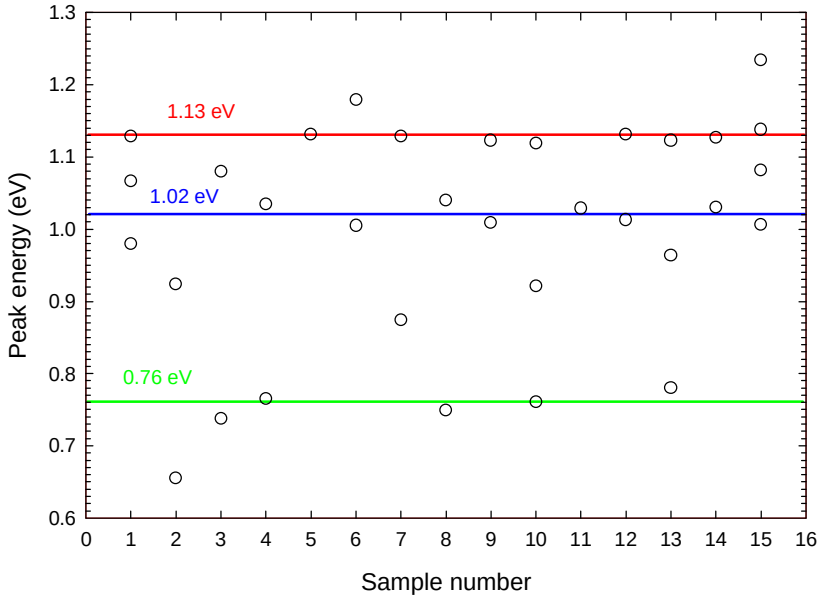

Fig. 3.11. *PL maxima energies of deep levels in CdTe crystals. In color are the energies of the most frequent levels. The sample number-sample coding is found in Tab. 3.5.*

3.2.3 Temperature dependence of photoluminescence

The temperature evolution of PL bands is not simple at all. The temperature not only dissociates neutral impurities (A^0, D^0), but also shifts the fundamental energy gap and the Fermi energy level. The temperature also influences strongly the relative concentration of free electrons and free excitons and causes changes in transport properties (mobility). It will be shown, that the intensity of many PL transitions do not quench monotonously with increasing temperature. Also, sometimes, the PL transitions do not shift monotonously energetically with increasing temperature.

Temperature evolution of PL spectra of CdTe samples SR317 and U17 are plotted in Fig. 3.12 and Fig. 3.13. Primary, they illustrate the fast quenching of PL radiation with temperature. Also, other rather complex effects can be seen. E.g., in Fig. 3.12 left the maximum intensity of the deep level near 1.15 eV is in proximity of 35 K. The type of transition is not known, but the PL maximum can be interpreted as due to a shift of the Fermi energy level. Other strange effect, that is not easy to be interpreted, is that PL of all transitions with very different binding energies is quenched at a similar speed (see Fig. 3.12 left and Fig. 3.13 left). It is also seen, that at 90 K, the intensities of the PL spectra approach fast to the noise level.

The classical expression currently used to describe the temperature quenching of integrated PL intensity is:

$$I(T) = \frac{I_0}{1 + C_1 \exp\left(-\frac{E_1}{kT}\right)}, \qquad \textit{Eq. 3.12}$$

where E_1 is activation energy of a transition responsible for the radiative quenching [Kru97]. On a larger temperature scale, this expression can be extended to include more activation processes:

$$I(T) = \frac{I_0}{1 + C_1 \exp\left(-\frac{E_1}{kT}\right) + C_2 \exp\left(-\frac{E_2}{kT}\right)} \qquad \textit{Eq. 3.13}$$

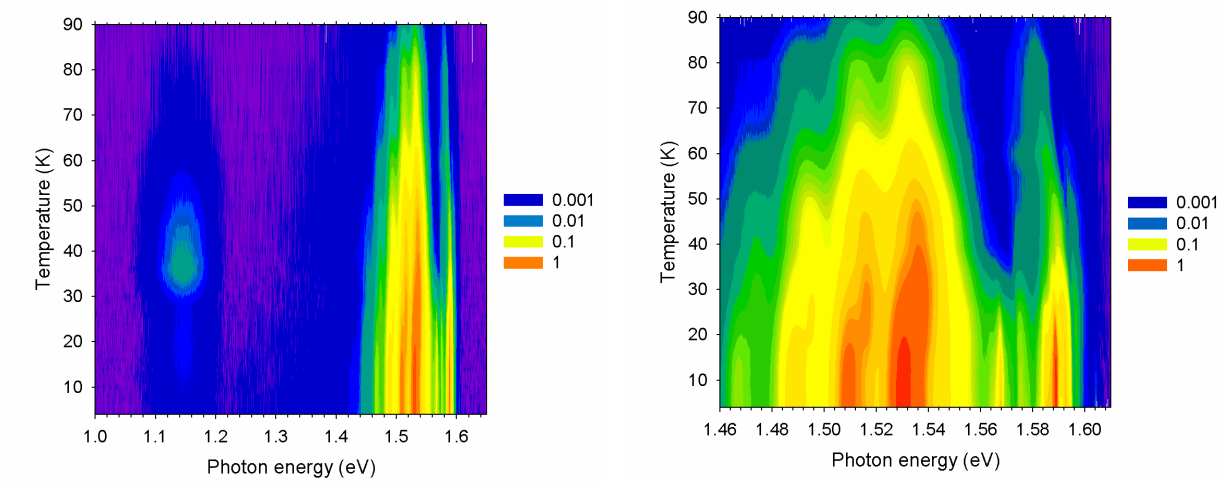

Fig. 3.12. *Logarithmic contour plots of temperature evolution of PL in CdTe SR317 (left), detail (right).*

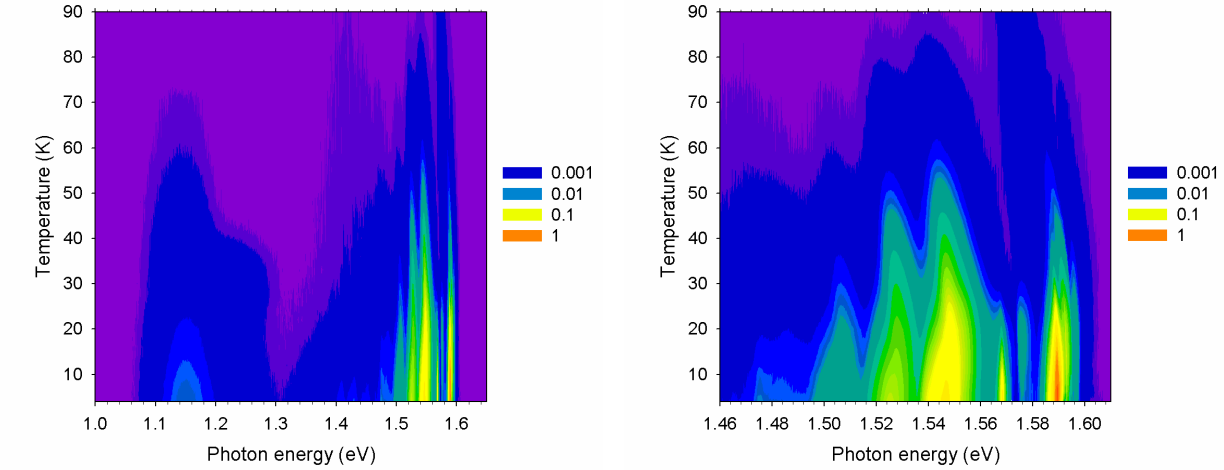

Fig. 3.13*. Logarithmic contour plots of temperature evolution of PL of CdTe U17 (left), detail (right). For the temperature shift of E_g, see section 3.3.5.*

However, the latter expressions do not describe well many of quenching processes observed. Especially, often one of the two activation energies yielded by fitting to Eq. 3.13 is a fraction of meV and there are great difficulties in interpreting of such energy. To better fit experimental data, [Kru97] proposed expression of type:

$$I(T) = \frac{I_0}{1 + C_2 T^{3/2} \exp\left(-\frac{E_2}{kT}\right)}, \qquad \textbf{Eq. 3.14}$$

the factor $T^{3/2}$ accounts for the temperature dependent cross capture coefficient. Identical expression was proposed before by [Zim92] to explain temperature quenching of bound excitons in CdTe. In this case, $T^{3/2}$ originates from temperature dependence of free-exciton density of states. In the real experiment, much more parameters influence the probability of radiative recombination on a given defect at given temperature (e.g. shift of the Fermi level energy, temperature dependence of the mobility of carriers).

General remark concerning quality of fits using equations 3.12 and 3.14 must be made. Almost no experimental data can be fitted enough well with one activation energy (3 free parameters). Using two activation processes (5 free parameters), the fitting parameters are not stable enough to give a feeling of reliable energies to be interpreted. Hence, we don't judge that

investigation of PL intensity quenching can be an absolute proof for interpretation of the involved transitions.

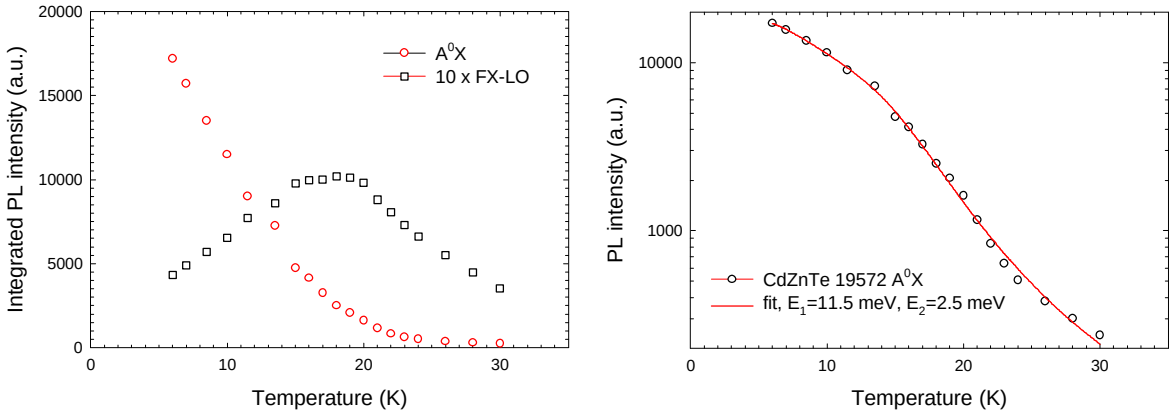

Fig. 3.14. *Temperature evolution of the dominant emissions in CdZnTe 19572 which are the acceptor bound exciton and free-exciton replica (left). Fitting to Eq. 3.13 with two activation energies is also plotted (right).*

Fig. 3.14 (left), Fig. 3.15 and Fig. 3.16 show non-monotonous evolution of integrated PL coming from FX-LO and D^0X bands. The non-monotonous quenching of excitons is observed only for several, high-quality crystals. The slight increase of free exciton PL with temperature together with fall of PL emitted by acceptor bound excitons was observed e.g. by [Tag75]. [Tag75] also derives thermal quenching energies for excitonic emission, but, they seem to be calculated from very small quantity of experimental points (3 points). These quenching energies are 4.5 and 7 meV for two different acceptor bound excitons, they correspond very precisely to the respective binding energies. Our fits do not support this simple and wanted interpretation.

Investigation of quenching of A^0X band is depicted in Fig. 3.14 (right). The two-energy model was used. The yielded activation energies are 11.5 and 2.5 meV. The first one can be attributed to the dissociation of free-excitons (R_X=10.5 meV) and the second one should account for the binding energy of the bound exciton. Unfortunately, the binding energy derived from PL spectra is about 7 meV. The old problem of too much fast quenching of acceptor bound excitons is well known [Zim92 and references therein].

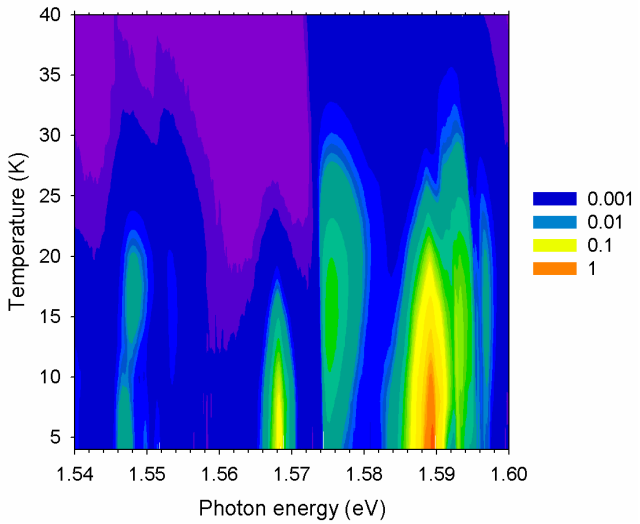

Fig. 3.15. *CdTe SU910 (high quality commercial sample). Temperature evolution of A^0D^0 and A^0e (near 1.547 eV and 1.549 eV respectively), FX-LO (near 1.576 eV) and bound-excitonic transitions (in the proximity of 1.589 and 1.593 eV).*

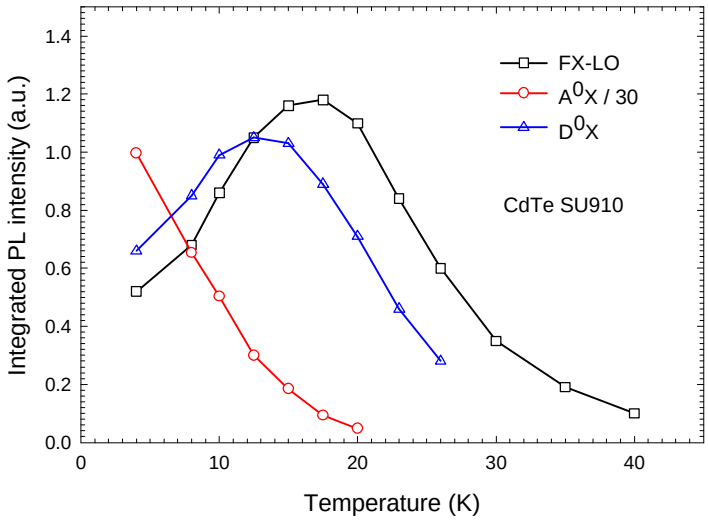

Fig. 3.16. *Non-monotonous temperature evolution of photoluminescence of free and donor-bound excitons for another high-quality CdTe.*

The quenching of donor bound excitons is slower compared to A^0X although the D^0X have smaller binding energy. Fig. 3.17 plots comparison of use of different models for temperature quenching of PL from donor bound excitons. In this case, one-energy models seem sufficient. Whereas the simplest model (Eq. 3.12) yields energy of 8 meV, the modified model (Eq. 3.14) gives 4 meV for the dominant quenching process. On one hand, the 8 meV activation energy could be ascribed to FX dissociation. On the other hand, within the second model, the 4 meV energy could be associated with bound exciton dissociation.

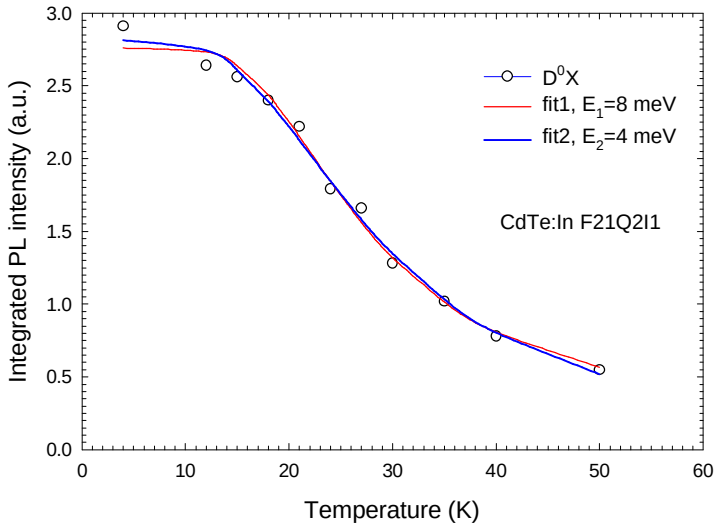

Fig. 3.17. *Temperature quenching of donor bound excitons and fittings for two different models. Fit1 and fit2 correspond respectively to Eq. 3.12 and Eq 3.14.*

Quenching of acceptor related PL is depicted in Fig. 3.18. Unfortunately, it is not simple to separate contributions of A^0D^0 and A^0e transitions because of non-trivial line-shapes. However, the A^0D^0 transitions are negligible for temperatures above 30 K. We can see that the fit (Eq. 3.13) yields a principal quenching energy of 28 meV. The binding energy of the present shallow acceptor is about 60 meV. Then again, the dominant quenching process is probably via an excited state of the acceptor so that the PL quenches more quickly than is expected from the defect binding energy. An effective configuration-coordinate model could describe the quenching

of the PL intensity; but the quenching energies obtained from the fit cannot be interpreted as directly observed parameters like binding energy of a defect.

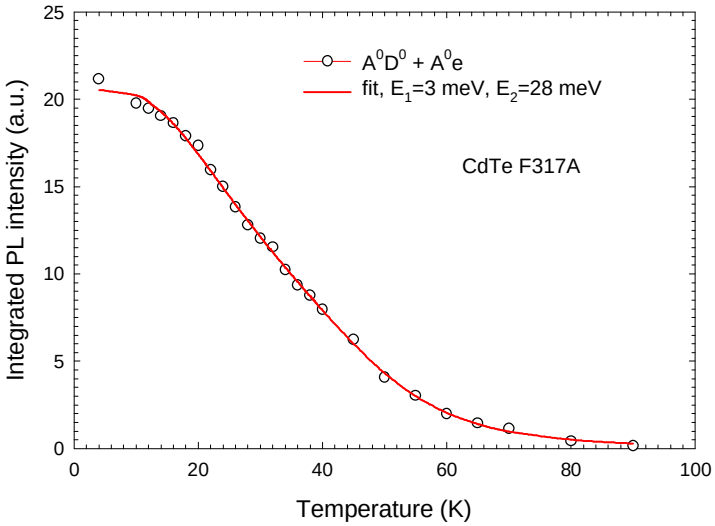

Fig. 3.18. *Quenching of acceptor to band transition photoluminescence in CdTe SR317.*

Fig. 3.19 plots temperature evolution of the maximum of band corresponding to the mixture of A^0D^0 and A^0e transitions. At low temperatures, the band can hardly be decomposed into the respective contributions. Only after the ionization of donors, the A^0e transition prevails. Fig. 3.19 shows comparison of E_g-E_B and E_g-E_B+k_BT/2 temperature dependencies to the experimental data (the k_BT/2 is the shift of PL maximum of a free-to-bound transition). The E_g-E_B+k_BT/2 dependence is closer to the experiment. Since the maximum of the A^0e transition theoretically shifts also with the increase of the thermal energy of free electrons, the acceptor binding energy should account also for this small contribution.

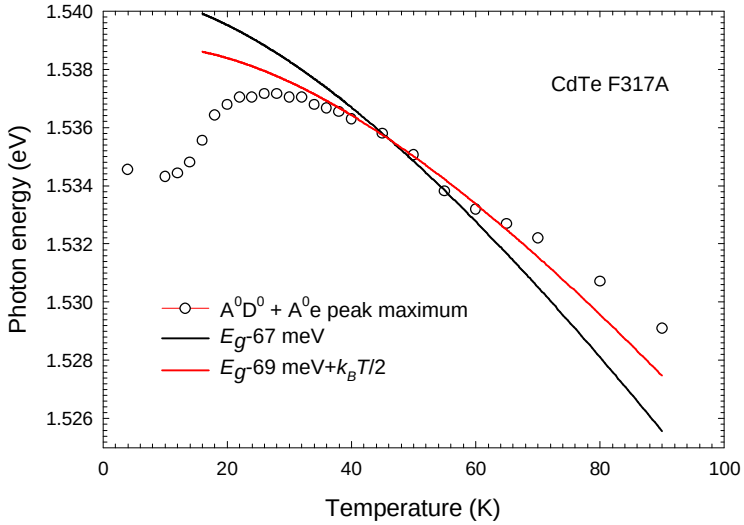

Fig. 3.19. *Temperature evolution of maximum of acceptor band which is composed both of donor to acceptor and acceptor to band transitions. In order to calculate the ionization energy of the acceptor correctly, addition of the thermal contribution of free electrons may be needed.*

3.2.4 Photoluminescence at high temperatures

This section is dealing with interpretation of edge photoluminescence for temperatures from 4 K to room temperature and even above it. Due to uncertainties in the knowledge of the fundamental

energy gap position at higher temperatures, many strange and confusing interpretations of the near band edge luminescence (NBEL) were proposed. Our explanation of NBEL will be based partially on our new temperature dependence of E_g, which can be found in chapter 3.3.5.

Recently, for example, room temperature (RT) photoluminescence has been reported to be suitable for mapping the concentration of zinc in the CdZnTe alloy [Li01]. It has been used to evaluate defect creation during technological manipulations [Rat03].

We will show that at temperatures 4-100 K, the edge PL is strongly affected by the free-exciton (FX) reabsorption. The reabsorption produces a dip in the PL spectrum, and the two resulting neighboring maxima were therefore sometimes interpreted as donor-hole (D-h) and FX emission [Yu95] or as ground FX state and upper exciton-polariton branch [Gon90].

The RT PL, if measurable, consists of one broad near band edge luminescence band [Gil85], [Lee94], [Agu95] and [Jai01]. At 300 K, the NBEL maximum is found close to 1.505 eV. The peak maximum was interpreted as FX resonance energy in [Gil85] and [Lee94] or as bound exciton transition dominating the emission spectrum in [Agu95]. [Jai01] affirms that the NBEL band is composed mainly from free-excitonic transitions and its phonon replicas. We will show that the NBEL band originates most probably from free electrons recombinating with holes trapped on potential fluctuations in samples of low quality.

Investigated CdTe samples can be divided into two groups differing in the temperature damping of PL. The first group exhibits PL that disappears fast with increasing temperature; generally, at 150 K it is not detectable anymore. These samples have rather sharp bound exciton (BX) lines (FWHM is 0.2-0.6 meV), which is a sign of a very good crystal quality. The crystals of the second group have much broader BX bands and simultaneously their PL is easily detectable at RT. This observation is depicted in Fig. 3.20. Letters code sample names (see Tab. 3.6).

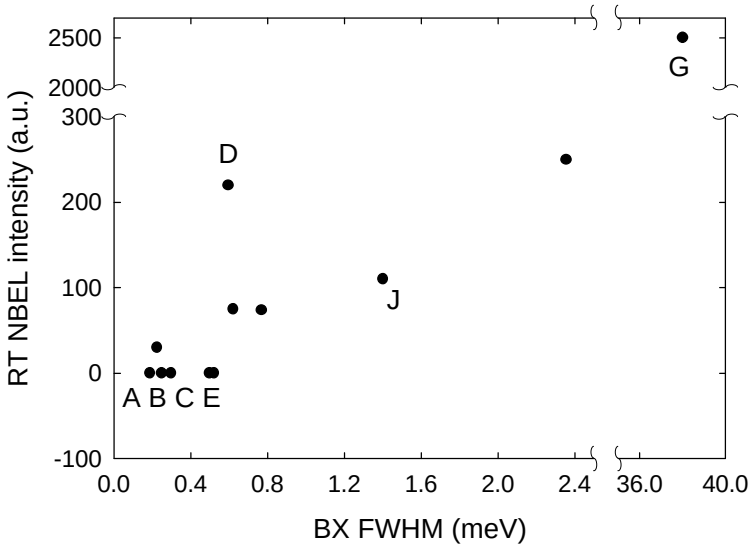

Fig. 3.20. *Correlation between the crystal quality expressed by the width of bound exciton lines at 4 K and the room temperature PL intensity. Samples A, B and C are high-quality crystals; samples J and G represent the low-end group.*

Letter	A	B	C	D	E	J	G
Sample	AF15	SR20	SU910	F26	U17	2003	PU1
Doping	CdTe:Sn	CdTe	CdTe	CdTe	CdTe	CdTe:Ge	CdTe

Tab. 3.6. *Correspondence between sample names and symbols in figures in this section.*

3.2.4.1 Reabsorption of luminescence by free excitons

Fig. 3.21 shows typical spectra of PL and absorption for chosen CdTe samples of different quality, at temperature of 4 K. Interpretation of the PL spectrum in the region of exciton-polariton energies at 4 K was done for example in [Sug76], [Coo89]. From the comparison of PL and absorption in Fig. 3.21, it is quite evident, that the highest-energy peak (1.597 eV), for samples A and D, is not the FX resonance as could be tentatively interpreted without the knowledge of the absorption spectrum. The peak at 1.597 eV could be interpreted as phonon-assisted recombination of excitons with higher velocities. At the $FX_{n=1}$ energy, we can observe a reabsorption minimum.

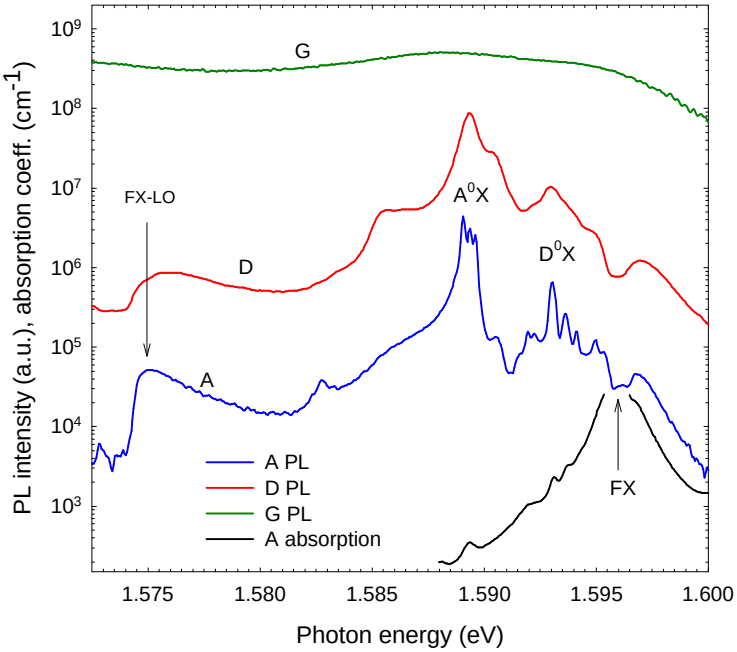

Fig. 3.21. *Absorption and PL for high and low quality CdTe single crystals at 4K. Arrows FX and FX-LO indicate the FX reabsorption and the FX emission assisted by the LO phonon, respectively. Photoluminescence of excitons bound to neutral acceptors and donors is denoted A^0X and D^0X. PL spectra are graphically vertically shifted (multiplied by a constant).*

The increased temperature results in a smearing of the exciton-polariton splitting being typically very small (0.6 meV [Sug76], 0.4 meV [Coo89]). For the ensuing analysis, the absorption coefficient above 25 000 cm^{-1}, where no transmission near the FX absorption has been detected, will be approximated by a Lorentz profile, which fits the experimentally observed absorption profile width and theoretically determined total absorption of FX states. Plots of both PL and absorption at higher temperatures are in Fig. 3.22. For temperatures of 40, 80 and 120 K, we find a remarkable coincidence between the characteristic dip in the edge PL and the FX resonance, which is very sharp as seen from the absorption spectra. We interpret thus the PL dip as the reabsorption of PL originating in the core of the crystal by the FX states close to the surface. A very similar interpretation was published already by [Tra82], where only PL spectra at 77 K of several semiconductors including CdTe were investigated. Our own interpretation was established independently of [Tra82]; the latter work has been cited only rarely in the ‘west’ literature and remains rather unknown. Moreover, our absorption measurements have brought an unambiguous proof of the reabsorption dip in PL spectra.

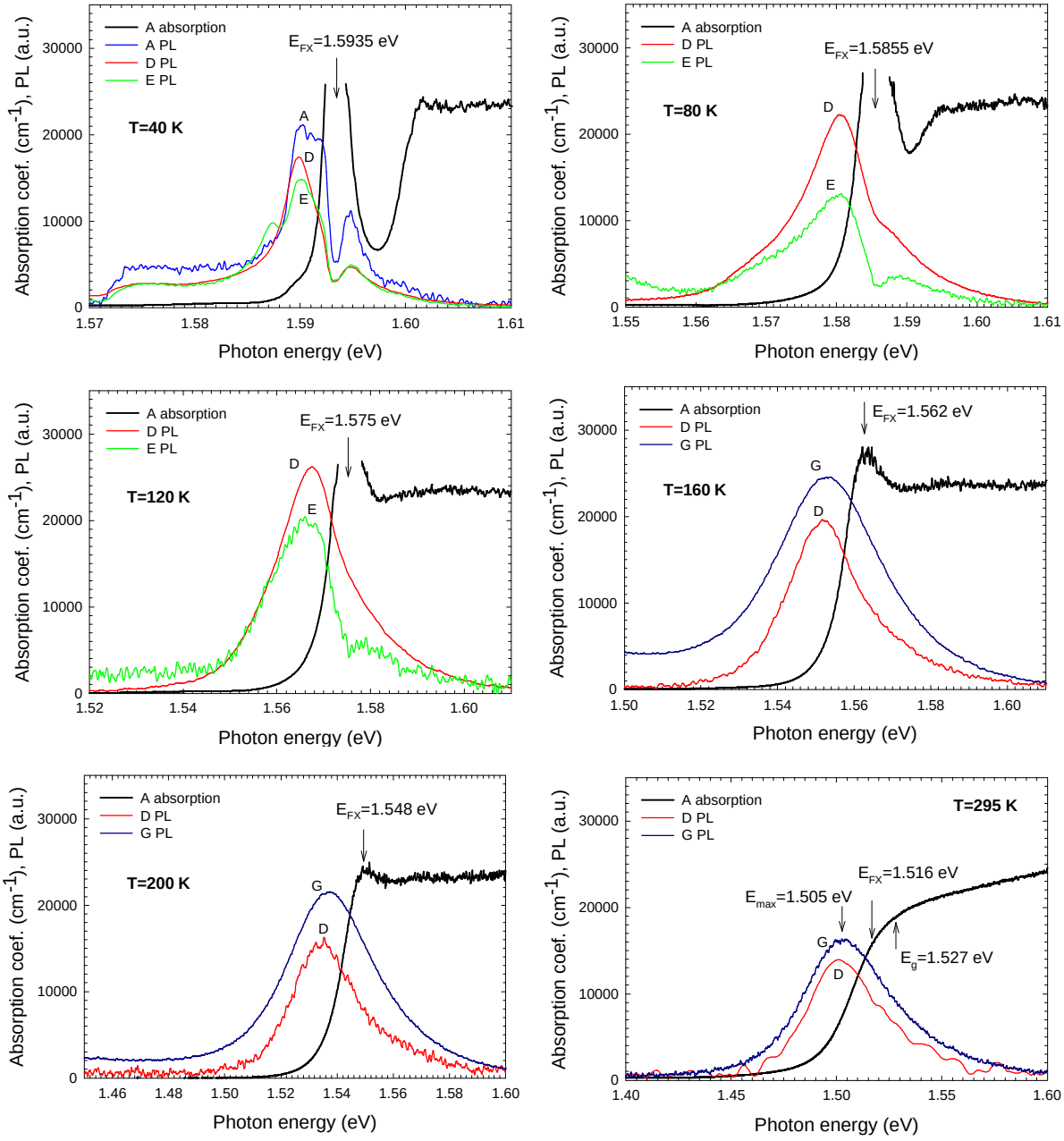

Fig. 3.22. *Near band edge photoluminescence spectra at different temperatures (in color). Absorption spectra (in black), free-exciton resonances (E_{FX}) and energy gaps (E_g) were deduced from numerical fitting of absorption spectra, see more in section 3.3.5.*

The FX resonance width depends on sample quality. For samples with a large crystal disorder, the PL spectrum does not show any dip at all. This characteristic PL dip, if present, can be used to determine the sample temperature (using a reliable temperature dependence of the E_g [Hor06a]) or the zinc content for the ternary $Cd_{1-x}Zn_xTe$ alloy [Fra00].

We will derive in this paragraph a simple theoretical model describing the photo-excited particle (electrons, holes or excitons) concentration profile near the sample surface in order to evaluate exactly the correction of the PL spectra for the variation of the absorption coefficient. We start with the simple steady form of diffusion-recombination equation for the concentration profile of photo-generated carriers $c(x)$

$$Aa_{exc}\exp(-a_{exc}x)+D\frac{d^2c(x)}{dx^2}-\frac{c(x)}{t}=\frac{dc(x)}{dt}=0, \qquad \textit{Eq. 3.15}$$

where the first term is the laser excited rate, the second term expresses concentration changes due to diffusion, and the third term describes recombination. Parameter A is proportional to the excitation intensity, a_{exc} is the absorption coefficient at the excitation energy, D is the (ambipolar) diffusion coefficient and t is the recombination lifetime. Assuming an infinite or zero surface non-radiative recombination rate, the boundary conditions are $c(x=0)=0$ in the first case and $dc/dx(x=0)=0$ in the second case. These conditions represent extreme cases, while the real experiment lies somewhere between them. Equation 3.15 is solved analytically and, for infinite surface recombination, $c(x)$ is given by:

$$c(x)=\frac{Aa}{\frac{1}{t}-Da^2}\left(\exp(-ax)-\exp\left(-\frac{x}{\sqrt{Dt}}\right)\right), \qquad \textit{Eq. 3.16}$$

whereas for zero surface recombination one obtains:

$$c(x)=\frac{Aa}{\frac{1}{t}-Da^2}\left(\exp(-ax)-a\sqrt{Dt}\,\exp\left(-\frac{x}{\sqrt{Dt}}\right)\right). \qquad \textit{Eq. 3.17}$$

Both profiles are plotted in Fig. 3.23 for chosen realistic values of parameters.

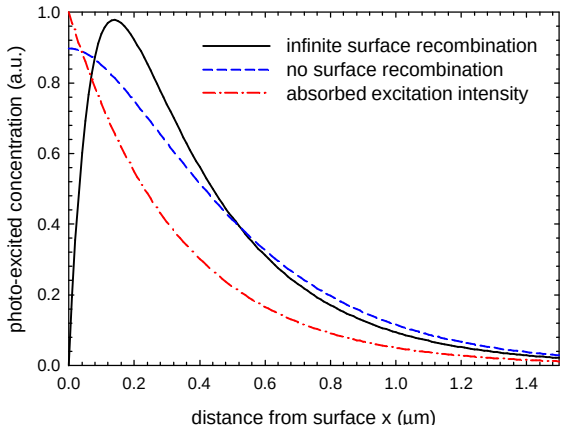

Fig. 3.23. *Calculated profiles of HeNe laser-excited carriers in CdTe with infinite surface recombination (full line), without surface recombination (blue dashed) and profile of the absorbed laser power (red dash-dotted). $D=1x10^{-5}$ m^2/s, $t=5x10^{-10}s$, $a_{exc}=3.5x10^6$ m^{-1}.*

The measured PL signal $PL_{measured}$ is a sum of contributions of PL density emitted by unit concentration of excited carriers PL_{ideal} coming from distances x (only $\exp(-ax)$ reaches the surface):

$$PL_{measured}(E)\approx PL_{ideal}(E)(1-R(E))\int_0^\infty c(x)\exp(-a(E)x)dx \qquad \textit{Eq. 3.18}$$

$$PL_{measured}(E)\approx PL_{ideal}(E)T(a(E)). \qquad \textit{Eq. 3.19}$$

The spectral modulation by the reflectivity R can be neglected in the analysis because its variation near the FX energy at high temperatures is not important (even at the lowest temperatures, the expression $1-R$ does not influence strongly the spectra (see Fig. 3.48)). The correction factor $T(a(E))$ can be calculated analytically for concentration profiles $c(x)$ given by Eqs. 3.16 and 3.17. For the case of infinite surface recombination it reads:

$$T(a) \approx \frac{a_{exc}}{1 - Dt\,a_{exc}^{\,2}} \left(\frac{1}{a_{exc} + a} - \frac{1}{a + \frac{1}{\sqrt{Dt}}} \right), \qquad \textit{Eq. 3.20}$$

and in the case of negligible surface recombination:

$$T(a) \approx \frac{a_{exc}}{1 - Dt\,a_{exc}^{\,2}} \left(\frac{1}{a_{exc} + a} - \frac{a_{exc} Dt}{1 + a\sqrt{Dt}} \right). \qquad \textit{Eq. 3.21}$$

Fig. 3.24 plots the absorption coefficient at 80 K and at RT in the vicinity of the FX resonance, the PL spectrum as measured $PL_{measured}(E)$ and the PL spectrum $PL_{ideal}(E)$ with the correction for strong reabsorption (for the case of infinite surface recombination). The result of the correction is that PL_{ideal} at 80 K is a single peak, whose intensity is slightly increased compared to $PL_{measured}$. The peak position is situated below the FX resonance. The origin of the band will be explained in the following section. At RT, the correction only slightly shifts the PL spectrum to higher energies and increases its intensity.

As the absorption coefficient at the excitation energy is several times smaller compared to the absorption coefficient at the FX resonance, the radiation at the FX energy cannot escape from the sample at a full intensity compared to photons of other energies where the absorption coefficient is low. It has to be pointed out that PL_{ideal} was obtained without any optimization of model parameters, which were deduced by PL independent methods.

The absorption dip due to the extremely high absorption coefficient at the FX energy is observed in simulated spectra using $T(a)$ function for both zero and infinite surface recombination, hence no conclusion can be drawn concerning the surface recombination kinetics. A mention should be done about the concept of the so called “dead layer”. If the infinite surface recombination is assumed (caused by electrical fields at the surface, surface defects, etc.), then, according to our model, the concentration of excited particles significantly decreases at a distance of 50-100 nm from the surface. At the same time, the PL signal comes from a region 150-200 nm deep. In such a case the model of the reabsorbing dead layer is well justified.

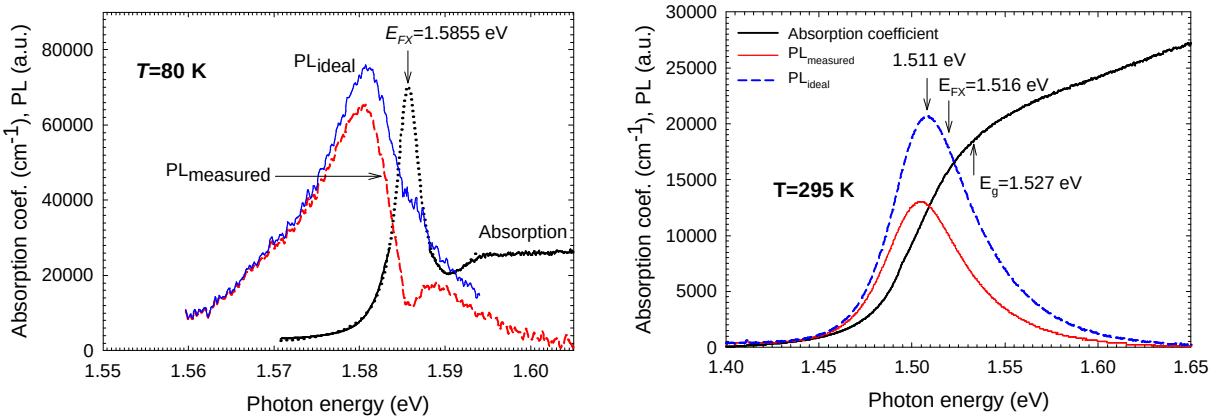

Fig. 3.24. *Correction of the PL for reabsorption at 80 K (sample E)(left) and at room temperature (sample J)(right). PL_{ideal} was obtained from Eq. 3.20. PL_{ideal} (in blue), $PL_{measured}$ (in red). The absorption spectrum (in black) consists of experimental data (thick line) and of modeled data (dotted).*

3.2.4.2 Room temperature photoluminescence

The reabsorption does not affect, however, the PL dip up to 120 K only. It also distorts the PL line-shape at higher temperatures (see Fig. 3.24 (right)). The PL maximum shifts via the

correction according to Eq. 3.20 to higher energy by several meV. In the following, this rectification of PL has been done.

The FWHM of the RT NBEL of different samples fluctuates within 43-55 meV. The NBEL maximum ranges from 1.495 to 1.505 eV. The low-energy side of the PL spectrum is described by:

$$PL(E) = c_1 \exp\left(\frac{E}{E_0}\right), \qquad \textit{Eq. 3.22}$$

whereas the high-energy wing was fitted to:

$$PL(E) = c_2 \exp\left(-\frac{E}{k_B T_{eff}}\right), \qquad \textit{Eq. 3.23}$$

where k_B is the Boltzman constant, c_1, c_2, E_0, T_{eff} are fitting parameters. The physical meaning of T_{eff} is the effective temperature of the free particles involved in the transition.

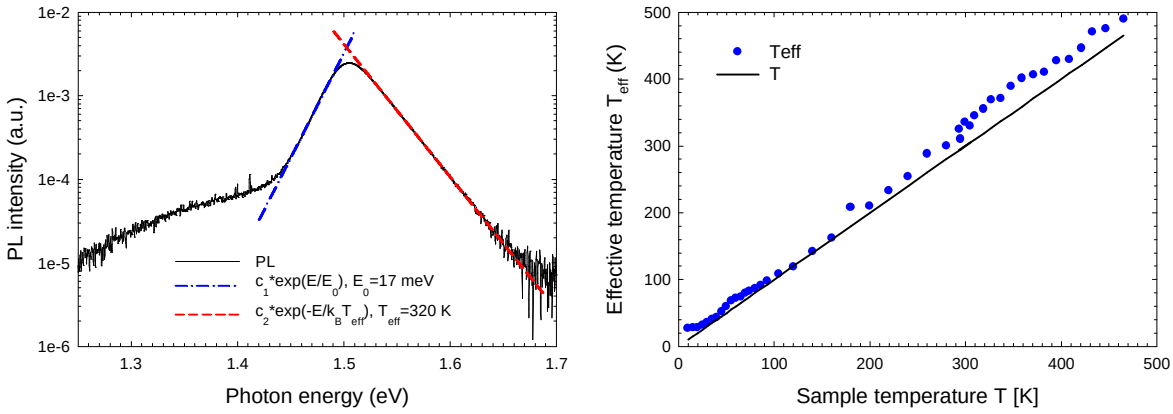

Fig. 3.25. *Left: analysis of the line-shape of the room-temperature photoluminescence spectrum, sample G. Right: correlation between the effective temperature T_{eff} from PL lineshape and the sample temperature T, sample G.*

The contiguous dependence T_{eff} vs T in Fig. 3.25 (right) proves that the NBEL band originates from processes involving at least one free particle. The maximum of NBEL lies slightly below the FX resonance, but the luminescence signal is detectable also above the band gap energy (see Fig. 3.25 (left)).

Fig. 3.26 shows the temperature evolution of the $E_g(T)$ dependence and evolution of dips and maxima of the edge PL for several samples, and also together data from [Gil85]. Based on the detailed analysis of the absorption coefficient of thin samples, we demonstrate that the maximum of the RT NBEL is below both the energy gap and the FX resonance (also see Fig. 3.24 right).

The question remains why the NBEL PL is not detected in high-quality samples, where, in principle, the band-to-band transitions should be more probable. Moreover, the maximum of the band-to-band luminescence would be expected approximately k_BT above the band gap energy.

We suggest the following interpretation of this effect: in crystals of lower quality, important fluctuations of the band extremes exist in the real space causing the capture of the photo-generated free particles, mainly the holes due to their larger effective mass. In the next step, free electrons are attracted by the localized hole and then they recombine radiatively. The localization hole energy corresponds to the NBEL maximum found below the fundamental

energy gap. In the high-quality samples the potential fluctuations are weak and the localization of free carriers does not take place. Free carriers can diffuse to a longer distance through the crystal and they are much more effectively captured by non-radiative recombination centers (deep defect, dislocation, surface) than in low-quality samples. Consequently, in high-quality crystals the PL radiation at room temperature is damped.

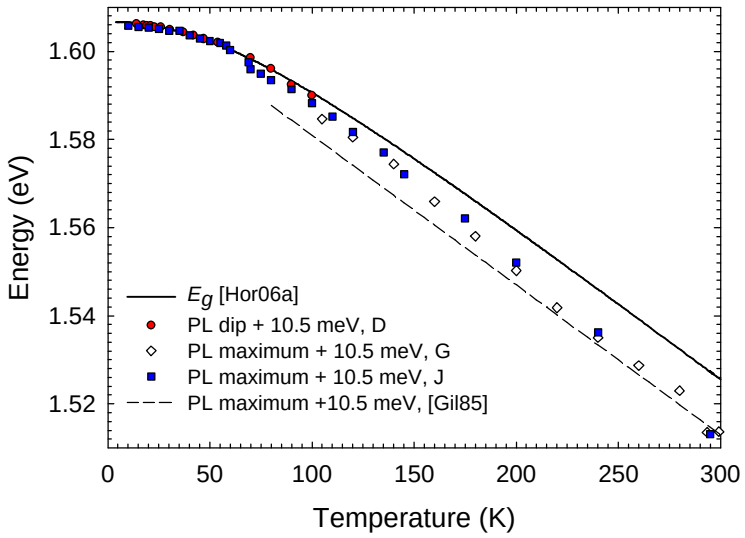

Fig. 3.26 *Temperature dependence of the dip and maximum positions of the NBEL luminescence (symbols). 10.5 meV is the FX binding energy. Comparison with literature (dashed). Temperature dependence of E_g from FX absorption measurements (thick line).*

3.2.5 Photoluminescence of CdZnTe

ZnTe has very similar defect structure to CdTe. The alloy CdZnTe with low zinc concentration (4-10%) has nearly the same properties as CdTe. E.g. the binding energies of defects are not much too different from CdTe. In practical use, sometimes, CdTe and CdZnTe are even mistaken. However, from the point of view of optical and especially photoluminescence properties very important differences are observed. First, high-resolution optical spectra let us to determine very precisely the band gap energy which next is used to calculate the zinc concentration. This will be described in more detail in chapter devoted to optical mapping. Second point is that the random or rather non-periodic distribution of zinc and cadmium atoms in the metal sublattice broadens sharp bound excitonic transitions typically by 1 to 2 meV. The composition influence on broadening was studied for example by [Ole85] or [Oet92]. The broadening causes that individual chemical defects can no longer be distinguished. Usually, in the excitonic part of photoluminescence spectra, three dominant bands are observed: free-exciton LO replica, acceptor and donor bound excitons. This is illustrated by Fig. 3.27.

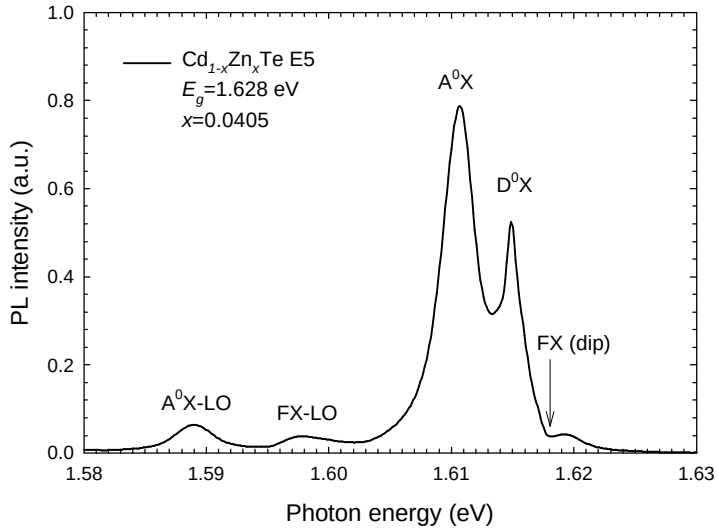

Fig. 3.27. *Typical photoluminescence spectrum of CdZnTe at 4 K.*

3.3 Absorption spectroscopy

At the beginning of this chapter, fundamental relations for experimental determination of absorption coefficient are described. In the next sections, different absorption contributions are exposed, spectrally ranging from free-carrier absorption in MIR to excitonic and band-to-band absorption in the NIR. Special attention is focused to the fundamental edge absorption, which was used for deriving a new temperature dependence of the fundamental energy gap.

3.3.1 Comments on absorption spectroscopy

Reflected and transmitted light ratio on a homogeneous, planparallel sample of a thickness d in normal incidence R_{tot} and T_{tot} are given by the well-known expressions:

$$R_{tot} = R + \frac{(1-R)^2}{1-R^2\exp(-2ad)} \qquad \textit{Eq. 3.24}$$

and

$$T_{tot} = \frac{(1-R)^2\exp(-ad)}{1-R^2\exp(-2ad)}. \qquad \textit{Eq. 3.25}$$

Solving the latter quadratic equation for $\exp(-ad)$, the absorption coefficient is calculated from:

$$a = \frac{1}{d}\ln\frac{(1-R)^2 + \sqrt{(1-R)^4 + 4T_{tot}^2R^2}}{2T}, \text{ where} \qquad \textit{Eq. 3.26}$$

$$R = \frac{(n-1)^2 + k^2}{(n+1)^2 + k^2}. \qquad \textit{Eq. 3.27}$$

The index of extinction k in the expression for R can be neglected for photon energies even in the proximity of the band gap, since the imaginary part of the complex index of refraction is small compared to the real part (except the FX resonance at low temperatures-see Fig. 3.50, Fig. 3.52 and Fig. 3.53). The energy dependence of the index of refraction n is described in section 3.4.2.

3.3.2 Absorption due to free holes

In this section we will describe mechanisms of absorption and light scattering in the MIR part of the spectra. Most of absorption processes are connected to free holes. However, sometimes, absorption by tellurium precipitates and its absorption superpose in this spectral range.

Of course, works on absorption coefficients at low energies in CdTe are classical. The most interesting ones are [Cap73], [Bec90] and [Sen01]. In the case of zero absorption, near the wavelength of 10 μm n is approximately 2.65, which gives R=0.204. Hence, the transmitted light through an ideal sample T_{tot} reaches 0.66. (The 10 μm wavelength is of great interest e.g. for infrared detector substrate applications because many detectors are illuminated through the substrate.)

Since all our investigated samples were p-type in this spectral range, we can limit ourselves to absorption processes connected to free holes. [Bec90] decomposes infrared absorption spectra of p-type material into 3 contributions: 1) intra-valence-band absorption, 2) valence band to acceptor absorption and 3) scattering by tellurium precipitates and inclusions. The measured absorption coefficient a is then sum of corresponding processes:

$$a = a_{ivb} + a_{imp} + a_{scat}. \qquad \textit{Eq. 3.28}$$

The line-shape of the intra-valence-band absorption a_{ivb} is given by [Bec90]:

$$a_{ivb}(E) = q_{ivb}(E)p\,, \qquad \textit{Eq. 3.29}$$

where p is hole concentration, E is the photon energy and q_{ivb} is absorption cross section, which is given by

$$q_{ivb}(E) \approx \sqrt{E}\,\exp\left(-\frac{m_2}{m_1 - m_2}\frac{E}{kT}\right)\left[1-\exp\left(-\frac{E}{kT}\right)\right]. \qquad \textit{Eq. 3.30}$$

[Bec90] gives q_{ivb}(0.124 eV)=2.9x10^{-16} cm^2 (at room temperature). It means that only highly doped p-type samples can show measurable absorption at the low energy part of the spectrum.

Extinction of the transmitted light by scattering is causing the decrease of transparency at higher energies. According to [Bec90], this contribution can be written as:

$$a_{scat}(E) = a_0 E^m\,, \qquad \textit{Eq. 3.31}$$

a_0 and m are fitting parameters.

Absorption spectra in Fig. 3.29 show contributions of these different mechanisms. Sample NUK 45 presents the strongest absorption from heavy to light-hole bands; sample 2003 has negligible absorption (absorption coefficients below 1 cm^{-1} are measured with difficulties). Sample AF13 has great losses by scattered light and also several distinct acceptor to valence band transitions are observed.

MIR and FIR absorption lines of shallow effective mass acceptors were studied in the 70's, but the transition energies are out of our spectral range; that is why we will not cite these works. [Mol82b] observed manifestation of excited states of Cu and Ag acceptors in PL using resonantly excited PL and as absorption lines in MIR. The absorption spectra show strong LO phonon replica. Major absorption lines were identified as 131 meV ($1S_{3/2}$-$2P_{5/2}$ (Γ_8^-) transition) and 134 meV ($1S_{3/2}$-$2P_{5/2}$ (Γ_7^-) transition) for copper and 92 meV ($1S_{3/2}$-$2P_{5/2}$ (Γ_8^-) transition) and 96 meV ($1S_{3/2}$-$2P_{5/2}$ (Γ_7^-) transition) for silver acceptor. (The ionization energy of Ag and Cu acceptors are respectively 108 and 146 meV.). The absorption lines near 0.283 eV are due to Fe^{2+} ions [Mua01]. Strong pollution by Fe is then detected in e.g. CdTe F2504 (see Fig. 3.28).

Fig. 3.28 depicts transmittance spectra, whereas Fig. 3.29 shows absorption coefficient of chosen samples. The pictures are plotted to illustrate different absorption mechanisms. A high-resistivity semiconductor shows a flat and high transmittance (sample 2003). The high absorption at low energies is due to acceptor and free-carrier absorptions (sample NUK45). High concentration of precipitates increases absorption at higher energies (sample AF13).

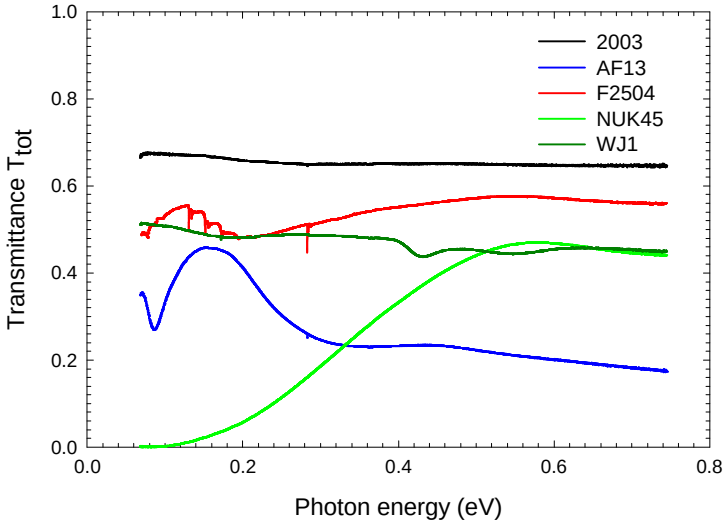

Fig. 3.28. *Representative transmittance spectra of different CdTe samples at 4 K. Sample 2003 has the highest resistivity, whereas sample NUK45 is p-type p>10^{16} cm^{-3}.*

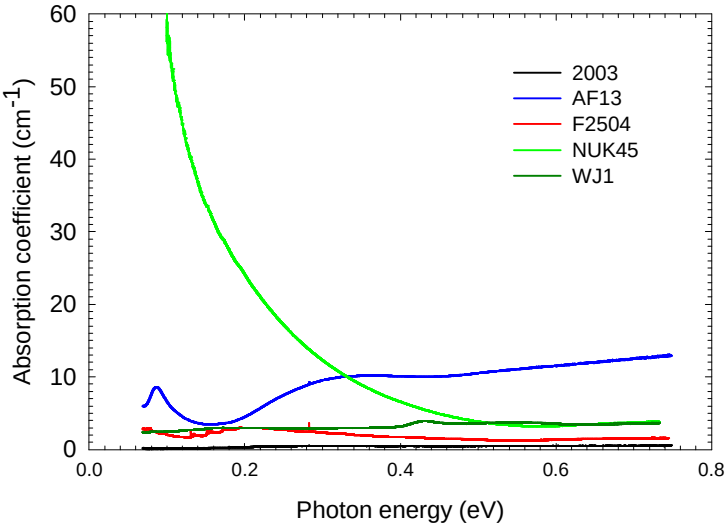

Fig. 3.29. *Absorption spectra for the same samples as in Fig. 3.28, showing different kinds of absorption mechanisms. E.g. acceptor to band transition near 90 meV in AF13, probably intra-valence band transitions for sample NUK45 and light scattering by inclusions for AF13.*

The free carrier transitions may manifest not only at low energies in MIR, but also in NIR as transitions from the spin-split band (SO). This transition is probably observed near 0.9 eV as small dip for transmittance spectra depicted in Fig. 3.30 [Cap73]. Because the transition is not found at the same energy for different samples, the transition from the SO band to acceptor impurities can also be considered.

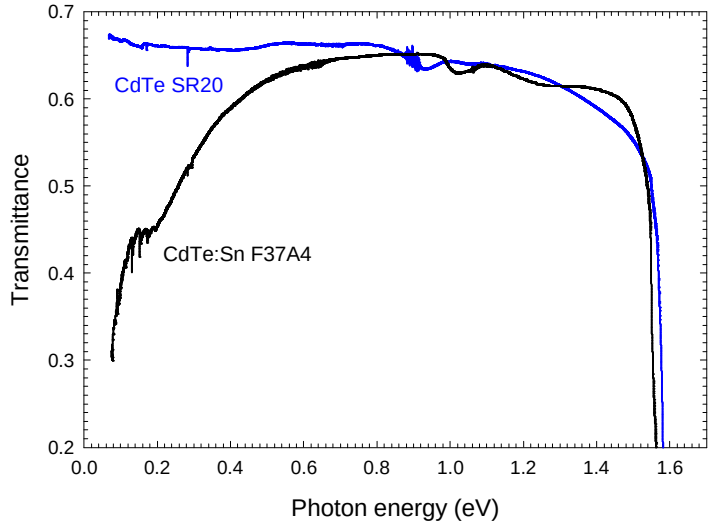

Fig. 3.30. *Transmittance spectra (at 4 K) of two representative samples (full-range of the spectrometer, combination of KBr and quartz beamsplitters and DTGS, GeD and SiD detectors).*

Surprisingly, the temperature evolution of the MIR absorption spectra is not strong (see Fig. 3.31 and Fig. 3.32). Fig. 3.31 shows, how probably the shift up and down of the Fermi energy level changes the free-carrier absorption.

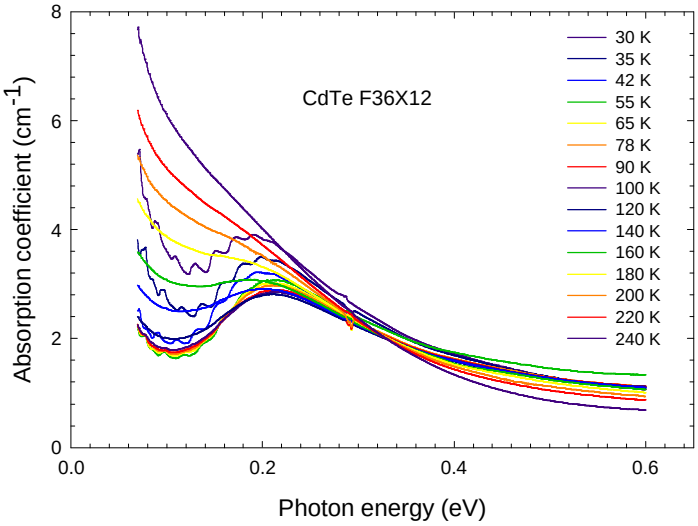

Fig. 3.31. *Temperature evolution of absorption coefficient. Low energy side of spectra is dominated by intraband transitions, while acceptor to band transitions with zero phonon line near 140 meV is also observed. Non-monotonous change of intra-band transitions corresponds to the temperature changes of the Fermi level. The wavy absorption (LO phonons replicas towards higher energies) corresponds to lowest temperatures.*

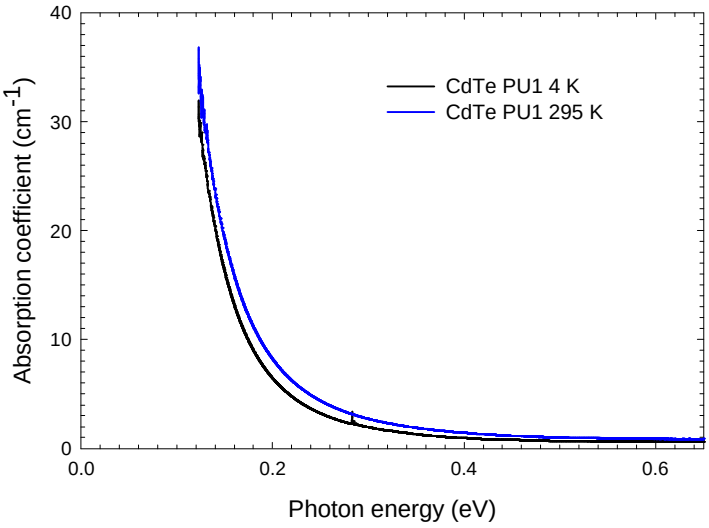

Fig. 3.32. *Absorption coefficient of intra-band transitions in PU1. Temperature dependence of most samples is unimportant.*

Fig. 3.33 depicts spectra of a CdTe sample before and after Cd annealing (500 °C, 10 h) which usually substantially reduces hole concentration by kicking out the substitutional acceptors (often Ag, Cu). The absorption lines of these acceptors disappear after annealing. The absorption near 0.283 eV is due to Fe^{2+} ions (see above).

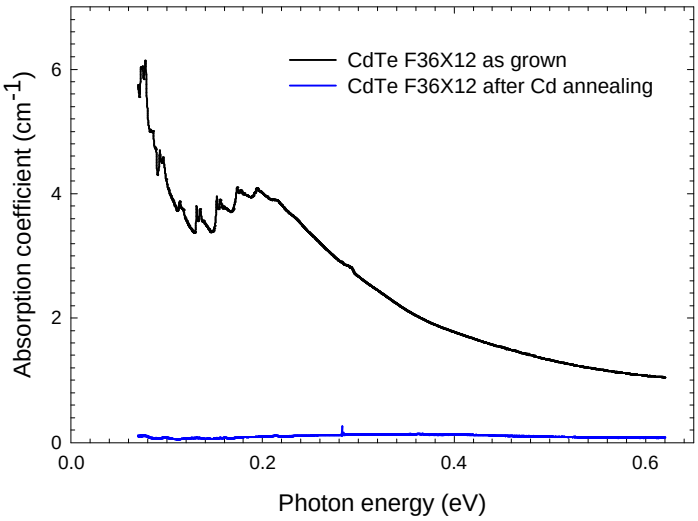

Fig. 3.33. *Effect of Cd annealing on infrared absorption (4 K). Cd annealing annihilates cadmium-substitutional acceptors, which simultaneously removes intra-band absorption.*

The effect of Te annealing is shown on three high-quality, commercial, originally identical samples 1072, 1076 and 1077 (see Fig. 3.34). The sample 1072 was subject of annealing in Te atmosphere at 500 °C for several hours. Its conductivity has risen about 20 times. Question is if the new acceptors were created by in-diffusion of impurities from the ampoule, formation of A-center complexes with residual donors or formation of other intrinsic (V_{Cd}) acceptors. Fig. 3.34 also shows, that for hole concentration $<10^{15}$ cm^{-3} the free-carrier absorption is hardly measurable.

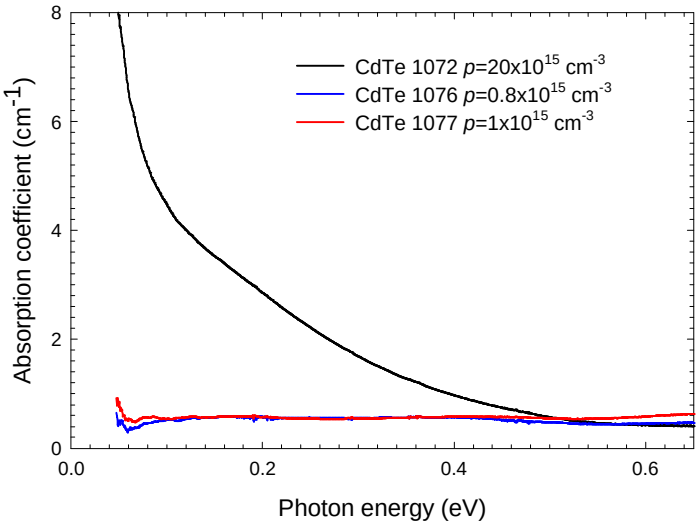

Fig. 3.34. *Dependence of absorption coefficient on p-doping (295 K).*

Both crystals AF13 and AF15 (CdTe doped by Sn) show strong scattering by precipitates or inclusions. Those microdefects can be tellurium microcrystals, but its origin could be in principle as well tin. The creation of precipitates is probable for dopants of low solubility.

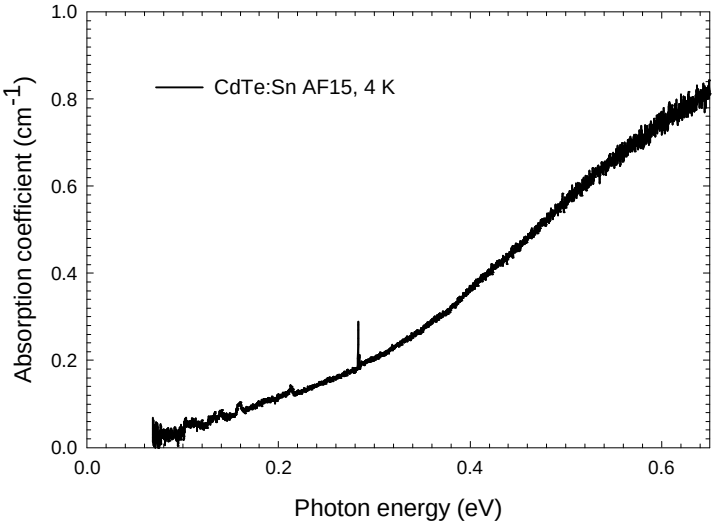

Fig. 3.35. *Increase of absorption with photon energy is due to light scattering. CdTe AF15 shows high concentration of probably tellurium precipitates in infrared microscopy.*

3.3.3 Absorption edge

By absorption edge commonly is understood the fast increase of absorption coefficient to values of about 50-100 cm^{-1} (range in which common thick samples transmit light) near the fundamental gap energy. To study effects at higher absorption values, thinner sample are needed, but very few works deal with them [Mar66], [Zim90]. Absorption edge energy is usually defined as energy corresponding to a given absorption level, for example to 20 cm^{-1}. However, the distance between the band gap energy and the absorption edge energy fluctuates a lot since this spectral region is very sensitive to defect-induced absorption.

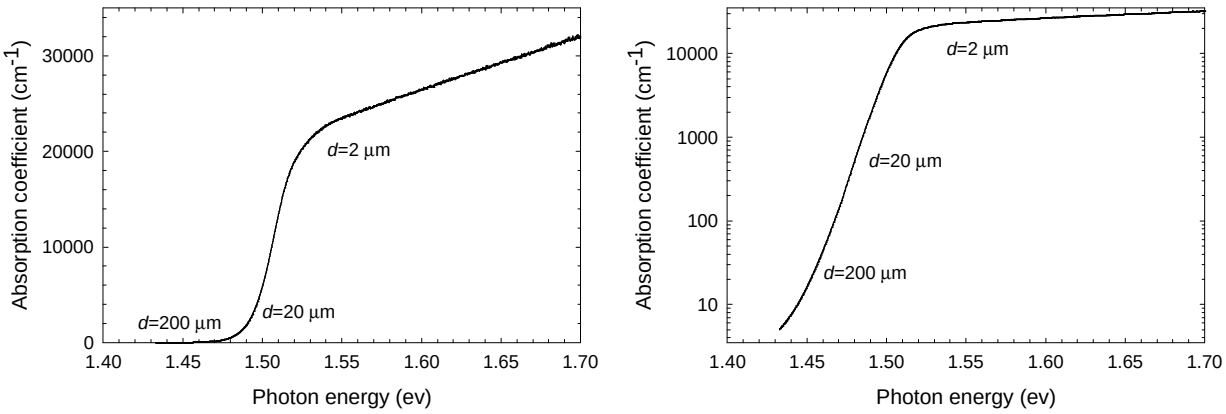

Fig. 3.36. *Absorption edge at 295 K for high quality CdTe (linear and logarithmic scale for comparison). Absorption coefficient below 100 cm^{-1} is influenced by defects, whereas higher values can be regarded as intrinsic (broadening by phonons).*

Fig. 3.36 shows measurement of absorption of high quality CdTe of different thickness at room temperature. The low values of absorption are influenced by defect absorption processes, which dominate the usually defined absorption edge. Values of more than 100 cm^{-1} represent the intrinsic absorption. The absorption edge in the large scale of values is of interest for example for modeling of carrier generation near the surface in the photoconductance technique.

The absorption edge at high temperature of a high quality sample is dominated by phonon broadening of the FX transition. At low temperatures, the low absorption tail posses interesting features. Very few samples of 1-2 mm thickness transmit light above the bound exciton region.

During our investigation this was case only of CdTe SU910, 1076 and CdZnTe 19572 (they are all commercial samples). Transmittance of five 1 mm thick CdTe samples with the closest position of absorption edge to E_g is depicted in Fig. 3.37.

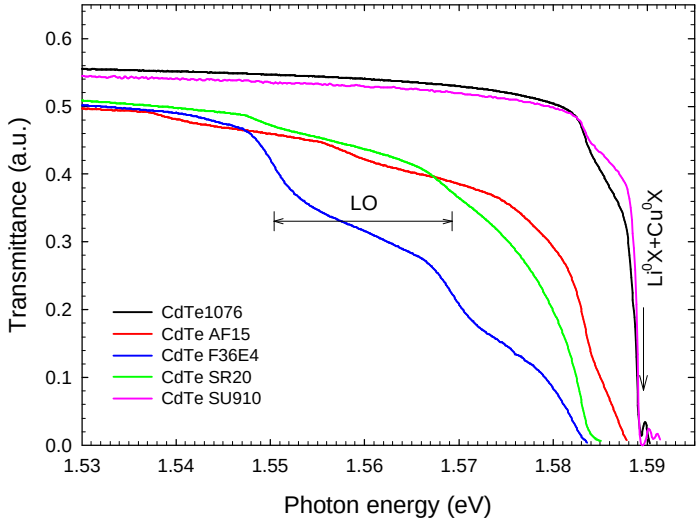

Fig. 3.37. *Absorption edge of high-quality CdTe samples (4 K). In the best case, the transmittance is limited by the bound exciton absorption.*

[Gri02] interpreted the spectra and published calculation of acceptor concentration as well as concentration of charged donors from the wavy shape of the absorption coefficient. We will follow this work to interpret the transmittance spectra. The absorption connected to band to defect transition is given by [Gri02]:

$$a(E) = \frac{16e^2P^2g}{3ce_0n\eta^2w}\left(\frac{\eta^2}{2m_ea_B^2}\right)^{5/2}\frac{\sqrt{E-E_g+E_A}}{\left(\frac{\eta^2}{2m_ea_B^2}+E-E_g+E_A\right)^4}. \qquad \textbf{Eq. 3.32}$$

P is the momentum matrix element, n is index of refraction, g is the acceptor degeneracy factor. The energy $h^2/2m_ea_b^2$ is approximately 0.3 eV for the effective-mass shallow acceptor [Gri02]. Then the absorption line-shape is basically a square root (the denominator is nearly constant). Waves at higher energies are mostly LO phonon replicas of the zero-phonon line.

To calculate the line-shape of acceptor absorption, first, the background absorption must be subtracted. This is a very difficult task. The background can be approximated roughly by an exponential function, but, depending on the crystal quality, the shape can be differing a lot. The comparison of model and experimental free-to-bound absorption transitions is plotted in ***Fig. 3.38***. The experimental structure is far from being as sharp as the model. Approximate acceptor ionization energies are then 68 meV for AF15, 58 meV for F36E4 and SR20 and 24 meV for 1076. The latter transition is deeper than an effective mass donor and simultaneously shallower compared to the effective mass acceptor. The energy of 24 meV, to our knowledge, has not been ascribed to any specific defect up to now. However, the ionization energies for others can be easily attributed to phosphorus (E_A=68 meV) and lithium or sodium (E_A=58 meV), see Tab. 2.3.

Absolute concentrations of the involved shallow acceptors can be computed from Eq. 3.32. For CdTe AF15 p=1.5 10^{14} cm^{-3}, for SR20 p=3.5 10^{14} cm^{-3} and for F36E4 p=1.3 10^{15} cm^{-3}.

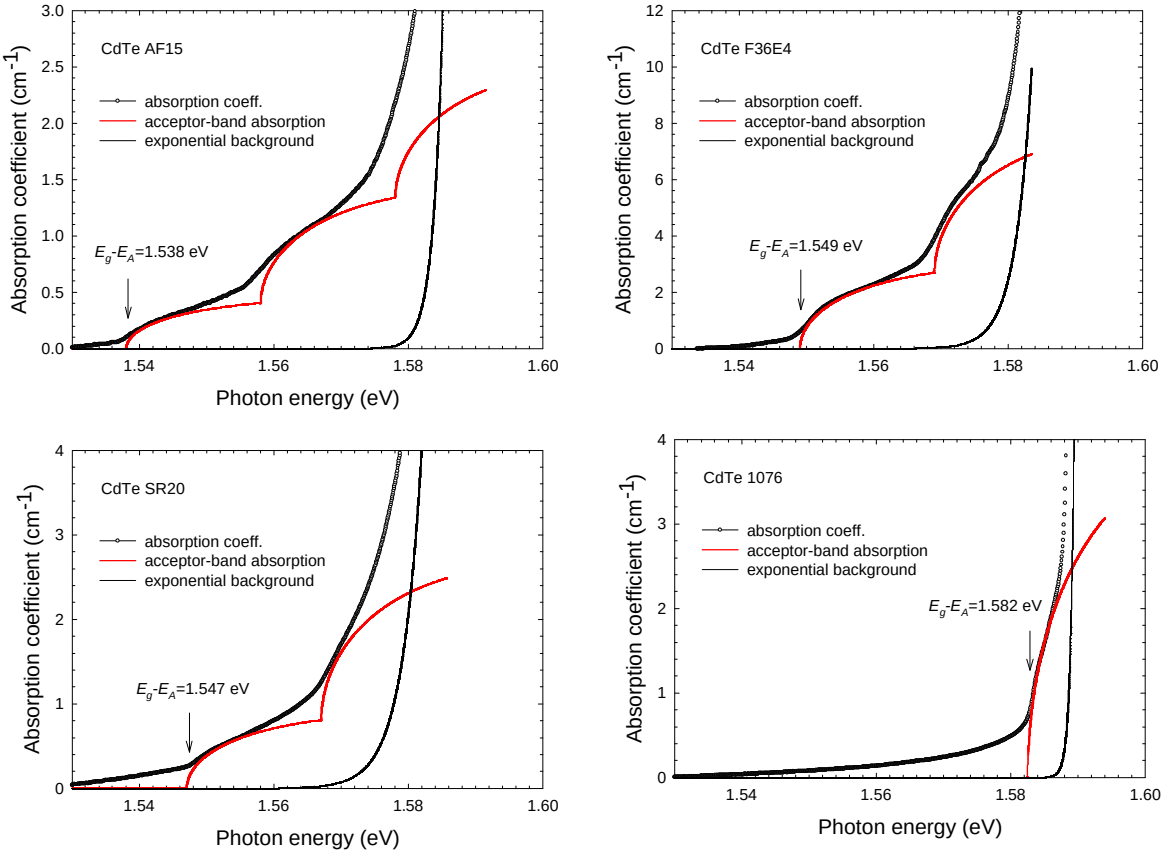

Fig. 3.38. *Absorption spectra of acceptor-band transitions.*

There is an interesting question, whether the A^0e transition is manifested in both PL and absorption spectra. In Fig. 3.39, these spectra are plotted for CdTe F26E4 and 1076. For F26E4, in the vicinity of 1.549 eV (absorption energy threshold), several emissions are superposed. The sharp peak originates from 2LO replica of A^0X. At lower energy, A^0D^0 transition can be seen; the high-energy side of the band at 1.549 eV is the A^0e transition. Then the interpretation of absorption seems correct. Unfortunately, for sample 1076, no intense emission is observed at 1.582 eV. A very little curvature at this energy could be interpreted as corresponding PL of the free-to-bound transition, but it is rather surprising, that for this particular defect the absorption technique is more sensitive than the PL one.

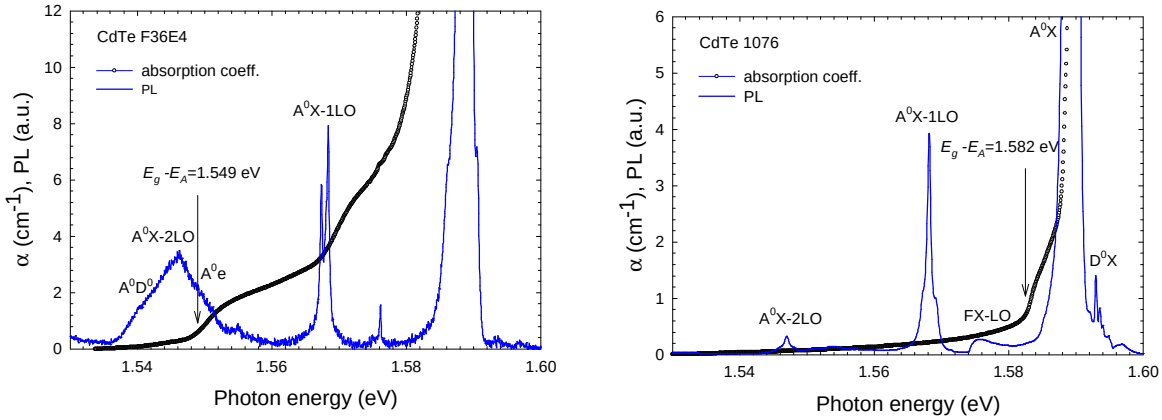

Fig. 3.39. *Comparison of absorption and photoluminescence spectra. For F36E4, the acceptor transition is visible in both spectra. For sample 1076, the PL signal from corresponding defect-band transition is not really strong or visible.*

3.3.4 Absorption by bound exciton states

Absorption by bound exciton states would be a precise method of determination of defect concentrations in relatively high-quality samples. The disadvantage is the need of very thin samples, especially for samples of a medium quality. Due to these obstacles, we could measure the absorption of shallow acceptor and donor BX only for several samples of undoped CdTe.

[Zim90] measured absorption of bound excitons on much thicker samples (200-300 μm), compared to our experiments (2-6 μm). This was possible due to better quality of samples and maybe due to use of more appropriate experimental setup for absorption spectroscopy for high absorption values (no use of FT spectrometer). Maximal integrated absorption of copper and silver bound excitons in [Zim90] was 0.1 eVcm^{-1} (compare with Tab. 3.7).

Absorption and PL spectra of our thin samples are plotted in Fig. 3.40 and Fig. 3.41. Transmittance of other samples showing also BX absorption lines is in Fig. 3.37. The BX absorption without the edge tail background is plotted in Fig. 3.42 and Fig. 3.43. Fig. 3.43 depicts absorption spectra of two exceptional samples (commercial ones) that transmitted light up to D^0X transitions without any need to be thinned down. The background absorption was fitted by expression *const*+exp((*E*/*E*$_0$)^*m*) with *m*≅1.9 and subtracted. Lorentzian line-shape fits successfully all BX peaks. Peak energies and integrated absorption values are given in Tab. 3.7.

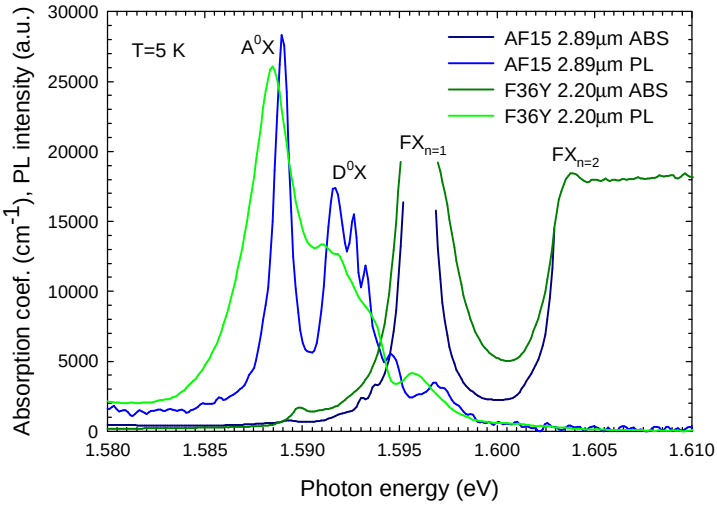

Fig. 3.40. *Photoluminescence and absorption spectra of thin self-standing samples*

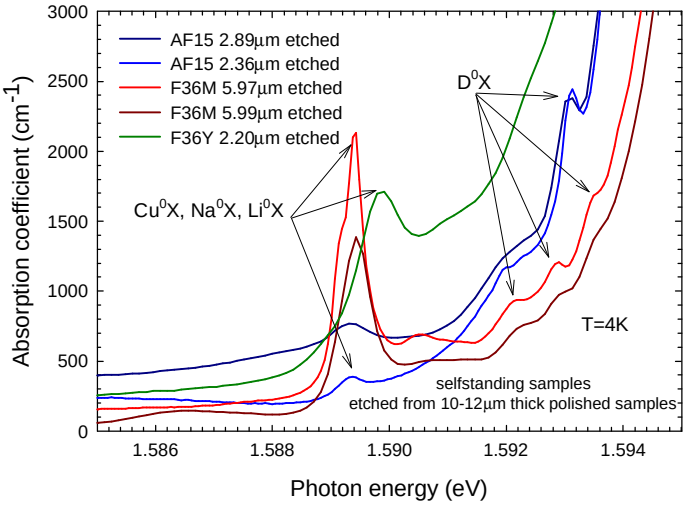

Fig. 3.41. *Free-excitonic absorption edge with superposed absorption of bound excitons.*

	1.5880 eV	1.5892 eV	1.5893 eV	1.5905 eV	1.5920 eV	1.5930 eV	1.5936 eV
AF15	0.2	-	0.4	-	0.3	0.3	0.25
F36Y	-	0.15	1.0	0.7	0.3	0.1	0.05
1076	-	-	0.015	0.02	no data	no data	no data
SU910	-	-	0.035	0.008	no data	no data	no data

Tab. 3.7*. Integrated absorption intensities for different bound excitons (in $cm^{-1}eV$).*

Fig. 3.42 (in blue) shows the PL spectra and its decomposition into single peaks for CdTe:Sn AF15. The PL and absorption spectra are quite similar. The intensity changes in individual peaks of bound excitons can be attributed to different occupation of states due to thermal distribution and to reabsorption effects by fundamental edge.

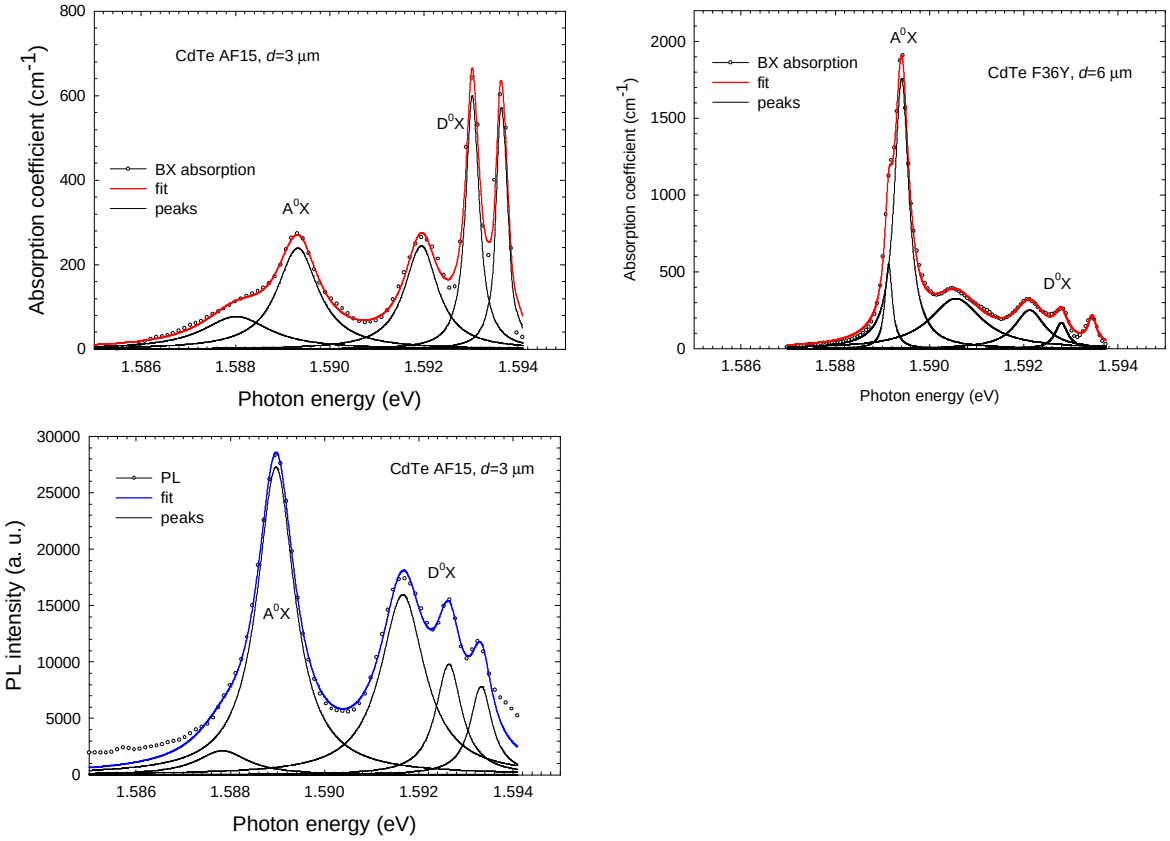

Fig. 3.42. *Absorption by bound excitonic states (red) and their photoluminescence (blue) in medium purity CdTe. Both absorption and PL lines are modeled by Lorentzian curves.*

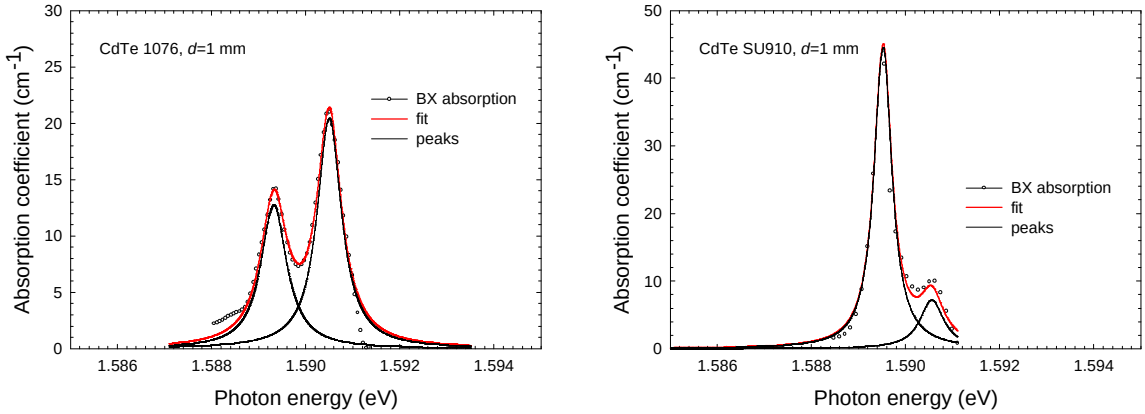

Fig. 3.43. *Absorption by bound excitonic states in high purity CdTe. Absorption spectra are from measurement on thick samples–above 1.591 eV the samples did not transmit anymore.*

3.3.5 Free exciton absorption and its temperature evolution

Absorption spectra of CdTe extending above the FX line are very sparse. Some measurements were published by [Mar66] and [Ali94]. [Mar66], measured absorption coefficient up to 1000 cm^{-1}, but could not track the temperature evolution of the FX absorption. [Ali94] shows temperature dependence of the FX peak up to 200 K, but the dependence is strangely deviated from other works. Also the spectrum (hand-drawn) at 2 K is strange because of relatively very small absorption of discrete exciton versus the continuum. [Lau90] measured transmittance of thin CdTe and CdHgTe samples (prepared by liquid phase epitaxy) but did not plot explicitly any absorption spectra of CdTe in his work.

This section is based on [Hor06a], where more details can be found. The main obstacle while wanting to perform measurements of free-exciton absorption is the small thickness of samples. As the absorption coefficient at the band gap energy is greater than 20 000 cm^{-1}, the transmittance through a 2 μm thick sample is about 1%. Preparation of such thin samples is not easy mainly because the material is very fragile. Freestanding samples as thin as 2 μm were prepared by etching from 12-15 μm thin polished slices. Even thinner samples were prepared by gluing samples on glass or sapphire substrates and polishing and etching. However, due to different thermal expansions coefficients, effects of strain like free-exciton line splitting were observed. For details, see [Nah06]. As this work is focused primary on crystal characterization, the strained samples will not be treated here at all.

Large scattering of the fundamental energy gap (E_g) values at high temperatures motivated our investigation of thin self-standing samples. E.g. at room temperature, values of E_g in literature are found to oscillate from 1.49 to 1.53 eV.

The absorption in the vicinity of the fundamental energy gap in a direct band gap semiconductor is well described by the Elliott theory [Pey93], [Ell57], which includes electron-electron interactions. A single electron theory predicting the well-known square root band-to-band absorption cannot be used in any case. The Elliott formula reads:

$$a(E)=\frac{e^2 w|d_{cv}|^2}{nce_0}\left(\frac{2m_r}{\eta^2}\right)^2\left[R_X\sum_{n=1}^{\infty}\frac{4p}{n^3}d\left(E-E_g+\frac{R_X}{n^2}\right)+q\left(E-E_g\right)\frac{pe^Z}{\sinh Z}\right], \qquad \textbf{Eq. 3.33}$$

where Z is defined as:

$$Z=p\sqrt{R_X/(E-E_g)}\,. \qquad \textbf{Eq. 3.34}$$

n is the index of refraction, the reduced mass is defined as $1/m_r=1/m_h+1/m_e$. d_{cv} is the matrix element, R_X is the exciton binding energy and q is the step function.

Fig. 3.44 demonstrates the relevance of use of the Elliott formula. Convolution was used to broaden the delta functions of discrete exciton absorption lines and the infinitely sharp increase of continuum excitonic absorption at the energy E_g. However, several deviations are observed in the experimental spectrum. First, it seems that different excitonic lines broaden differently. The broadening is stronger for excited exciton levels. Also the continuum absorption shows much important broadening than the convolution procedure produces. The surplus absorption near 1.616 eV is explained as LO phonon assisted free-exciton transition [Dil68].

The problem how to correctly include the disorder and temperature broadening into the Elliott formula is complex. For further analysis of temperature evolution of absorption spectra we have chosen another approach. The absorption is dominated by the ground state free-excitonic transition, which is superposed on background absorption constituted by the tail of the continuum transitions. Hence, we have fitted the absorption spectra in the below energy gap region to a Lorentzian or Gaussian peak and an exponential function, respectively corresponding to the discrete free-exciton and tail of interband transitions. Spectra and the fits are depicted in Fig. 3.45. Fitting parameters for the free-exciton peak are plotted in Fig. 3.46. The integrated free-

exciton absorption, which is yielded approximately constant from the fit, shows good physical meaning of the fitting procedure at high temperatures. Also the free-excitonic FWHM is consistent with temperature broadening that is due mainly to LO phonons [One93]:

$$FWHM = \Gamma_0 + \frac{\Gamma_1}{\exp\left(\frac{\Theta_D}{T}\right) - 1}, \qquad \textit{Eq. 3.35}$$

where the parameter Q_D is close to the Debye temperature and G_0 and G_1 are fitting parameters. The fit yields Q_D=180 K. This value corresponds to energy of 15 meV, which is close to the well known LO phonon energy in CdTe of 21 meV. In fact, the parameter Q_D describes rather the mean phonon energy, which is 16 meV. Then the agreement is excellent. Phonons are the main responsible mechanism as well for broadening, as well for temperature shift of the fundamental energy gap (see further).

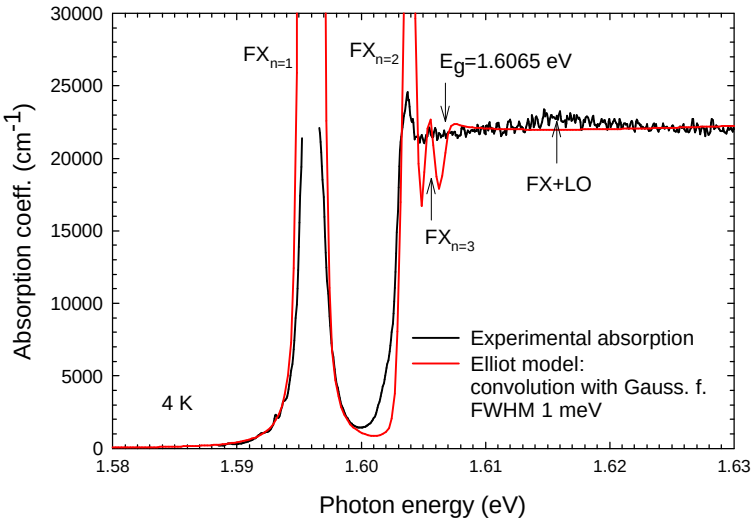

Fig. 3.44. *Excitonic effects near the fundamental absorption edge in CdTe. Elliott model convoluted with Gaussian broadening function (red) and experimental absorption for 2.3 mm thin CdTe sample AF15 (black). Absorption above 20 000 cm^{-1} can be slightly distorted; however agreement between the theory and the experiment is relatively good.*

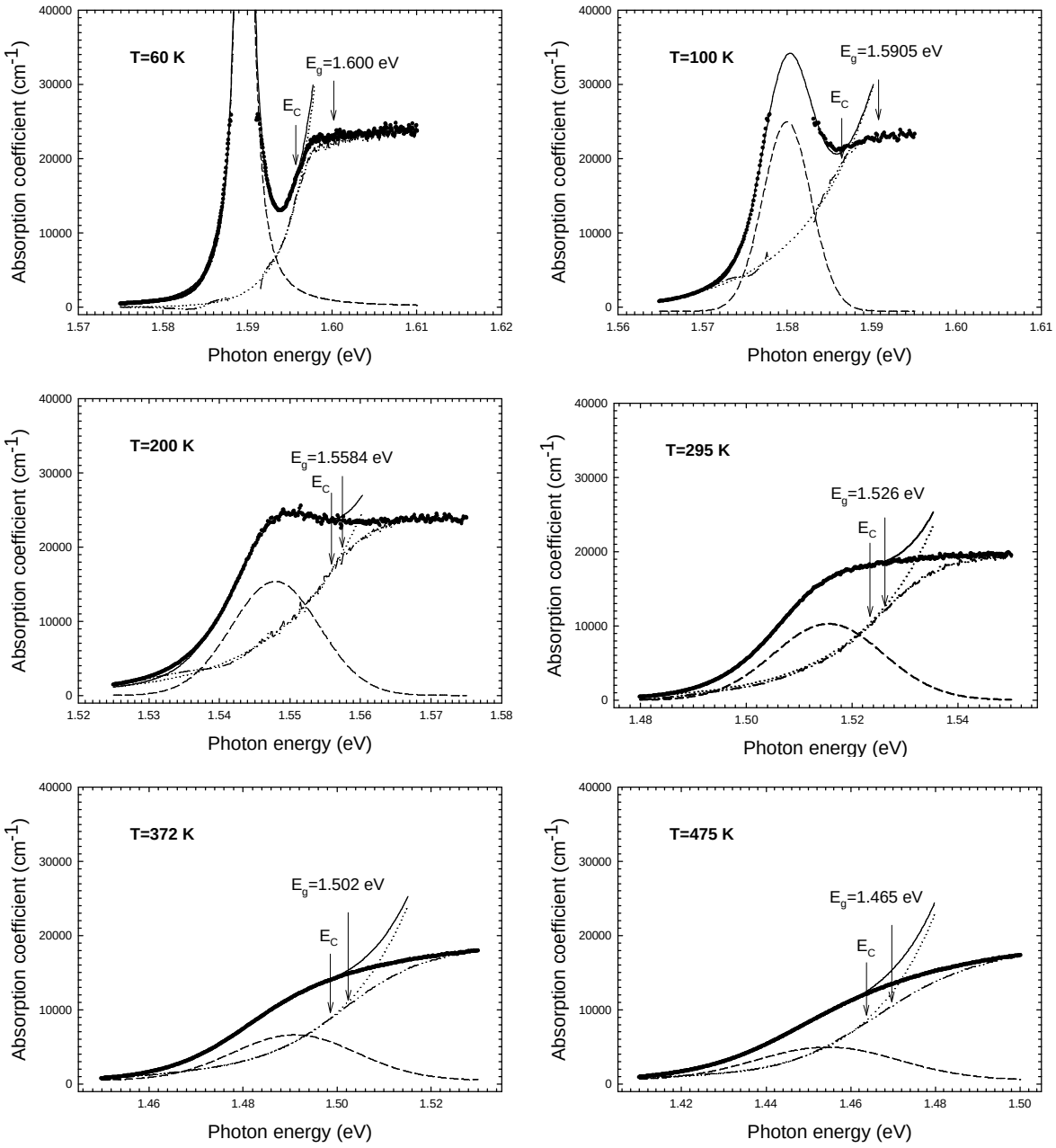

Fig. 3.45. *Temperature evolution of absorption spectra in the vicinity of the fundamental energy gap in Cdte (thick line). The absorption edge is decomposed into free-exciton absorption (dashed line) and exponential background function (dotted line). The sum (thin line) of these two contributions is fitted to the experimental absorption with upper energy limit E_C. Above the E_C energy, the fit has no physical meaning.*

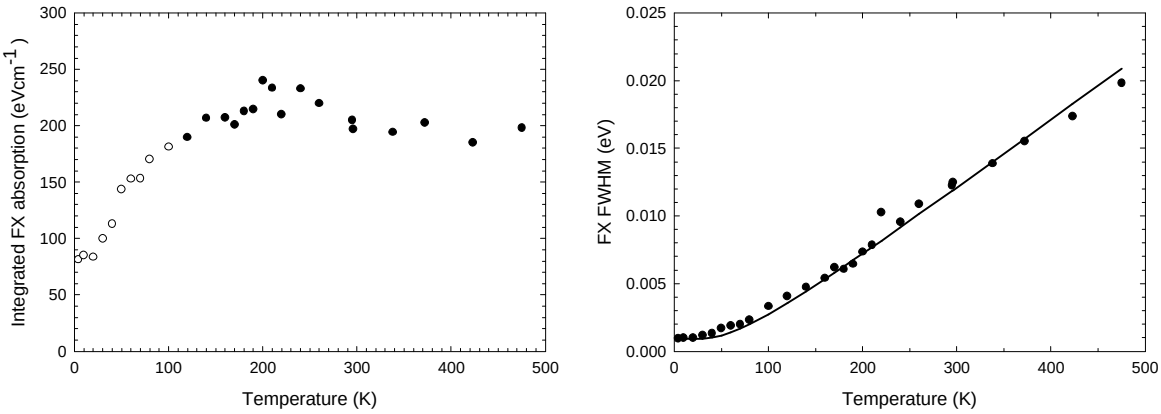

Fig. 3.46. *Temperature dependence of fitting parameters for free-exciton absorption. Left: integrated FX absorption: reliable values for temperatures higher than 100 K (full circles), less reliable values (open circles). Right: FWHM for the free-exciton peak. Experimental data (points) and fit to Eq. 3.35 (line).*

The temperature dependence of the band gap energy is being expressed by many formulas. Most of them are empirical or semi-empirical:
Varshni expression [Var67]:

$$E_g(T) = E_g(0) - aT^2/(b+T), \qquad \textbf{Eq. 3.36}$$

Manoogian-Wooley (M-W) expression [Man84]:

$$E_g(T) = E_g(0) - UT - V\Theta\left(\coth(\Theta/2T) - 1\right), \qquad \textbf{Eq. 3.37}$$

and Vina equation [Vin84]:

$$E_g(T) = E_B - a_B\left(1 + \frac{2}{\exp(\Theta/T) - 1}\right). \qquad \textbf{Eq. 3.38}$$

The recent expression proposed by Pässler [Pas03]

$$E_g(T) = E_g(0) - \frac{a\Theta}{2}\left[\left(1 + \sum_{n=1}^{3} a_n(n)\left(\frac{2T}{\Theta}\right)^{n+n} + \left(\frac{2T}{\Theta}\right)^{5+n}\right)^{\frac{1}{5+n}} - 1\right], \qquad \textbf{Eq. 3.39}$$

with

$$a_1(n) = \frac{5+n}{6}\left(\frac{p}{2}\right)^{2+(n-1)^2/2},\ a_2(n) = \frac{1-n}{2},\ \text{and}\ a_3(n) = \frac{(5+n)(1+n)^2}{3n(2+n)} \qquad \textbf{Eq. 3.40}$$

is based on self-consistent calculations.

Tab. 3.8 resumes parameters that fit best the four above-mentioned expressions. Based on the standard deviation values, the Pässler expression seems to be the most appropriate for description of $E_g(T)$ in the whole temperature range 0-500 K and can be extrapolated to much

higher temperatures as well. A review and comparison of relevant measurements of the temperature dependence of E_g is also depicted in Fig. 3.47.

Varshni expression (Eq. 3.36)						
$E_g(0)$ (eV)	α (meV/K)	β (K)		E_g(300 K) (eV)	S_N (meV)	
1.6077	0.372	110.0		1.526	0.84	[Hor06a]
1.606	0.325	78.7		1.529	-	[Lau90]
1.602	0.461	160.1		1.512	-	[San96]
M-W expression (Eq. 3.37)						
$E_g(0)$ (eV)	U (x10^{-5} eV/K)	V (x10^{-4} eV/K)	Θ (K)	E_g(300 K) (eV)	S_N	
1.6077	8.66	1.31	191	1.526	0.73	[Hor06a]
1.6066	5.0	1.8	183	1.513	-	[Fon00]
Vina expression (Eq. 3.38)						
E_B (eV)	a_B (eV)	Θ (K)		E_g(300 K) (eV)	S_N	
1.6323	0.02664	153		1.525	0.78	[Hor06a]
Pässler expression (Eq. 3.39)						
$E_g(0)$ (eV)	α (meV/K)	Θ (K)	ν	E_g(300 K) (eV)	S_N	
1.6066	0.354	160.4	1.09	1.526	0.64	[Hor06a]
1.606	0.309	104	0.75	1.528	-	[Lau90]+[Pas03]

Tab. 3.8. *Fitting parameters for Varshni, M-W, Vina and Pässler expressions of $E_g(T)$. E_g(300 K) and standard deviation values (S_N) are also given.*

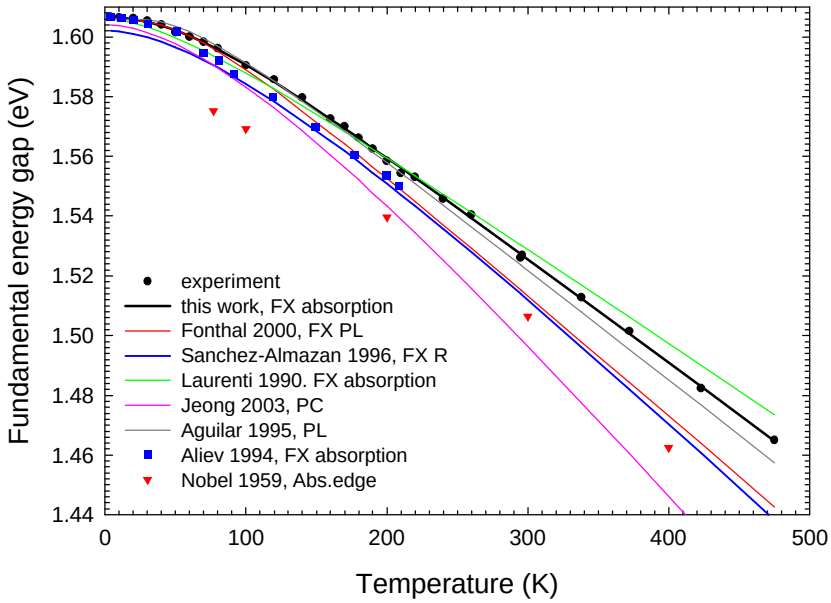

Fig. 3.47. *Temperature dependence of the fundamental energy gap for CdTe (our data are fitted to Eq. 3.39). Except our data and those of Nobel, above RT values are only extrapolations.*

3.4 Reflectance spectroscopy

3.4.1 Comments on reflectance spectroscopy

Reflectance spectroscopy and its modulated derivations are valuable techniques, which can provide precise information on the band structure of solids, not only semiconductors. The Kramers-Krönig (K-K) transform of reflectance spectra of wide range yields all the optical functions such as complex index of refraction and complex dielectric function or absorption coefficient. Works concerning CdTe deal usually with modeling the optical functions in the range 1-6 eV at rather elevated temperatures [Ada93], [Kim95], [Kim97]. Relatively small interest was focused on high-resolution spectra at liquid helium temperature near the fundamental energy gap E_g (or E_0). Together with problems of modeling the dielectric function (many models do not include the continuum exciton absorption consistently), no persuading conclusion could have been done till now concerning the precise position of the fundamental energy gap at room temperature [Lee94].

In region of weak absorption, the optical function can be determined quite easily by absorption spectroscopy. However, absorption measurements are not possible for most photon energies since thickness of investigated samples would be needed inferior to a fraction of 1 μm. Then, the reflectance and its derivations (electroreflectance, photoreflectance, and other) are used. Absorption and other optical spectra can be deduced from reflectance spectrum by the Kramers-Krönig analysis.

Reflectance spectroscopies are used to calculate the band structure of solids, in particular to determine critical points and amongst them the fundamental energy gap. In particular one may be interested in determining the energy gap of CdTe at room temperature. It seems that this is a simple task, but we will demonstrate it is not.

Fig. 3.48 shows temperature evolution of reflectivity spectra. They consist of sum of signals of light reflected from the front and the back side in the transparency region. The reflectivity in the transparency region is so high because the sample was mounted on a sample holder with gold surface. Then a part of the reflections comes also from the gold layer. The spectrum above the absorption edge energy can be identified with reflectance.

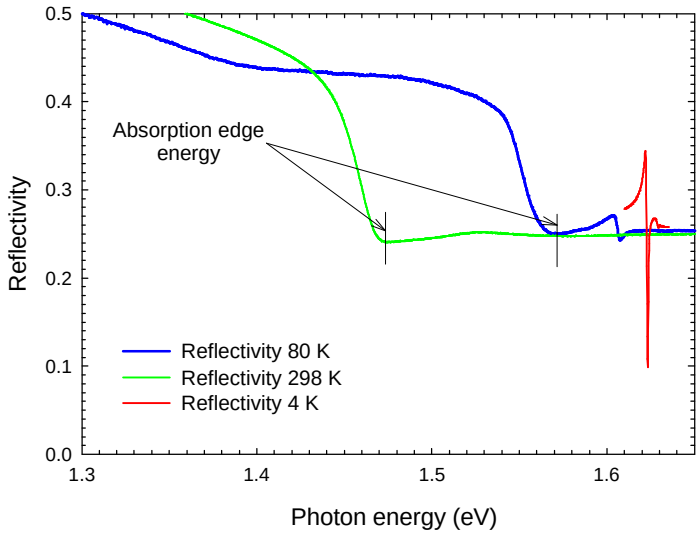

Fig. 3.48. *Reflectivity spectra of CdZnTe E10 at 4 K, 80 K and at room temperature.*

3.4.2 Index of refraction

Index of refraction *n* will be an important parameter in the following. Let's cite a reliable work dealing with spectral and temperature dependence of *n*. [Hli01] reports on determining the refractive index from interference pattern on a thin slab (55 μm) of CdTe. The values of *n* at 4 K and 295 K are plotted in Fig. 3.49.

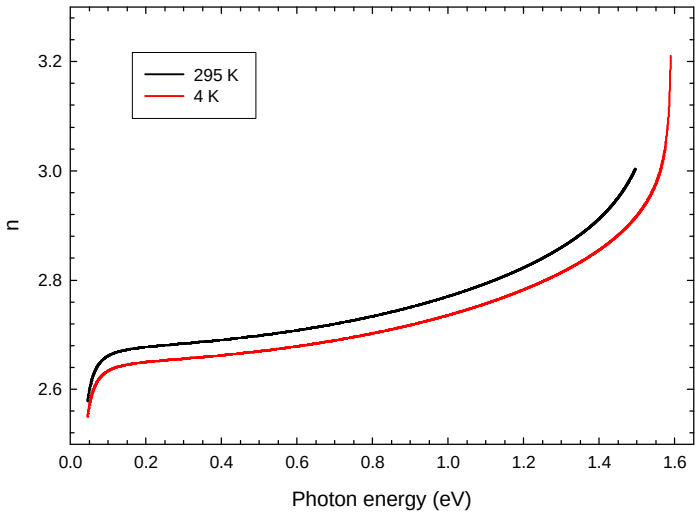

Fig. 3.49. *Refractive index of CdTe in the transparency region from [Hli01].*

3.4.3 Kramers-Krönig verification of reflectance and absorption

Let's analyze the measured reflectance and absorption spectra. The comparison via K-K relations could show distinct properties of analyzed surface (reflectance) and unperturbed crystal (absorption). Fig. 3.50 shows the imaginary part of complex index of refraction (k) at room temperature. Data for k between 1.3-1.7 eV were measured with high precision on good quality thin samples (thicknesses of 2, 20, 200, 2000 μm). The remaining spectral data are taken from [Ada93].

The real part of the complex index of refraction is calculated using

$$n(E) = 1 + n_{bcg} + \frac{2}{p}\int_{0.1eV}^{5.5eV} \frac{E'k(E') - Ek(E)}{E'^2 - E^2} dE'. \qquad \textbf{Eq. 3.41}$$

To obtain good agreement of absolute value of the refractive index, a constant n_{bcg}=0.85 was added (accounting for contributions of unknown low and high energy absorptions). The refractive index in the proximity of the fundamental band gap energy is plotted in Fig. 3.50 (right).

Comparison of measured and calculated reflectance is in Fig. 3.51. The two reflectance curves differ basically only by the slope of the background baseline. Probably, this is caused by experimental imperfections while measuring reflectance spectra (problem of reliable reference spectrum).

The reflectance maximum for both reflectance experiment and K-K transform of absorption is found near 1.505 eV. As the modeling of the reflectance line-shape is not trivial, the simple position of reflectance maximum can be used for the determination of energy gap in CdZnTe. However the difference (about 20 meV) between the reflectance maximum and the energy gap is not evident at all.

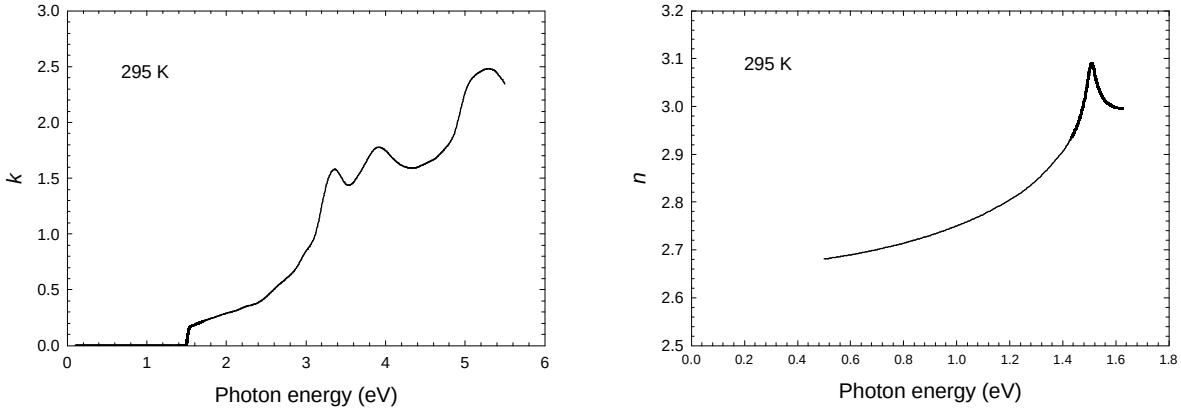

Fig. 3.50. *Absorption spectrum (295 K) given as index of extinction k is composed from our own experimental data (0.1-1.7 eV) and data for higher energies, which were taken from [Ada93]. Index of refraction n obtained via K-K transform. The precise offset calibration was done using [Hli01].*

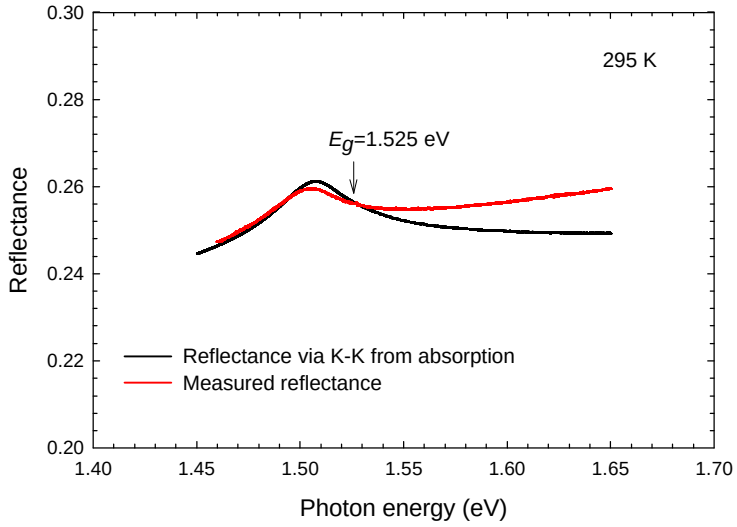

Fig. 3.51. *Reflectance spectra as measured (red) and obtained from K-K transform from absorption spectrum (black). The small disaccord is probably due to experimental imperfections when measuring reflectance.*

At liquid helium temperature, we again want to compare the K-K transform of the absorption coefficient measured on thin sample (thickness of 2 μm) with the reflectance spectrum measured on high quality CdTe crystal. The imaginary part of the complex refraction index is plotted in Fig. 3.52, as well as the calculated real part (using K-K transform). Reflectance spectra and group index are also depicted. The FWHM of the free exciton line in the absorption spectrum was 1 meV, that is sign of the lowered crystal quality due to sample preparation by polishing. This is confirmed by small modulation of calculated reflectance spectrum compared to the directly measured one (the measured reflectance spectrum is obtained from a deeply etched surface). If the absorption spectrum is modeled in a way that the ground exciton state is made much narrower, keeping the integrated absorption constant (FWHM=0.2 meV), after K-K transform, one obtains spectra in Fig. 3.53. Again, from the comparison of measured and calculated reflectance, it is clear that the free exciton line-width is slightly smaller then 0.2 meV. Both modeled and measured reflectance spectra are in quite a good agreement.

A remark concerning the line-widths of exciton lines in the high quality CdTe crystals should be made. The narrowest line of bound exciton observed in photoluminescence on available CdTe samples was 0.2 meV. Thus the free-excitonic line-width of about 0.2 meV as obtained from the reflectance analysis shows very good quality of the surface layer. To explain: PL spectrum of bound excitons provides information from depths of about 200-400 nm below the surface, whereas the reflectance near FX resonance tests only the surface of approximately 100 nm depth (the FX absorption coefficient reaches maximum of 300 000 cm^{-1} for 0.2 meV FWHM). Another proof of high crystalline quality is the reflectance feature of first excited state of the free exciton near 1.603 eV (distance between the ground and the first excited state is 1.603-1.596 eV=7 meV, which is consistent with the well known value of 10 meV for binding energy of the free exciton).

The calculation of the group index may be important while studying time and spectrally resolved properties near the free exciton energy. The group index was measured by the technique of time of flight of PL radiation in [Ser98]. However, only values up to 30 can be measured in this way on thick samples. Our values for high quality samples reach more than 1000 for the group index.

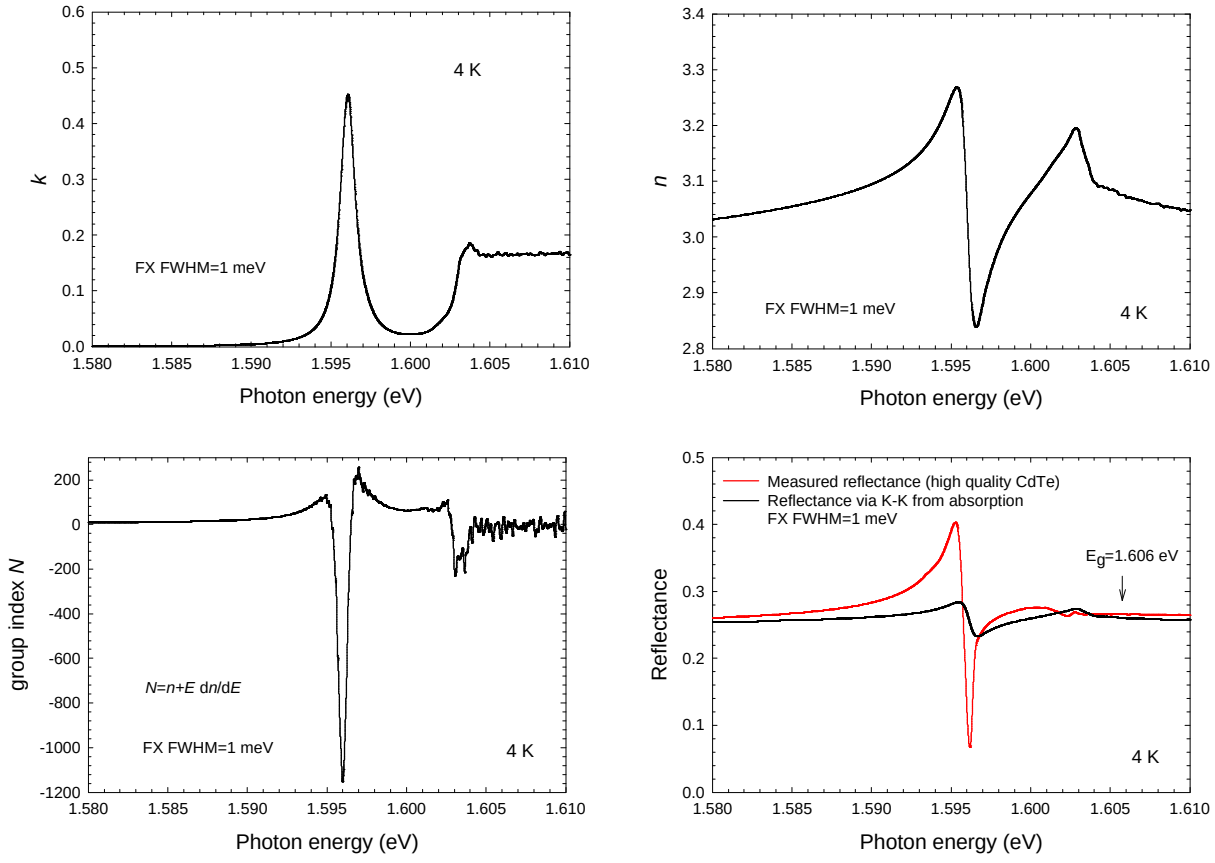

Fig. 3.52*. The measured extinction index* k*, its K-K transform to refractive index n, reflectance and group index for 2 mm thin self-standing CdTe sample (all in black). The FWHM of the free exciton line is 1 meV. In red is plotted the experimental reflectance recorded on another high-quality bulk CdTe (AF15).*

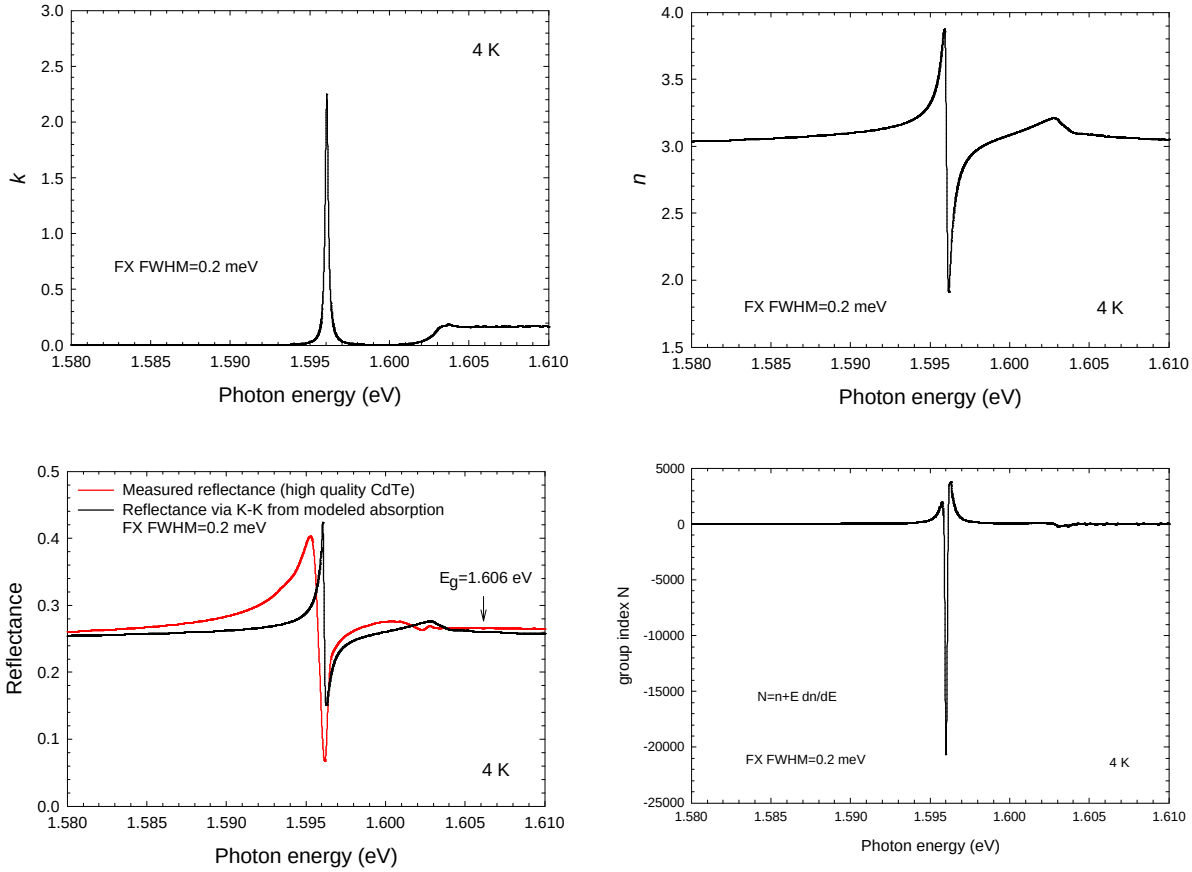

Fig. 3.53. *The same as in Fig. 3.52, but the absorption spectrum was modeled in such a way, that the FWHM of the free exciton is 0.2 meV.*

4 Optical mapping of CdTe and CdZnTe wafers

4.1 Comments on optical mapping

Visualization of spatial distribution of defects is potentially a very interesting application of optical methods. There are several advantages: optical characterization is non-destructive, contactless and it can have very good spatial resolution (the case of photoluminescence) and it can be cheap (methods run at room temperature). Works on optical mapping of CdTe and CdZnTe are quite numerous; these techniques are relatively new (beginning in the 80's).

1D mapping can be performed as a line scan through a sample with intentionally prepared inhomogeneities while studying diffusion and annealing effects like in [Soc94] or [Hor05]. This is suitable technique for liquid helium temperatures since the sample in a typical cryostat can be easily moved along one direction. For characterization of wafer homogeneity, 2D experimental setup is needed. Sometimes, very sophisticated techniques are used to yield interesting properties of CdTe compounds. [Sch90] treats distribution of tellurium inclusions in CdTe by detecting the PL signal emitted by microcrystalline tellurium near 0.5 eV. [Ton96], [Li01] and [Fur04] studied the distribution of zinc in CdZnTe by mapping the room temperature PL with high spatial resolution. [Rat03] measured spatial distribution of ratio of band edge and deep band PL in order to characterize defect creation during technological manipulation (creation of contacts). [Tri92] describes mapping of scattered laser light by microdefects. In the same work, mapping by PL technique at RT is used to find areas with high density of dislocations (minima of the integrated PL signal). [Tri92] also announced preparation of liquid helium temperature PL mapping on CdTe, but this work has not appeared till now, to our knowledge. Distribution of deep bands, A-center and band edge PL at liquid nitrogen was subject of [Fie02]. Similar technique was employed by [Guk97], who presented single wavelength scanning at liquid nitrogen temperature. [Guk97] investigated PL intensity variation across dislocation etch pits and grain boundaries. [Tob95] presented a zinc mapping technique using PLE spectroscopy at low temperature (15 K). A setup for PLE spectroscopy equipped with a 2D CCD camera was used to map the composition of substrates without any moveable parts.

Reflectance-based methods have usually worse spatial resolution because they operate with white light. Contrary, spatial resolution of about 1 μm is achieved quite easily at RT PL characterization. At lower temperature, in a vacuum liquid nitrogen cryostat with one window, [Guk97] reports spatial resolution of about 5 μm. Emission spectroscopy mapping possessing the highest spatial resolution is the cathodoluminescence (CL). This method can easily represent variations of optical properties across grain boundaries or dislocations [Bub88].

From this small recherché, it seems that room temperature PL is the most used optical mapping method. [Taj90] cleared out general problems of RT PL mapping in semiconductors. In industry of crystal growth (InP), PL at RT was used to imagine zones of equal PL intensity in order to visualize crystal growth process, but not to determine distribution of specific defects [Zap1]. In view of our findings about RT PL band in section 3.2.4.2, we cannot deny, that use of this method to map zinc concentration seems a little doubtful to us.

In the following, we will present low temperature (at about 10 K) optical mapping of CdTe and CdZnTe wafers. Contrary to liquid nitrogen temperature, liquid helium temperature allows us to record maps of bound excitons, the PL signal is several orders greater and also the width of PL lines is much smaller. We will explain, why the liquid helium PL is the ultimate technique for mapping: it provides rich information on defects while in the same time it includes absorption mapping via the FX reabsorption (for CdZnTe). The following text is based on our recent works [Hor05], [Hor06b] and [Hor06c].

4.2 Experimental details

Whereas the one-spot optical spectra were obtained in a classical experimental setup, the mapping configuration (Fig. 4.1) deserves more attention.

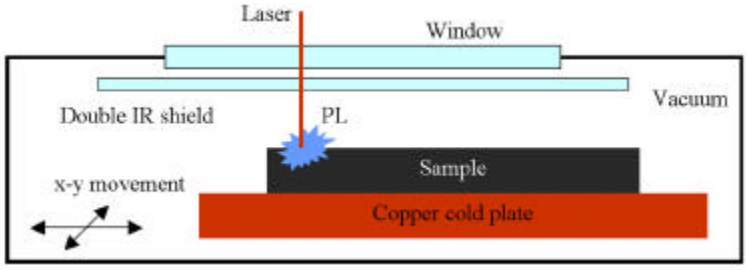

Fig. 4.1. *Scheme of experimental setup for PL mapping measurements.*

Contrary to the classical cryostat, where the sample is in contact with exchange gas, in the mapping cryostat the sample is placed in vacuum on a copper cold plate. The copper plate assures the only cooling stream. Thermal radiation is shielded using two cooled SiO_2 glass windows. To obtain the best thermal contact, the bottom part of sample is grinded to maximal planarity. With both perfectly polished planar sample and sample plate, the cold plate/semiconductor thermal contact is the best and the temperature of the upper surface as low as 6-8 K can be reached with moderate liquid helium consumption (2 l/h). By contrast, with surfaces of "usual" quality, using sample mounting with thermo-conducting grease (Apiezon N, Cry-con), the thermal contact was bad and the minimum reached sample surface temperature was poor 20-30 K. Moreover, using thermo-conducting grease unavoidably creates mechanical strain when cooled down so that CdTe samples which are very fragile often brake into pieces.

Surfaces of samples (wafers) for optical mapping were prepared in a specialized optical atelier. The mapped surfaces are standard chemically-mechanically etched by bromine-methanol solution to provide the best possible homogeneity of the surface quality. Homogeneity of the signal collection is assured also by the fact that only the sample is moved, but the optical path is fixed. The usual spectral resolution is 0.2 meV (on the full range of the detector spectral region!) with time of as low as 5 s (only several 'scans') to record a non-noisy spectrum from a sample that exhibits standard PL efficiency. The spatial resolution of the positioning system is 1 μm, the diameter of the laser spot is about 30 μm, but the step used for large wafer characterization is 1 mm due to time limits. Then, a typical mapping experiment when ≈1000 spectra are recorded, takes approximately 5 hours, the consumption of liquid helium is ≈10 liters.

The x-y movement stage of the mapping cryostat receives commands from the computer via the RS232 communication interface. The OPUS program, which provides communication and data transfer from the FTIR spectrometer, offers possibility to build and run macro-programs including sending commands to both the spectrometer and to the x-y stage of the cryostat. Thus a simple macro of less then 10 lines (2 cycles, a command for recording and saving a spectrum with given parameters, commands for the relative movement of the stage) is sufficient for recording spectra from a predefined sample surface area. The numerical processing of recorded spectra is done also using macros in the native environment of the OPUS program. It has built-in functions for Fourier transform, integration, curve fitting, peak picking and other common manipulations of optical spectra. Thus, to obtain a PL intensity map of a CdTe sample for a given PL band, the integration within a constant range is very often enough. In CdZnTe, where the band gap energy shifts with zinc concentration, a minima peak-picking is necessary for finding the FX reabsorption feature. Broad deep level intensities can be calculated also using just the integration. Contrary, the intensities of sharp lines of bound excitons are usually calculated via maxima peak-picking procedure, which yields not only energy positions but also intensities and line-widths of found peaks.

4.3 Mapping of zinc concentration in CdZnTe

4.3.1 Comments

Many optical methods can be used for the determination of zinc concentration in $Cd_{1-x}Zn_xTe$ (primary, the energy gap is to be determined).

Derived reflectance methods (photoreflectance, electroreflectance, ellipsometry and other) are widely used to obtain the dielectric function of materials. Advantage of reflectance is in the simplicity of experimental setup. Contrary to the photoluminescence, specific features of the fundamental energy gap are observed even at room temperature. Except our measurements [Hor06c], to our knowledge, no mapping using reflectance was made public up to now on the CdZnTe system.

The use of transmittance on thick samples is questionable for wafer characterization in practice as the position of the absorption edge depends on the crystal quality. The absorption edges differ commonly by 10-20 meV ($\Delta x \approx 0.03$) for different samples at RT as well as at lower temperatures. Absorption spectroscopy is also sometimes used [Hir00], however this method can only reflect the relative and approximate shift of the energy gap.

Low temperature photoluminescence spectra, as was explained at paragraph 3.2.4.1, contain information about both emission and absorption. Energy gap can be deduced as well as from free-exciton reabsorption feature, as well from emission of bound excitons. But using the intrinsic absorption effect is more reliable, of course.

Photoluminescence maximum at RT (if observable at all) for CdTe fluctuates from sample to sample and lies below the free-exciton resonance and E_g (see paragraph 3.2.4.2).

Neither the transmittance nor PL at RT is therefore suitable for absolute evaluation of zinc composition. RT reflectance could be used for this purpose, but it requires an exact knowledge of the complex dielectric function in the vicinity of E_g (the optical function is not known with sufficient energy resolution and its exact modeling is not trivial). We will show, that the low temperature PL is the most appropriate for mapping of zinc concentration, as well for mapping of concentrations of crystal defects.

Zinc concentration x is obtained from [Fra00]:

$$E_g(x) = 1.606 + 0.520x + 0.254x^2 . \qquad \textbf{Eq. 4.1}$$

ΔE_g is the difference of band gap energies between $Cd_{1-x}Zn_xTe$ and CdTe.

The ΔE_g-x calibration (for low zinc concentration) is plotted in Fig. 4.2. It is nearly a linear dependence.

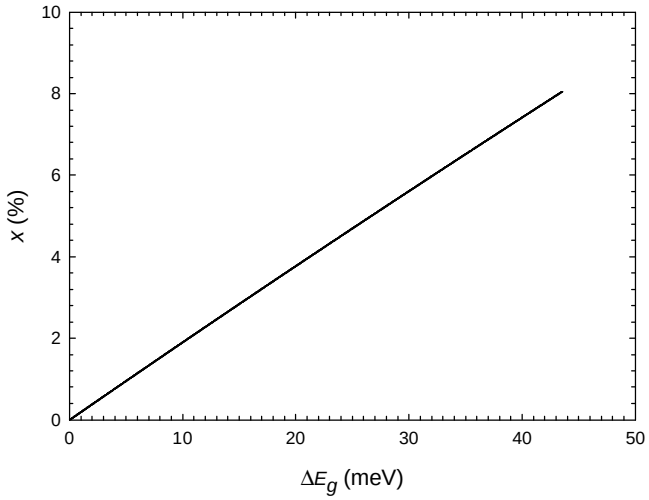

Fig. 4.2. *Zinc concentration x in $Cd_{1-x}Zn_xTe$ versus the band gap energy shift DE_g.*

4.3.2 Zinc concentration maps

Fig. 4.3 shows maps of zinc concentration established by different methods. The band gap energy at room temperature was obtained by adding 18 meV to the reflectance maximum (for more detail see 3.4.3 and 3.3.5). At liquid nitrogen temperature the oscillation of FX resonance in reflection spectrum was used. Absorption edge position was shifted to be in accord with the PL measurements at low temperature, which was calibrated according to [Fra00].

Investigated sample E10C was cut along the growth axis, which is denoted as z-axis. *Z*=0 mm is where the solidification began, *Z*=20 mm is the heel. The growth began intentionally at the free surface of the melt. Nominal zinc concentration was 0.035. Profiles of zinc concentration are plotted in Fig. 4.4. The same zinc concentration lines show the propagation of the liquid-solid interface during the solidification. For the particular case, it means that the growth has begun as wanted – at the free surface of the melt in a crucible. It shows that the walls were hotter and that a lot of heat was dissipated towards the upper direction probably by radiation. Also, the axial symmetry is not perfect.

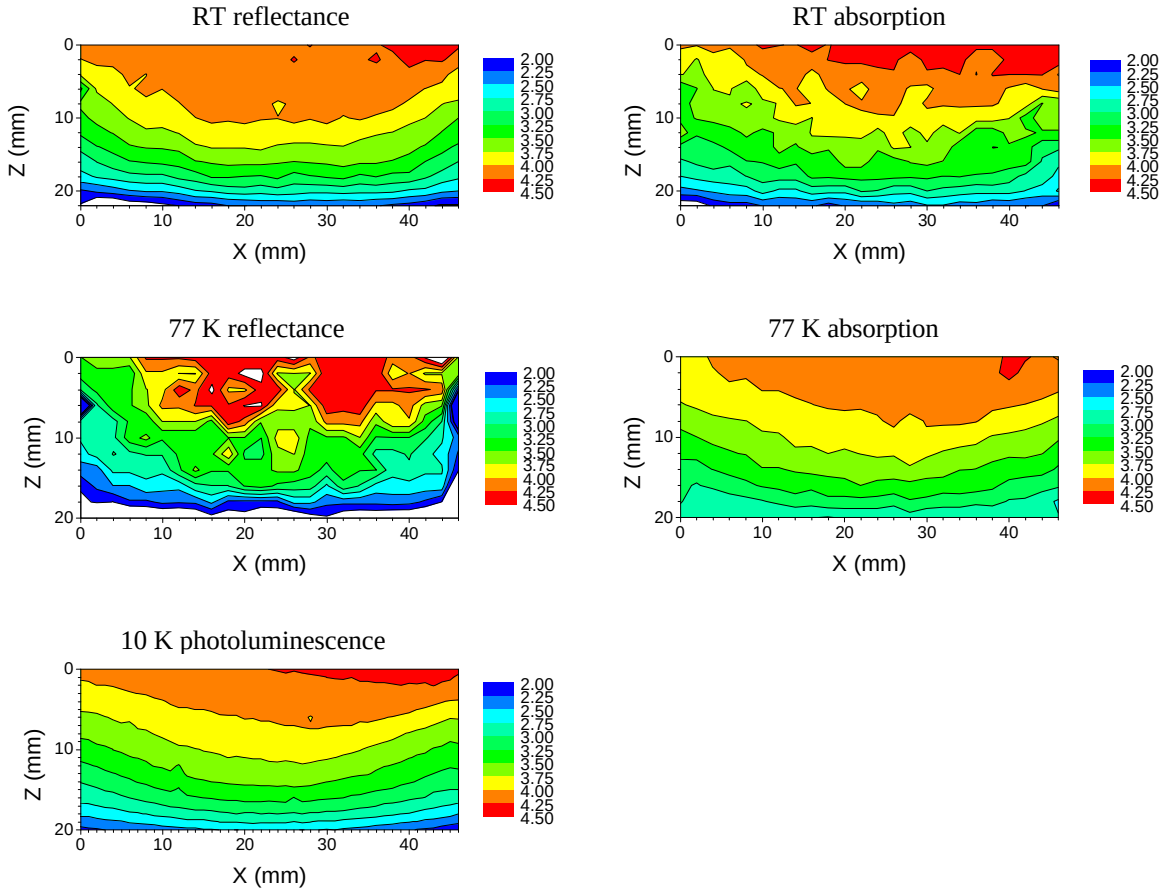

Fig. 4.3. *CdZnTe E10C. Zinc concentration maps (% zinc) recorded at different temperatures by various optical techniques. Ticks show density of measured points. The scale is the same for all graphs.*

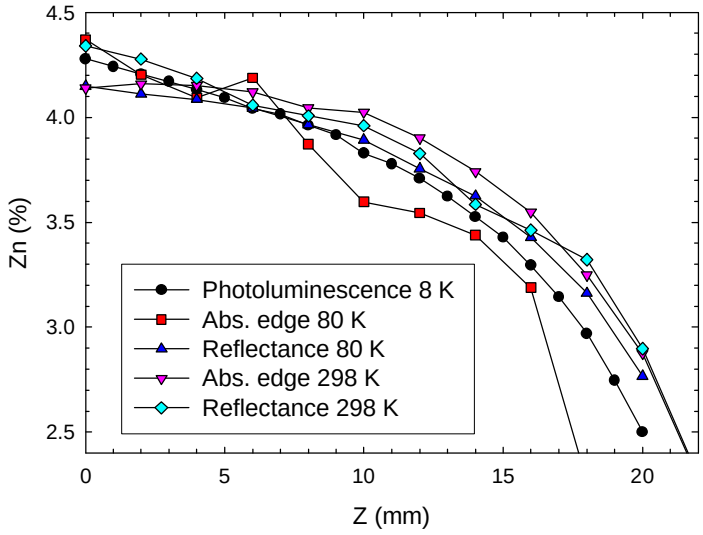

Fig. 4.4. *CdZnTe E10C. Zinc segregation profiles determined by different techniques.*

Method	error in *x*	Spatial resolution	Absolute	Time per one spectrum (s)
Photoluminescence at 10K	0.0005	30 μm	Y	10
Reflectance at 80 K	0.002	1 mm	Y	60
Absorption at 80 K	0.01	1 mm	N	20
Reflectance at 298 K	0.005	1 mm	Y	200
Absorption at 298 K	0.01	1 mm	N	20

Tab. 4.1. *Characteristics of the zinc mapping methods under study.*

Errors of determination of *x* were estimated in Tab. 4.1. The best resolution in zinc concentration is obtained by the liquid helium PL; its superiority is of course due mainly to the lowest temperature. Further reason for choosing the liquid helium PL as the prime method is the best spatial resolution. More, apart information about the band gap energy, PL gives the information about defect concentrations. This information is hardly accessible by other optical methods.

Finally, the segregation coefficient for zinc (from the near axis region of the PL map in Fig. 4.3) calculated using the standard formula

$$c_{Zn}(g) \approx (1-g)^{k_{Zn}-1} \qquad \textit{Eq. 4.2}$$

is k_{Zn}=1.15±0.05. g is the solidified fraction. This value is in agreement with values reviewed in [Kuc96], which range from 1.14 to 1.2.

Although the Fig. 4.4 shows a nice segregation profile of zinc concentration for the crystal E10 (in the central part), for most crystals one hardly finds such an ideal situation.

Sample E10A1 was cut in a plane perpendicular to the growth axis. In an ideal case, the zinc concentration would be constant. Fig. 4.5 shows typical variations of zinc concentration near the central part of ingot (x=0 mm, y=35 mm) and near the crucible wall (x=25 mm, y=0 mm). The most important result is that local minima are found near the crucible walls. This can be explained that the walls being hotter, they cause heat exchange by convection currents. Hence, places where zinc concentration is locally low have solidified much later than the surrounding material.

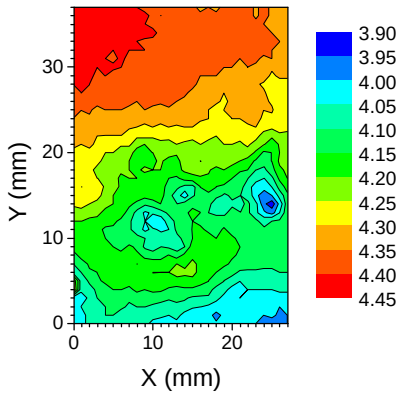

Fig. 4.5. *Zinc concentration (% zinc) map for CdZnTe E10A1 recorded at liquid helium temperature (10 K) by photoluminescence. Ticks show density of measured points. Local zinc minima are well visible. Zinc resolution is maximal possible.*

4.4 Mapping of defects by photoluminescence spectroscopy

4.4.1 Comments and theory

As stated in the introduction to this chapter (section 4.1), the characterization by the low temperature PL mapping is not a widespread technique. This section aims to show possibilities of low temperature PL mapping in imaging the distribution of crystal defects and especially in determining the segregation coefficients of impurities. It will be shown that a simple relation involving segregation coefficient of dominant non-radiative center connects the segregation coefficient of concentration of a defect and segregation coefficient of corresponding PL intensity. Despite possible absence of information about the non-radiative center, segregation coefficients of PL intensities bring valuable information about the relative segregation of specific defects. The text is based on [Hor06b].

Determination of concentration of defects is practically limited to liquid helium temperatures. In fact, absorption spectroscopy can see transitions involving deeper levels at high concentrations even at room temperature. But low temperature methods provide information on much more defects whose concentration is very low. For low doped and undoped CdTe crystals, well-resolved absorption lines of bound exciton states are observed. In principle, absorption into bound exciton states can be measured and calibrated to concentration. However, samples must be thinned down to 10-20 μm in order to overcome the high edge absorption coefficient. Hence in practice, for 2D wafer mapping only the photoluminescence can be used.

Let's consider situation when one radiative (R) and one non-radiative (NR) recombination centers exist with respective segregation coefficients k_R and k_{NR}. Their concentration profiles $c_R(g)$ and $c_{NR}(g)$ are given by the normal freezing equation:

$$c_R(g) = c_{R0} k_R (1-g)^{k_R - 1} \qquad \textbf{Eq. 4.3}$$

and

$$c_{NR}(g) = c_{NR0} k_{NR} (1-g)^{k_{NR} - 1}, \qquad \textbf{Eq. 4.4}$$

where g is the solid fraction, c_{R0} and c_{NR0} are nominal concentrations. PL intensity is given by:

$$PL(g) \approx \frac{p_R(g)}{p_R(g) + p_{NR}(g)} \approx \frac{c_R(g)}{c_R(g) + K c_{NR}(g)} \approx \frac{1}{1 + K \frac{c_{NR0}}{c_{R0}} (1-g)^{k_{NR} - k_R}}, \qquad \textbf{Eq. 4.5}$$

p_R and p_{NR} are probabilities of radiative and non-radiative recombination and K is a proportionality constant. For dominant non-radiative recombination, the expression can be simplified to:

$$PL(g) \approx \frac{c_{R0}}{c_{NR0}}(1-g)^{k_R - k_{NR}}. \qquad \textit{Eq. 4.6}$$

Thus the segregation coefficient of distribution of the PL intensity of a particular defect is shifted by k_{NR}-1 compared to the concentration segregation coefficient. Hence, if the segregation coefficient of the present non-radiative center were known or if the one of a well-known defect observed in PL were known, segregation coefficients of all remaining defects could be determined absolutely by the PL mapping technique.

Another approach to determine concentrations consists in finding an intrinsic band in the spectrum to which other photoluminescence intensities could be related. Radiative band-to-band transitions have not been observed in CdTe at low temperatures. Free-exciton emission is too weak and not completely understood up today. Only reliable PL emissions that are of intrinsic origin are LO phonon replicas of FX. Amongst them the most intensive is the first one (FX-LO). In a quasi-equilibrium PL experiment, we can suppose that the PL intensity of FX-LO ($PL_{FX\text{-}LO}$) is proportional to FX concentration c_{FX}

$$PL_{FX-LO} \approx c_{FX}. \qquad \textit{Eq. 4.7}$$

In a similar way, the PL intensity of exciton bound on a defect PL_{defect} is proportional to both FX c_{FX} and defect c_{defect} concentrations

$$PL_{defectX} \approx c_{defect} c_{FX} \qquad \textit{Eq. 4.8}$$

Hence, combining Eqs. 4.7 and 4.8, we obtain

$$c_{defect} \approx \frac{PL_{defect}}{PL_{FX-LO}}. \qquad \textit{Eq. 4.9}$$

This formula is valid for PL experiment below saturation of bound exciton and FX decay. The method can be used only in high purity crystals because increasing defect concentration rapidly quenches FX-LO intensity. From this point of view, a low quality crystal can be defined as having total defect concentration greater than approximately 10^{16} cm^{-3}. Of course, a sufficient condition for this is a high carrier concentration (>10^{16} cm^{-3}) at room temperature.

4.4.2 Photoluminescence maps

4.4.2.1 CdZnTe E10C

First let's examine the segregation of PL intensities on sample the E10C (its zinc concentration map is shown above in Fig. 4.3). The PL spectrum (Fig. 4.6) consists of deep level DL1 and DL2 with respective maxima near 1.15 eV and 1.2 eV, shallow acceptor to band transition with binding energy 54 meV. Bound excitons are also present, unfortunately they cannot be separated into acceptor and donor contributions across the whole wafer surface. Free exciton replica is weak and superposed to other residual emissions. The integrated PL intensities are plotted in Fig. 4.7 and Fig. 4.8.

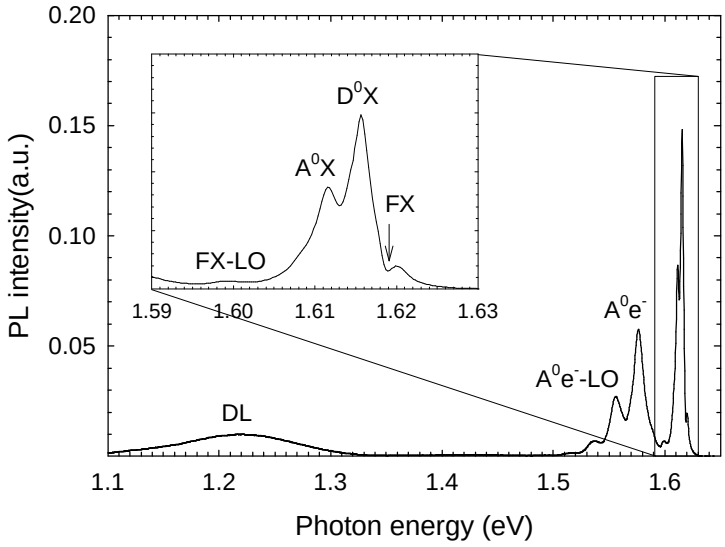

Fig. 4.6. *PL spectrum of E10 from the region of crystal growth beginning.*

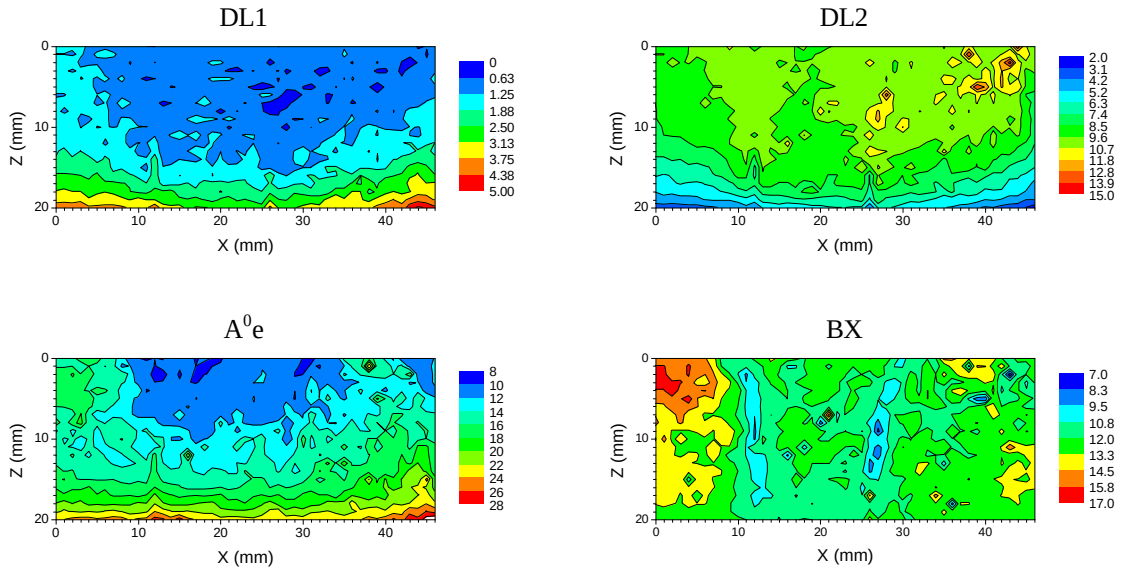

Fig. 4.7. *PL mapping of CdZnTe E10C recorded at liquid helium temperature (10 K). Deep levels DL1 and DL2, acceptor to band transition A^0e and integrated excitonic emission BX. Ticks show density of measured points. Blue regions in the excitonic photoluminescence map correspond to grain boundaries.*

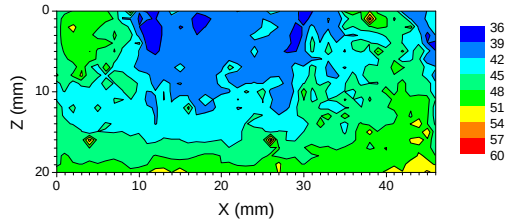

Fig. 4.8. *PL mapping of CdZnTe E10C. Total integrated photoluminescence intensity.*

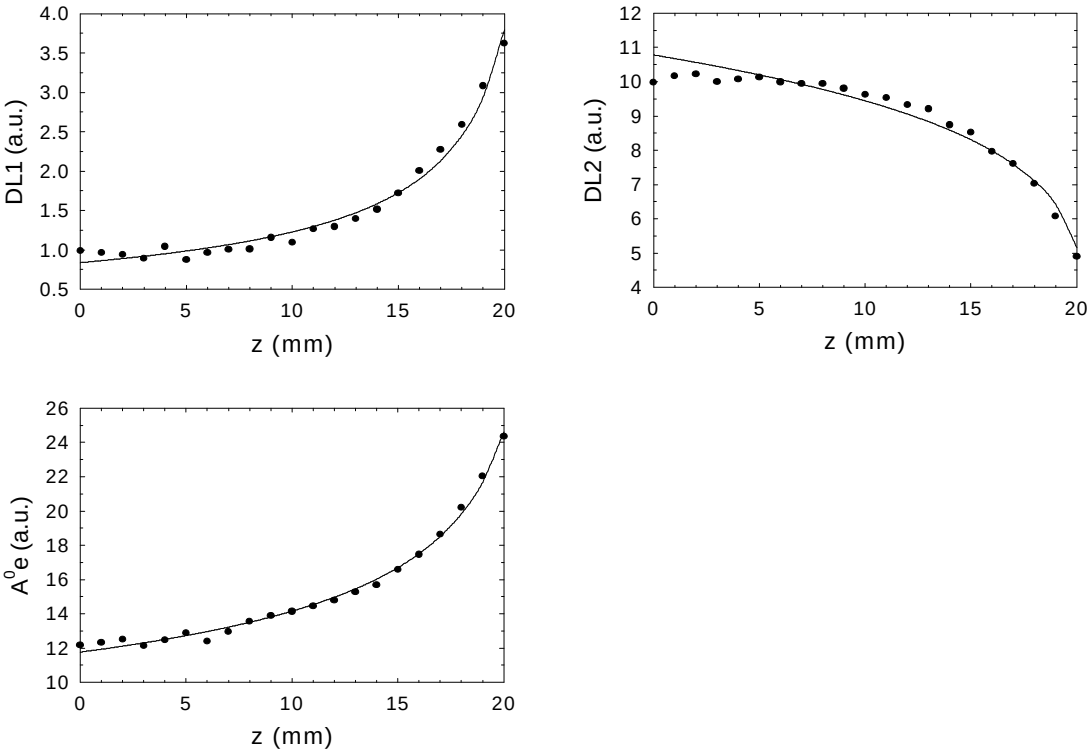

Fig. 4.9. *Profiles of PL intensities of deep levels DL1 and DL2 and of acceptor-to-band transition. Experimental data (points), fittings to normal freezing equation (lines).*

In Fig. 4.9, profiles of PL intensities of selected defects are plotted. Those profiles are taken from the maps in Fig. 4.7, from the near axis part of the ingot. The data were fitted to Eq. 4.2 type; calculated segregation coefficients for respective defects are shown in Tab. 4.2.

The dominant shallow acceptor PL intensity is distributed with k=0.7. This defect could be identified with Na or Li acceptor substituting the cadmium position. [Mol84] gives ionization energies of 59 meV and 58 meV for Na and Li respectively. The acceptor binding energy from our PL spectra is 54 meV. In [Kuc96], value of k=0.3 is proposed for Li and k=0.05 for Na. If we assume that the present shallow acceptor is Cd-substitutional lithium, then the concentration segregation coefficients can be obtained from Eq. 4.6. Segregation coefficients calculated with this assumption are in Tab. 4.2. Segregation coefficient of the non-radiative center has value of 0.6.

	[Zn]	DL1	DL2	A^0e	NR center
Segregation coefficient of PL intensity	-	0.45±0.1	1.2±0.15	0.7±0.15	-
Segregation coefficient of concentration	1.15±0.05	0.05±0.1	0.8±0.15	0.3±0.15	0.6±0.1

Tab. 4.2. *Segregation coefficients of PL intensities and segregation coefficients of concentrations.*

Unfortunately, the attribution of the shallow acceptor to Li may be incorrect since the mass spectroscopy analysis shows larger concentration of Na (Tab. 1.2). Also, the difference in binding energies obtained from PL spectra and those from literature indicate that the shallow acceptor may not necessary be Li or Na. In the same time, we cannot take the values in Tab. 4.2 really seriously for another reason. The migration of impurities in the solid phase taking place during the crystal cooling-down can influence the distribution of defects very strongly. The latter effect will be dominating the PL intensity distribution in CdTe:In crystal in section 4.4.2.3.

4.4.2.2 CdZnTe E10A1

Fig. 4.10 shows PL maps of integrated PL intensities. PL intensities show local maxima and minima that are exactly correlated with local zinc minima in Fig. 4.5. The inhomogeneous distribution of PL intensities is due probably uniquely to segregation processes connected with above-mentioned convection in the melt. An interesting feature is that PL intensities of e.g. shallow acceptors changes on a short scale by a factor of 2-3. If similar factors determine the distribution of the concentrations also, this can be explanation for fluctuation of electrical properties, which is sometimes observed.

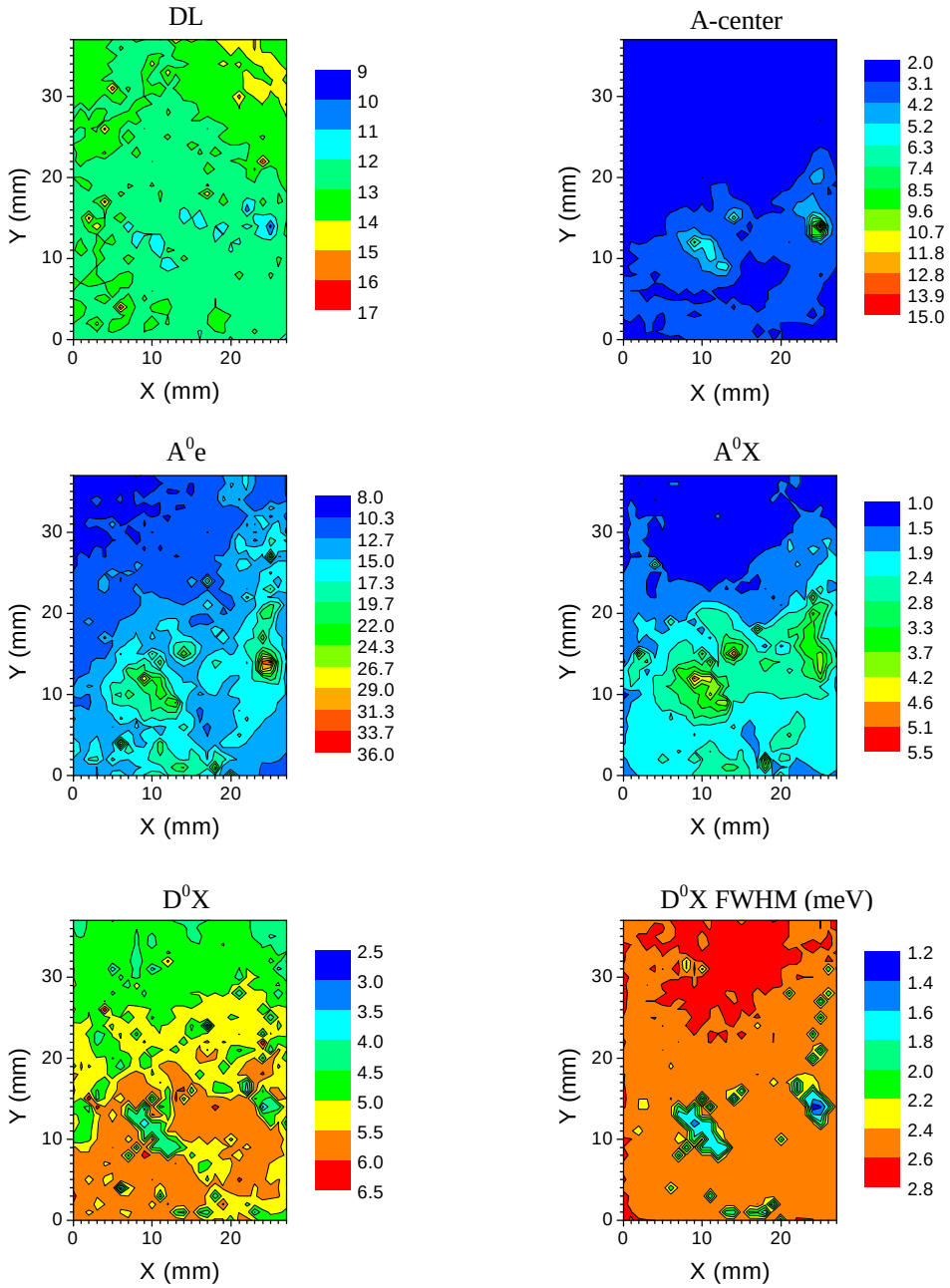

Fig. 4.10. *PL intensity maps of CdZnTe E10A1 recorded at liquid helium temperature (10 K). Deep level DL, A-center, shallow acceptor to band A^0e, shallow acceptor bound exciton A^0X, shallow donor bound exciton D^0X and its FWHM (meV). PL intensity of deep level correlates with the zinc concentration, whereas A-center and shallow acceptor PL anti-correlate. Ticks show density of measured points.*

4.4.2.3 CdTe:In E3314

Chosen wafers cut from In-doped CdTe E3314 were mapped by PL with spatial resolution 1x1 mm^2. The sample temperature estimated from the PL spectra is about 10 K. PL maps together with schematic representation of the sample placement are depicted in Fig. 4.12. The PL spectra (Fig. 4.11) show DAP transitions with ZPL near 1.453 eV. This could be the indium A-center. The 1.492 eV seems to correspond to DAP band of silver acceptor (the Coulombic shift is about 6 meV). Silver presence is manifested also by the bound exciton at 1.5885 eV ($A3^0X$). The other bound excitons at 1.5883 ($A2^0X$) and 1.580 eV ($A1^0X$) probably come from unknown complexes. The intensity of donors (D^0X) was obtained by integration in the corresponding spectral region; even though the donor peak is not resolved at all in the spectra. No PL signal was detected between 0.46-1.1 eV. Also, no emission of FX replicas is observed.

PL maps must be interpreted carefully. The A-center bands are highly efficient recombination centers. Hence, excitonic PL is probably strongly damped in regions where A-center emission is strong. It means, that differences in the distribution of the $A1^0$ defect are even stronger. Exactly speaking, we cannot decide, whether the other defects manifested by excitonic emission ($A1^0$, $A2^0$, D^0) have minimum concentration in the central part or not.

No segregation values can be extracted from the maps taken along the growth axis. The wafer cut perpendicularly to the growth axis shows nice axial symmetry of distribution of PL intensities. The distribution of defect PL can hardly be given by the temperature field during solidification. The conclusion is that the PL distribution, for the particular case, was rather governed by migration of defects during a non-equilibrium cooling-down process.

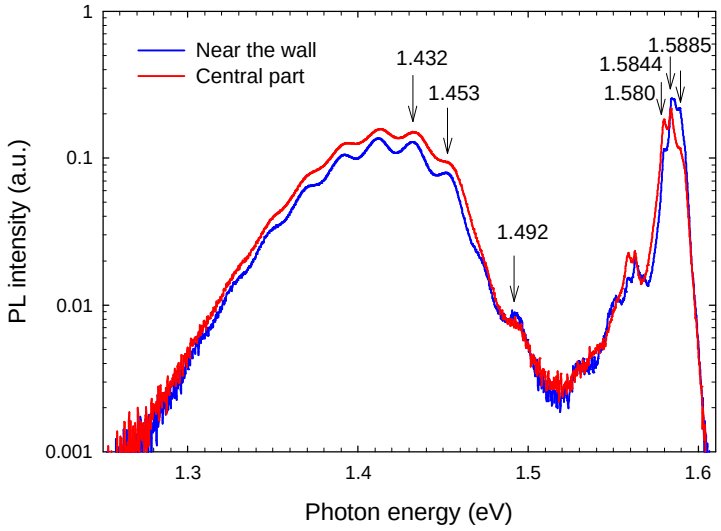

Fig. 4.11. *Representative spectra of inner and outer part of crystal E3314.*

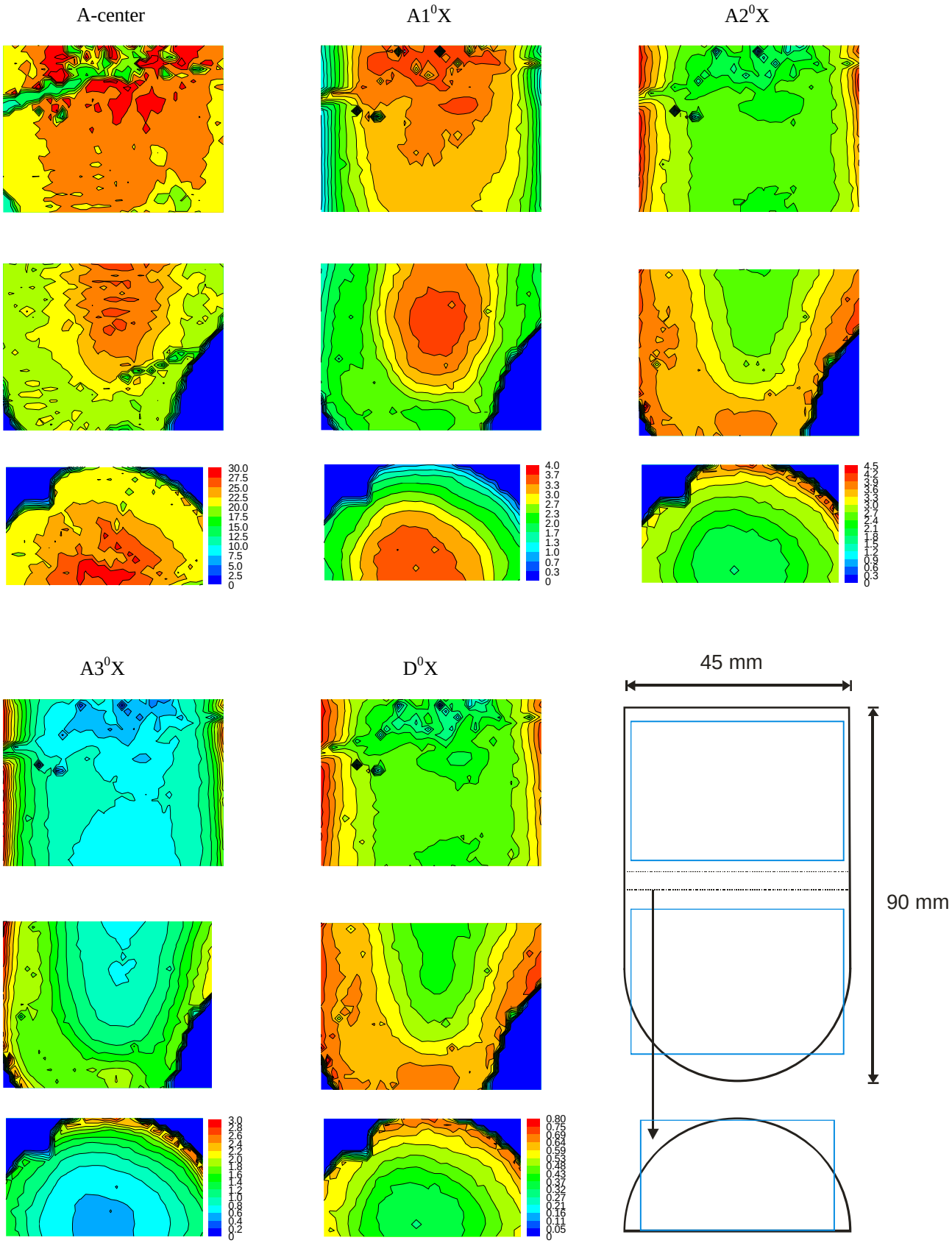

Fig. 4.12. *PL maps of CdTe:In E3314. Scheme of placement of maps (right down). Spatial resolution is 1x1 mm^2.*

4.4.2.4 CdTe SR317

Two of several hundred spectra recorded while constructing the PL maps of CdTe SR317 are plotted in Fig. 4.13. PL emission consists of bands whose chemical origin is badly understood. The acceptor bound excitons in the proximity of 1.589 eV (denoted as $A_1{}^0X$) are probably due to alkali elements. $A_2{}^0X$ excitons are located near 1.5905 eV. Shallow acceptor-to-band transition with E_B=77 meV is called A^0e. The A and A_1 or A and A_2 acceptors can be in principle chemically identical.

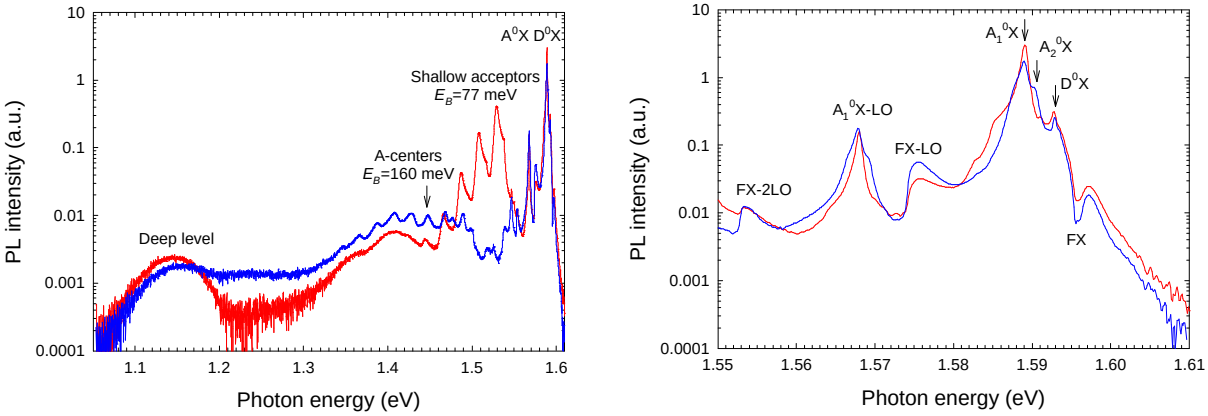

Fig. 4.13. *Representative PL spectra of CdTe SR317, wide and narrow edge spectral regions.*

PL maps and its placement within the crystal are depicted in Fig. 4.14 and Fig. 4.15. The spatial step is 2x2 mm^2. Seven of the PL maps represent integrated PL intensity; the remaining ones show ratios of bound and free-excitonic PL intensities. The problems of temperature regulation during the growth probably cause the surprising shapes and large inhomogeneities of PL intensities. Basically, the maps are symmetrical around the growth axis. Some complementary distributed PL bands are observed as the deep level (DL) and the A-center. The upper central part seems to be of quite good quality (strong FX-LO emission, low A-center emission and low acceptor concentrations $A_1{}^0$ and $A_2{}^0$). This pure region looks encircled by a ring of high-intensity points ($A_1{}^0X$ map). These points are a side-effect due to the discrete sampling, in fact, there is a continuous half-circle of strong PL emissions of acceptor bound excitons. The maps of PL ratios must be regarded very carefully, since small FX-LO intensities give rise to large false concentrations especially in the areas with no PL signal (down corners of the sample).

In this particular case, we cannot think about estimating the segregation coefficients of defects since the solidification of the crystal was not probably continuous. The growth has begun in the upper part of the ingot (see Fig. 4.15) as expected (the Fig. 4.15 is upside down from the point of view of crystal growth setup). The purest region is found close to the growth beginning, but this is basically all that can be concluded from having a look on the PL maps.

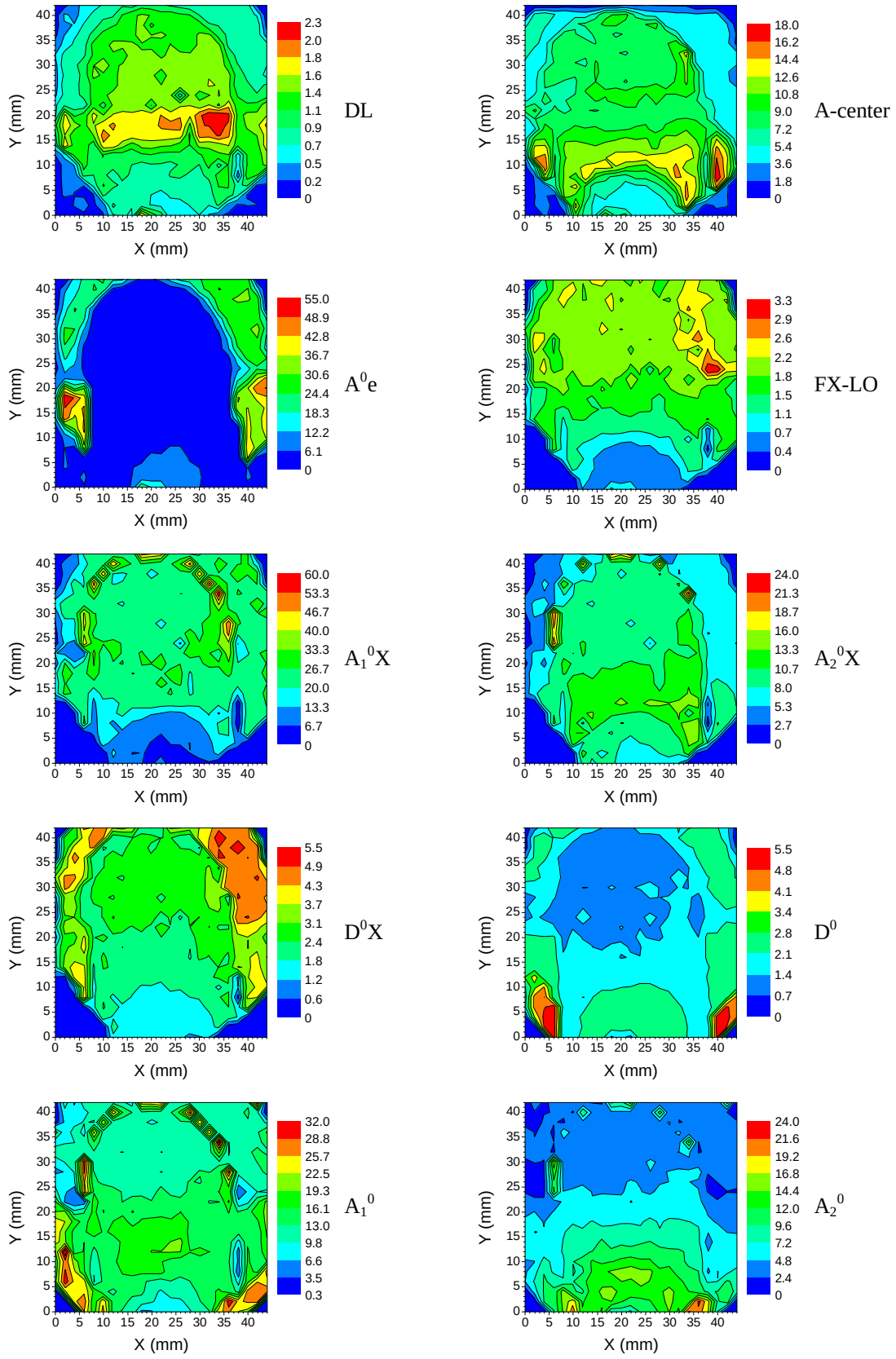

Fig. 4.14. *Maps of distribution of PL intensity of CdTe SR317 (DL, A-center, A^0e, FX-LO, $A_1{}^0X$, $A_2{}^0X$ and D^0X) and distribution of PL intensity ratios ($A_1{}^0=A_1{}^0X/FX\text{-}LO$, $A_2{}^0=A_2{}^0X/FX\text{-}LO$, $D^0=D^0X/FX\text{-}LO$). Spatial step is 2x2 mm^2.*

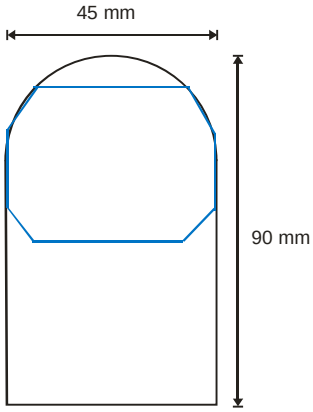

Fig. 4.15. *Placement of the PL map (in blue) of CdTe crystal SR317 on the vertical crystal cross-section (in black). The corners were covered with a paper mask. Consideration of distribution of PL intensities should omit especially the down corners of the rectangular PL maps in Fig. 4.14.*

4.4.2.5 Photoluminescence line-scanning

The PL spectra described in this section were measured in the flow liquid helium cryostat; the sample is mounted in direct contact with helium exchange gas. Hence all spectra are taken at temperature of 4 K. The classical cryostat let us to record only 1D scans of PL intensity, moving the sample manually (using a rough micrometer stage), with maximum spatial resolution of 0.125 mm. Part of this was published as [Hor05].

CdTe samples of cubic shape were shortly annealed mostly in cadmium atmosphere. Then polishing and etching was used to remove one half of the sample so that PL profile from surface through the sample core could be measured (see Fig. 4.16). Galvanomagnetic measurements show that a p-n junction is created typically several hundred microns below the surface. CdTe samples grow usually as p-type; the cadmium annealing produced a surface n-type layer, whereas the sample core remained p-type. Optical investigation confirms results of electrical measurements.

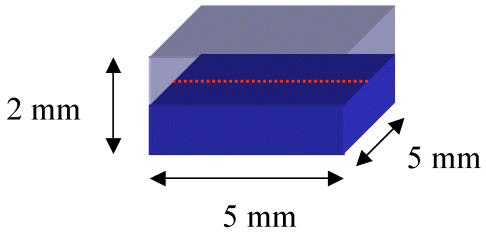

Fig. 4.16. *Scheme of sample shape subject to PL line-scanning after non-homogeneous annealing. The dimensions are only approximate.*

Cadmium annealing significantly influences PL spectra of CdTe. Profiles of photoluminescence bands for three chosen samples are plotted respectively in Fig. 4.18, Fig. 4.19 and Fig. 4.21. These samples (two undoped and one indium doped CdTe) were annealed at 500 °C for times from 16 to 23 hours. The sudden change of PL intensities in the profiles in depth from 200 to 1000 μm corresponds to the switch of electrical properties. The different depths of p-n junction and asymmetries of the PL profiles are explained by different concentration of cadmium vacancy, which are to be filled by cadmium atoms entering the annealed sample.

Fig. 4.17 and Fig. 4.18 show respectively spectra and profiles for CdTe F36P4A. The acceptor type PL bands remain in the p-type sample core, whereas the n-type surface layer shows almost none of these emissions. Deep level near 1.147 eV is distributed in a similar way. Only the Y band, which is attributed to defects trapped at dislocations [Hil97] is more intensive in the

n-type region. The core convex profile of Cu_{Cd} and Li_{Cd}, bound excitons could be interpreted as migration of defects towards the interior of the sample. However, the interpretation is difficult, because the sudden change of defect concentration influences the local quasi-equilibrium of photo-generated excitons and electrons. Normalization to e.g. free-excitonic emission would be appreciated, however this emission is present only in the surface n-type layer.

Possibility to perform the correction of the emission of bound excitonic PL was in the case of CdTe F36J11, where FX-LO was intense enough even in the p-type sample core (see spectra in Fig. 4.20). PL profiles in Fig. 4.19 show that after normalization (Eq. 4.9), the acceptor concentration is approximately constant in the sample core (compare Fig. 4.19 right and left). The ratio of shallow acceptor concentration in the core is about 300 higher compared to the surface. It means that the RT hole (minority carriers) concentration in the surface layer should be about 10^{13} cm^{-3} (the core concentration is similar to the as-grown concentration which is approximately10^{15} cm^{-3}). This is confirmed by temperature dependent galvanomagnetic measurements [Hor05], [Bel05a], [Bel05b] and [Bel05c].

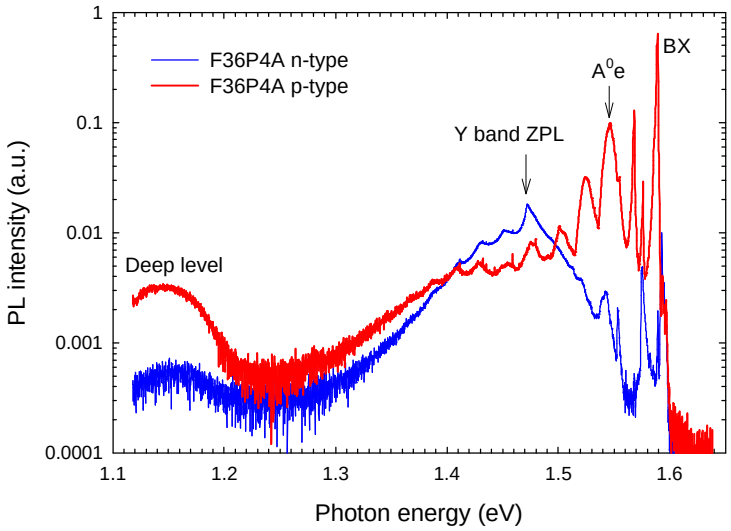

Fig. 4.17. *PL spectra of the core (in red) and of the surface layer (in blue) of CdTe F36P4A.*

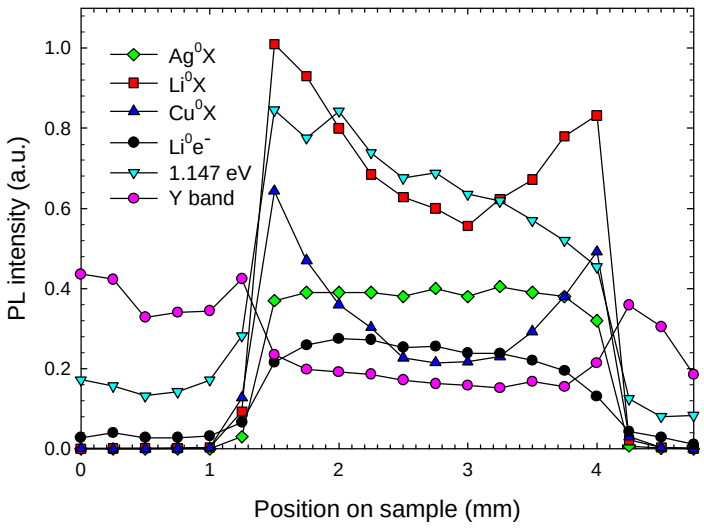

Fig. 4.18. *Line-scan of integrated PL intensities through the sample F36P4A annealed in liquid cadmium at 500°C for 16 hours.*

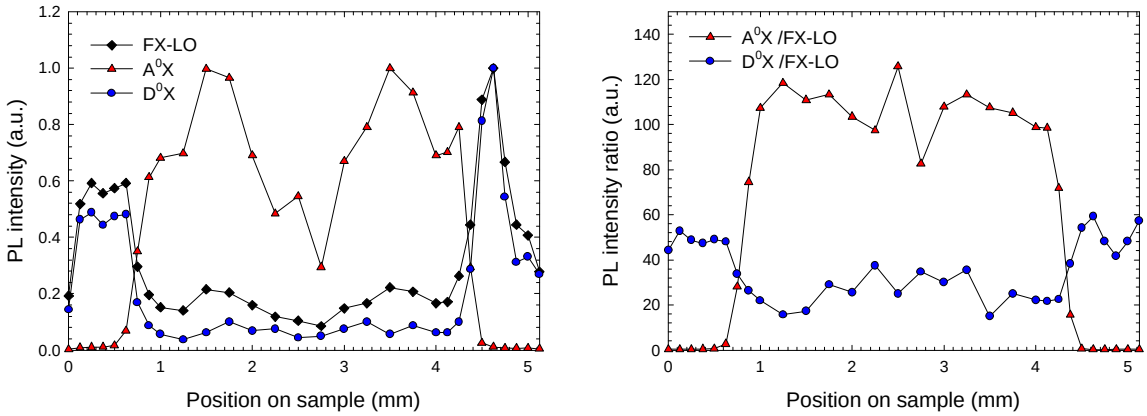

Fig. 4.19. *F36J11 annealed in cadmium vapor at 500°C for 23 hours. PL intensities (left) and relative concentrations (right).*

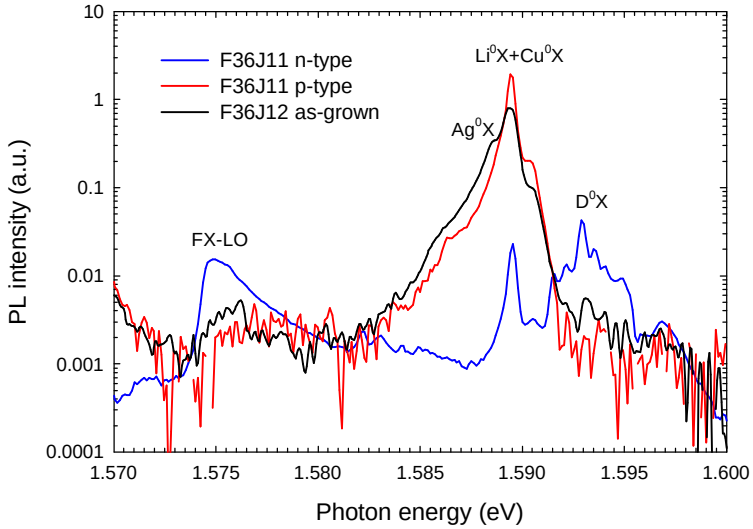

Fig. 4.20. *PL spectra taken from n-type, p-type and as-grown samples of CdTe F36J11 and neighboring F36J12. Sum of silver, lithium and copper bound excitons is denoted also as A^0X.*

In indium doped CdTe (PL profiles in Fig. 4.21, PL spectra in Fig. 4.22), the effect on electrical properties is similar, but PL profiles show changes rather in distribution of indium-related defects. In the surface n-type layer, an increase of indium donors with simultaneous decrease of indium A-center and acceptor defects is observed. The PL intensity of the 1.584 eV bound exciton is found to increase by the annealing the most. The 1.584 eV line corresponds probably to a defect including cadmium vacancy, two substitutional indium atoms and another cadmium atom [Wor95].

PL line-scanning method is an easier and more reliable technique compared to the PL mapping for several reasons. The temperature can be controlled in a much better way; there is a reliable way to reach temperature of 4 K on the surface of the sample without any complicated sample mounting techniques. Also the ‘manual’ processing of about 20-40 spectra assures better interpretation of the PL profiles. Thus, in our case, the PL mapping and the PL line-scanning are rather complementary methods.

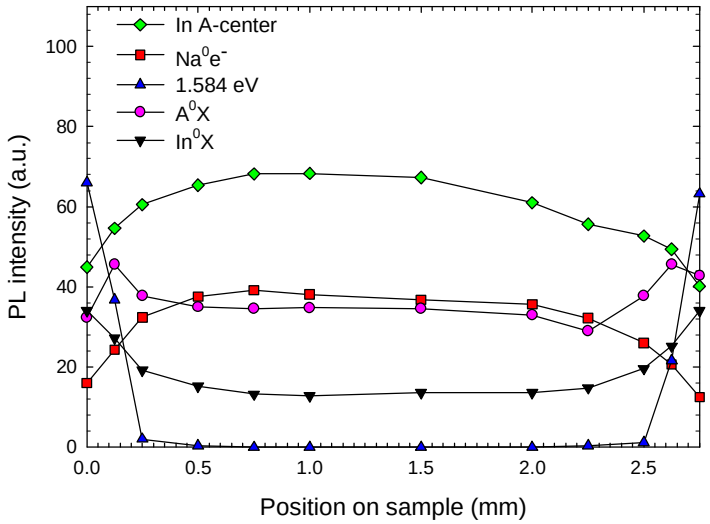

Fig. 4.21. *PL intensities profiles in F21Q2A2 annealed in cadmium vapor at 500°C for 16 hours.*

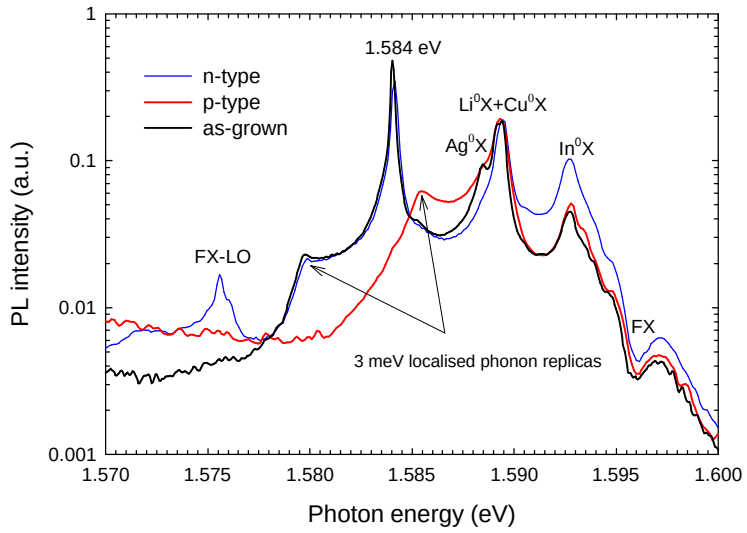

Fig. 4.22. *PL spectra taken from n-type, p-type and as-grown samples of CdTe:In F21Q2A2. The 1.584 eV line corresponds probably to a defect including cadmium vacancy, substitutional indium atoms, but does not correspond to the indium A-center.*

5 Conclusion

The first part of this work is dealing with defect description and assignment; it presents a review of published data. The data were assorted in such an order to be useful to the optical spectroscopy, especially to the photoluminescence. The experience of investigating optical properties (mainly photoluminescence and absorption) of numerous CdTe and CdZnTe samples of various origin was gathered in the chapter 3. Finally the knowledge about intrinsic and extrinsic effects was used in chapter 4 which deals with spatial characterization of CdTe and CdZnTe samples and wafers

5.1 Optical properties of CdTe

We have studied possibilities of determination of specific chemical defects and their concentrations by optical methods. Although mainly PL spectra show large number of various transitions, only very small part of them can be identified without doubts. The reasons are sometimes fundamental like superposition of very closely lying transitions (the case of acceptor and donor bound excitons); another reason is that till now convincing identification experiments with CdTe crystals of ultimate purity were not performed. However, we can quite well distinguish photoluminescence transitions related to acceptor and donor impurities even if they cannot be assigned chemically.

In undoped CdTe crystals grown in the Institute of Physics in Prague, presence of alkali elements Na or Li is almost ever observed as bound excitonic photoluminescence. Nearly at the same energy, Cu bound exciton is probably found. Presence of silver is sometimes manifested also by the corresponding bound exciton. Some of the shallow acceptor-to-band transitions were identified with phosphorus and sodium. Amongst deeper levels we could identify only mid-gap levels correlating with Sn, Ge and In doping. Low temperature absorption measurements have proved presence of Fe, Ag and Cu in most of undoped CdTe crystals produced by our institute.

We have tried to determine concentrations of some particular defects by optical means. These methods and their estimated applicable ranges are found in Tab. 5.1. All the methods require liquid helium temperatures, of course. The techniques, which can reflect concentrations of several distinct defects (ratio of bound and free excitonic PL, absorption of bound excitons), are limited to investigation of states of bound excitons in rather very pure crystals.

Technique	Applicable concentration
PL BX/FXLO ratio	10^{13}-10^{15} cm^{-3}
Absorption of bound excitons	10^{12}-10^{15} cm^{-3}
Absorption free-to-bound	10^{14}-10^{15} cm^{-3}
Absorption of free carriers	10^{16}-10^{17} cm^{-3}

Tab. 5.1. *Optical methods for determination of absolute concentrations.*

Apart investigation of optical properties of defects, we have studied intrinsic absorption spectra of thin self-standing CdTe platelets and we have established a new and reliable temperature dependence of the fundamental energy gap in CdTe. Thus we were able to remove uncertainty in interpretation of the near band edge photoluminescence emission at higher temperatures.

5.2 Optical mapping of CdTe and CdZnTe

In the chapter 4, we have reviewed published works and described various optical techniques which are used to visualize spatial variations of important quantities of CdTe and $Cd_{1-x}Zn_xTe$

crystals. The most wanted parameter to be mapped is usually the zinc concentration *x*. In the section 4.3, we have compared parameters of the most frequent methods (reflectance, transmittance, PL, all of them at various temperatures). We have shown, that low temperature PL spectra contain, apart the information about defects, also direct information about the free-excitonic absorption. This reabsorption feature was used for high-resolution (spatial and energetic) mapping of zinc concentration of large CdZnTe wafers. Apart the expected segregation of zinc along the growth axis, we have demonstrated existence of previously unobserved local zinc minima in some wafers.

In section 5.2, the PL mapping together with recognition of a specific defect via an independent method was proposed to calculate the absolute segregation coefficients of the other defects. We have shown that in some cases the segregation is not the dominant process governing the distribution of defects in the final crystal wafer. The migration of impurities during cooling-down due to non-equilibrium thermodynamical conditions was found to be the main source of inhomogeneities apart the segregation. In all wafers (as-grown samples) that we have investigated by the PL mapping, we have found large inhomogeneities of the distribution of PL intensities.

We have applied the low temperature PL line-scanning to calculate relative concentration profiles of acceptor and donor impurities using normalization of bound-excitonic PL intensities to the first free-exciton replica. These experiments were carried out on shortly annealed CdTe samples in order to investigate the influence of cadmium in-diffusion on electrical and PL properties. The experiment has confirmed the extreme influence of cadmium vacancy on acceptor defects. Although the chemical nature of involved acceptor defects is not reliably determined, we have been able to track the variation of its concentration over more than two orders of magnitude.

6 References

[Ada93] S. Adachi, T. Kimura, and N. Suzuki, *Optical properties of CdTe: Experiment and modeling*, J. Appl Phys. **74**, 3435 (1993).

[Agu95] J. Aguilar-Hernandez, G. Contreras-Puente, H. Flores-Liamas, H. Yee-Madeira and O. Zelaya-Angel, *The temperature-dependence of the energy band gap of CSVT-grown CdTe films determined by photoluminescence*, J. Phys., D: Appl. Phys. **28**, 1517 (1995).

[Ali94] G.N. Aliev, O.S. Koshchug, R.P. Seysyan, *Vysokotemperaturnaja granica effektivnosti eksiton-poljaritonnich processov v kristallach telluridov kadmia i zinka*, Fyzika tverdogo tela **36**, 373 (1994).

[Bar75] C.E. Barnes, and K. Zanio, *Photoluminescence in high-resistivity CdTe:In*, J. Appl. Phys. **46**, 3959 (1975).

[Bec90] U. Becker, P. Rudolph, R. Boyn, M. Wienecke and I. Uthe, *Characterization of p-type CdTe Bridgman crystals by infrared extinction spectra*, phys. stat. sol. (a) **120**, 653 (1990).

[Bel05a] E. Belas, R. Grill, P. Horodyský, P. Moravec, J. Franc, and P. Höschl, *Defect distribution in CdTe after Cd saturated annealing*, phys. stat. sol. (c) **2**, 1155 (2005).

[Bel05b] E. Belas, J. Franc, R. Grill, A.L. Toth, P. Horodyský, P. Moravec, and P. Höschl, *Regular and Anomalous-Type Conversion of p-CdTe during Cd-Rich Annealing*, Journal of Electronic Materials **34**, 957 (2005).

[Bel05c] E. Belas, R. Grill, A.L. Toth, P. Moravec, P. Horodyský, J. Franc, P. Höschl, H. Wolf, and T. Wichert, *Electrical and Optical Properties of In-Doped CdTe After Cd-Rich Annealing*, IEEE Transactions on nuclear science **52**, 1932 (2005).

[Bon92] D. Bonnet, *The CdTe solar cells–an overview*, International Journal of Solar Energy **12** (1992).

[Bry68] J.F. Bryant, E. Webster, *The luminescence emission of cadmium telluride at 77°K*, J. Phys. D **1**, 965 (1968).

[Bub88] L. O. Bubulac, *Spatial origin of various PL lines in CdTe at 77 K*, J. Cryst. Growth **86**, 536 (1988).

[Cap73] V. Cápek, K. Zimmerman, C. Konák, M. Popova and P. Polívka, *Valence band structure of CdTe*, phys. stat. sol. (b) **56**, 739 (1973).

[Cap94] Edited by P. Capper, *Properties of Narrow Gap Cadmium-based Compounds*, Institution of Electrical Engineers, London (1994).

[Coo89] D.E. Cooper, P.R. Newman, *Exciton-polariton dynamics and photoluminiscence line shapes in cadmium telluride*, Phys. Rev. B **39**, 7431 (1989).

[Cui05] Y. Cui, U. Banin, M.T. Bjork, A.P. Alivisatos, *Electrical Transport through a Single Nanoscale Semiconductor Branch Point*, Nano Letters **5**, 1519 (2005).

[Dil68] J. Dillinger, C. Konák, V. Prosser, J. Sak, and M. Zvára, Phonon-assisted exciton transitions in A2B6 semiconductors, phys. stat. sol. **29**, 707 (1968).

[Ell57] J.R. Elliott, *Intensity of optical absorption by excitons*, Phys. Rev. **108**, 1384 (1957).

[Fie02] M. Fiederle, V. Babentsov, J. Franc, A. Fauler, K.W. Benz, R.B. James, and E. Cross, *Defect structure of Ge-doped CdTe*, J. Cryst. Growth **243**, 77 (2002).

[Fie99] M. Fiederle, T. Feltgen, J. Meinhardt, M. Rogalla, and K.W. Benz, *State of the art of (Cd,Zn)Te as gamma detector*, J. Cryst. Growth **197**, 635 (1999).

[Fon00] G.Fonthal, L. Tirado-Mejía, J.I. Marín-Hurtado, H. Ariza-Calderón, J.G. Mendoza-Alvarez, *Temperature dependence of the band gap energy of crystalline CdTe*, J. Phys. Chem. Sol. **61**, 579 (2000).

[Fra00] J. Franc, P. Hlídek, P. Moravec, E. Belas, P. Höschl, L. Turjanska, R. Varghová, *Determination of energy gap in $Cd_{1-x}Zn_xTe$ (x=0-0.06)*, Semicond. Sci. Technol. **15**, 561 (2000).

[Fra90] J.M. Francou, K. Samynadayar, J.L. Pautrat, *Shallow donors in CdTe*, Phys. Rev. B **41**, 12035 (1990).

[Fur04] R. Furstenberg, J.O. White, J.H. Dinan, and G.L. Olson, *High-resolution mapping of infrared photoluminescence*, J. Electron. Mat. **33**, 714 (2004).

[Gil85] N.C. Giles-Taylor, R.N. Bicknell, D.K. Blanks, T.H. Myers, J.F. Schetzina, *Photoluminescence of CdTe: A comparison of bulk and epitaxial material*, Vac. Sci. Technol. A **3**, 76 (1985).

[Gon90] J. Gonzales-Hernandez, E. Lopez-Cruz, D.D. Allred, W.P. Allred, *Photoluminescence studies in $Zn_xC_{1-x}dTe$ single crystals*, J. Vac. Sci. Technol. A **8**, 3255 (1990).

[Gri02] R. Grill, J. Franc, P. Hlídek, I. Turkevych, E. Belas, and P. Höschl *Defect-induced optical transitions in CdTe and $Cd_{0.96}Zn_{0.04}Te$*, Semicond. Sci. Technol. **17**, 1282 (2002).

[Guk97] A.Gukasyan, A.Kvit, and Y.Klevkov, *High-resolution PL characterization of impurity segregation and their complex formation on extended defects in CdTe*, Sol. Stat. Com. **97**, 897 (1997).

[Hal61] R.E. Halsted, M.R. Lorenz, and B. Segall, *Band edge emission properties of CdTe*, J. Phys. Chem. Solids **22**, 109-116 (1961).

[Ham00] J. Hamann, A. Burchard, M Deicher, T. Filtz, V. Ostheimer, F. Strasser, H. Wolf, ISOLDE collaboration, and T. Wichert, *Identification of Ag-acceptors in $^{111}Ag/^{111}Cd$ doped ZnTe and CdTe*, J. Cryst. Growth **214/215**, 207 (2000).

[Ham98] J. Hamann, A. Burchard, M Deicher, T. Filtz, V. Ostheimer, C. Schmitz, H. Wolf, T. Wichert and the ISOLDE collaboration, *Identification of Ag-acceptor related photoluminescence in ^{111}Ag doped CdTe*, Appl. Phys. Lett. **72**, 3029 (1998).

[Hil97] S. Hildebrandt, H. Uniewski, J. Schreiber, and H.S. Leipner, *Localization of Y luminescence at glide dislocation in cadmium telluride*, J. Physique III **7**, 1505 (1997).

[Hir00] R. Hirano, A. Hichiwa, H. Maeda, and T. Yamamoto, *Evaluation of Zn uniformity in CdZnTe substrates*, J. Electron. Mat. **29**, 654 (2000).

[Hli01] P. Hlídek, J. Bok, J. Franc, and R. Grill, *Refractive index of CdTe: Spectral and temperature dependence*, J. Appl. Phys. **90**, 1672 (2001).

[Hor05] P. Horodyský, E. Belas, J. Franc, R. Grill, P. Hlídek, A. L. Tóth, *Photoluminescence mapping of p-to-n conversion of CdTe by annealing in Cd atmosphere*, phys. stat. sol. (c) **2**, 1189 (2005).

[Hor06a] P. Horodyský, P. Hlídek, *Free exciton absorption in bulk CdTe: temperature dependence*, phys. stat. sol. (b) **243**, 494 (2006).

[Hor06b] P. Horodyský, J. Franc, R. Grill, P. Hlídek, and P. Höschl, *Impurity segregation in CdZnTe by photoluminescence mapping*, phys. stat. sol. (c) **4**, 730 (2006).

[Hor06c] P. Horodyský, J. Franc, R. Grill, P. Hlídek, P. Moravec, J. Bok and P. Höschl, *Mapping of zinc content in $Cd_{1-x}Zn_xTe$ by optical methods*, J. Electron. Mat. **35**, 1491 (2006).

[Hor1] P. Horodyský, R. Grill, and P. Hlídek, *Band-edge photoluminescence in CdTe*, phys. stat. sol. (b), in press.

[Jai01] S. Jain, *Photoluminescence study of cadmium zinc telluride*, Thesis, West Virginia University, Morgantown (2001), (available at http://www.as.wvu.edu/phys/mbe/theses/jain.pdf).

[Jeo03] T.S. Jeong and P.Y. Yu, *Temperature dependence of the photocurrent in p-type CdTe*, J. Kor. Phys. Soc. **43,** 1101 (2003).

[Kei65] T.H. Keil, *Shapes of impurity absorption bands in solids*, Phys. Rev. **140**, A601 (1965).

[Kim04] T.W. Kim, E.H. Lee, K.H. Lee, J.S. Kim, and H.L. Park, *Formation and optical properties of CdTe self-assembled quantum rings with electronic states embedded in ZnTe barriers*, Applied Physics Letters **84**, 595 (2004).

[Kim95] C.C. Kim, and S. Sivananthan, *Modeling the optical dielectric function of II-VI compound CdTe*, J. Appl. Phys. **78**, 4003 (1995).

[Kim97] C.C. Kim, M. Daraselia, J.W. Garland, and S. Sivananthan, *Temperature dependence of the optical properties of CdTe*, Phys. Rev. B **56**, 4786 (1997).

[Kru91] J. Krustok, A. Loo, and T. Piibe, *Deep-level photoluminescence of doped CdTe in the 0.8 eV region*, J. Phys. Chem. Solids **52**, 1037 (1991).

[Kru96] J. Krustok, V. Valdna, K. Hjelt and H. Collan, *Deep center luminescence in p-type CdTe*, J. Appl. Phys. **80**, 1757 (1996).

[Kru97] J. Krustok, H. Collan, and K. Hjelt, *Does the low-temperature Arrhenius plot of the photoluminescence intensity in CdTe point towards an erroneous activation energy?*, J. Appl. Phys. **81**, 1442 (1997).

[Kuc96] L. Kuchar, J. Drápala, L. Lunácek, *Purification methods of Cd, Te and CdTe and periodicity of segregation cofficients of admixtures*, J. Cryst. Growth **161**, 94 (1996).

[Kuh92] T.A. Kuhn, W. Ossau, A. Waag, R.N. Bicknell-Taussius, and G. Landwehr, *Evidence of a deep donor in CdTe*, J. Cryst. Growth **117**, 660 (1992).

[Lau90] J.P. Laurenti, J. Camassel, A. Bouhemadou, B. Toulouse, R. Legros, and A. Lusson, *Temperature dependence of the fundamental absorption edge of mercury cadmium telluride*, J. Appl. Phys. **67**, 6454 (1990).

[Lee94] J.L. Lee, N.C. Giles, D. Rajavel, C.J. Summers, *Room-temperature band-edge photoluminiscence from cadmium telluride*, Phys. Rev. B **49**, 1668 (1994).

[Li01] Z.-F. Li, W. Lu, G.S. Huang, J.R. Yang, L. He, S.C. Shen, *Microphotoluminescence mapping of CdZnTe: Zn distribution*, J. Appl. Phys. **90**, 260 (2001).

[Lis85] K. Lischka, C. Brunthaler, and W. Jantsch, *Deep donor levels due to isolated Fe in CdTe*, J. Cryst. Growth **72**, 355 (1985).

[Man03] L. Manna, D.J. Milliron, A. Meisel, E.C. Scher, A.P. Alivisatos, *Controlled growth of tetrapod-branched inorganic nanocrystals*, Nature Materials **2**, 382 (2003).

[Man84] A. Manoogian, J.C. Wooley, *Temperature-dependence of the energy-gap in semiconductors*, Can. J. Phys. C **62**, 285 (1984).

[Mar66] D.T.F. Marple, *Absorption edge in CdTe: experimental*, Phys. Rev. **150**, 728 (1966).

[Mat03] X. Mathew, *Photo-induced current transient spectroscopy study of traps in CdTe*, Solar Energy Mat. & Solar Cells **76**, 225 (2003).

[Mol82a] E. Molva, J.P. Chamonal, J.L. Pautrat, *Shallow acceptors in cadmium telluride*, Phys. Stat. Sol. **109**, 635 (1982).

[Mol82b] E. Molva, J.P. Chamonal, G. Milchberg, K. Saminadayar, B. Pajot, and G. Neu, *Excited states of Ag and Cu acceptors in CdTe*, Sol. Stat. Com. **44**, 351 (1982).

[Mol84] E. Molva, J.L. Pautrat, K. Saminadayar, N. Magnea, *Acceptor states in CdTe and comparison with ZnTe. General trends*, Phys. Rev. B **30**, 3344 (1984).

[Mon86] B. Monemar, E. Molva, and Le Si Dang, *Optical study of complex formation in Ag-doped CdTe*, Phys. Rev. B **33**, 1134 (1986).

[Mor06] P. Moravec, P. Höschl, J. Franc, E. Belas, R. Fesh, R. Grill, P. Horodyský and P. Praus, *Chemical polishing of CdZnTe substrates fabricated from crystals grown by the vertical-gradient freezing method*, J. Electron. Mat. **35**, 1206 (2006).

[Mua01] O. Mualin, E.E. Vogel, M.A. de Orue, L. Martinelli, G. Bevilacqua, and H.-J. Schulz, *Two-mode Jahn-Teller effect in the absorption spectra of Fe^{2+} in II-VI and III-V semiconductors*, Phys. Rev. B **65**, 035211 (2001).

[Nah06] P. Nahálková, P. Nemec, D. Sprinzl, E. Belas, P. Horodyský, J. Franc, P. Hlídek, P. Malý, *Spin dynamics in bulk CdTe at room temperature*, Materials Science and Engineering B **126**, 143 (2006).

[Naw04] M. Nawrocki, L. Klopotowski, and J. Suffczynski, *Optical spin injection and tunneling in asymmetric coupled II–VI quantum wells*, phys. stat. sol. (b) **241**, 680 (2004).

[Neu83] G.F. Neumark and K. Kosai, in *Semiconductors and semimetals*, Vol. 19, Academic press, San Diego (1983).

[Neu97] G.F. Neumark, *Defects in wide band gap II-VI crystals*, Mat. Sci. Eng. R **21** (1997).

[Nob59] D. de Nobel, *Phase equilibria and semiconducting properties of cadmium telluride*, Philips Res. Rep. **14,** 361 (1959).

[Obe02] M. Obert, B. Wild, G. Bacher, A. Forchel, R. Andre, Le Si Dang, *Optical confinement in CdTe-based photonic dots,* Applied Physics Letters **80**, 1322 (2002).

[Oet92] K. Oettinger, D.M. Hofmann, A.L. Efros, B.K. Meyer, M. Salk and K.W. Benz, *Excitonic line broadening in bulk grown $Cd_{1-x}Zn_xTe$*, J. Appl. Phys **71**, 4523 (1992).

[Ole85] D.J. Olego, J.P. Faurie, S. Sivananthan, and P.M. Raccah, *Optoelectronic properties of $Cd_{1-x}Zn_xTe$ film grown by molecular beam epitaxy on GaAs substrates*, Applied Physics Letters **47**, 1172 (1985).

[One93] M. O'Neil, M. Oestreich, W.W. Ruhle, D.E. Ashenford, *Exciton radiative decay and homogeneous broadening in $CdTe/Cd_{0.85}Mn_{0.15}Te$ multiple quantum wells*, Phys. Rev. B **48**, 8980 (1993).

[Pas03] R. Pässler, *Semi-empirical descriptions of temperature dependences of band gaps in semiconductors*, phys. stat. sol. (b) **236**, 710 (2003).

[Pau85] J.L. Pautrat, J.M. Francou, N. Magnea, E. Molva, and K. Saminadayar, *Donors and acceptors in tellurium* compounds; the problem of doping and self-compensation, J. Cryst. Growth **72**, 194 (1985).

[Pey93] N. Peyghambarian, S.W. Koch, A. Mysyrowicz, Introduction to semiconductor optics, p.149 (1993). Prentice Hall, Englewood Cliffs (1993).

[Pie01] S. Pietralunga, A. Milani, A. Zappettini, M. Martinelli, *Experimental characterization of ternary $Cd_{0,9}Zn_{0,1}Te$ as a basic material for all-optical processing in the 1.5mm range*, Journal of Optical society of America **18**, 176 (2001).

[Rat03] S. Rath, P.J. Sellin, M.B.H. Breese, H. Herman, L.C. Alves, A.H. Holland, *Microscopic evaluation of spatial variations in material and charge transport of CdZnTe radiation detectors*, Nucl. Inst. Meth. Phys. Res. A **512**, 427 (2003).

[Row74] J.M. Rowe R.M. Nicklow, D.L. Price, and K. Zanio, *Lattice dynamics of cadmium telluride*, Phys. Rev. B **10**, 671 (1974).

[San96] F.G. Sanchez-Almazan, H. Navarro-Contreras, G. Ramirez-Flores, M.A. Vidal, O. Zelaya-Angel, M.E. Rodriguez, and R. Baquero, *Temperature dependence of the band gap of $Cd_{1-x}Zn_xTe$ alloys of low zinc concentrations*, J. Appl. Phys **79** 7713 (1996).

[Sch90] H. Schmidt, J.W. Tomm, and K.H. Herrmann, *Middle infared photoluminescence maping of II-VI semiconductor wafers*, J. Crys. Growth **101**, 474 (1990).

[Sen01] S. Sen, D.R. Rhiger, C.R. Curtis, M.H. Kalisher, H.L. Hettich and M.C. Currie, J. Electron. Mat. **30**, 611 (2001).

[Ser98] B. Sermage, S. Petiot, C. Tanguy, Le Si Dang and R. André, *$Cd_{0.88}Zn_{0.12}Te$ group index measurements near the exciton energy at low temperature*, J. Appl. Phys. **83**, 7903 (1998).

[Set92] S. Seto, A. Tanaka, Y. Masa, and M. Kawashima, *Chlorine-related photoluminescence lines in high-resistivity Cl-doped CdTe*, J. Cryst. Growth **117**, 271 (1992).

[Shi98] H. Shin, and C. Sun, *Photoluminescence spectra of Cl-doped CdTe crystals*, J. Cryst. Growth **186**, 354 (1998).

[Sla64] G.A. Slack, S. Galginaitis, *Thermal Conductivity and Phonon Scattering by Magnetic Impurities in CdTe*, Phys. Rev. **133**, A253 (1964).

[Soc94] N.V. Sochinskii, M.D. Serrano, V.N. Babentsov, N.I. Tarbaev, J. Garrido, and E. Dieguez, *Short-time annealing of as-grown p-CdTe wafers*, Semicond. Sci.Technol. **9**, 1713 (1994).

[Sta95] W. Stadler, D.M. Hofmann, H.C. Alt, T. Muschik, B.K. Meyer, E. Weigel, G. Müller-Vogt, M. Salk, E. Rupp, and K.W. Benz, *Optical investigation of defects in $Cd_{1-x}Zn_xTe$*, Phys. Rev. B **51**, 10619 (1995).

[Sug76] S. Suga, K. Cho, P. Hiesinger, T. Koda, *Luminescence of exciton-polaritons in semiconductors*, J. Lumin. **12/13**, 109 (1976).

[Tag75] T. Taguchi, J. Shirafuji, and Y. Inushi, *Excitonic emission in cadmium telluride*, phys. stat. sol. (b) **68**, 727 (1975).

[Taj90] M. Tajima, *Characterization of semiconductors by photoluminescence mapping at room temperature*, J. Cryst. Growth **103**, 1 (1990).

[Tob95] S.P. Tobin, J.P. Tower, P.W. Norton, D. Chandler-Horowitz, P.M. Amirtharaj, V.C. Lopez, W.M. Duncan, A.J. Syllaios, C.K. Ard, N.C. Giles, J. Lee, R. Balasubramanian, A.B. Bollong, T.W. Steiner, M.L.W.Thewalt, D.K.Bowen, and B.K. Tanner, *A comparison of techniques for nondestructive composition measurements in CdZnTe substrates*, J. Electron. Mat. **24**, 697 (1995).

[Ton96] J.E. Toney, B.A. Brunett, T.E. Schlesinger, J.M. Van Scyoc, R.B. James, M. Schieber, M. Goorsky, H. Yoon, E. Eissler, and C. Johnson, *Uniformity of CdZnTe grown by high-pressure Bridgman*, Nucl. Inst. Meth. Phys. Res. A **380**, 132 (1996).

[Tra82] V.V. Travnikov, V.V. Krivolapchuk, *Exciton diffusion and resonance radiation self-absorption*, Fizika tverdogo tela **24**, 961 (1982).

[Tri92] R. Triboulet, A. Durand, P. Gall, J. Bonnafe, J.P.Fillard, and S.K. Krawczyk, *Qualification by optical means of CdTe substrates*, J. Cryst. Growth **117**, 227 (1992).

[Tur04] I. Turkevych, *High temperature properties of CdTe*, Ph.D. Thesis, Charles University, Prague (2004).

[Var67] Y.P. Varshni, *Temperature dependence of the energy gap in* semiconductors, Physica **34**, 149 (1967).

[Vin84] L. Vina, S. Logothetidis, and M. Cardona, *Temperature dependence of the dielectric function of germanium*, Phys. Rev. B **30**, 1979 (1984).

[Wor95] L. Worschech, W. Ossau, and G. Landwehr, C*haracterization of a strain-inducing defect in CdTe by magnetoluminescence spectroscopy*, Phys. Rev. B **52**, 13965(1995).

[www1] www.evidenttech.com, www.qdots.com.

[www2] Web of Science at http://portal.isiknowledge.com.

[Yu95] Z. Yu, S.G. Hofer, N.C. Giles, T.H. Myers, C.J. Summers, *Interpretation of near-band-edge photoreflectance spectra from CdTe*, Phys. Rev. B **51**, 13789 (1995).

[Yu96] P.Y. Yu, and M. Cardona, *Fundamentals of semiconductors*, Springer-Verlag, Berlin Heidelberg New York (1996).

[Zap1] A. Zappettini, private communication.

[Zha03] A.W. Zhao, G.W. Meng, L.D. Zhang, T. Gao, S.H. Sun, Y.T. Pang, *Electrochemical synthesis of ordered CdTe nanowire arrays*, Applied Physics A **76**, 537 (2003).

[Zim90] H. Zimmermann, R. Boyn, C. Michel, and P. Rudolph, *Absorption-calibrated determination of impurity concentrations in CdTe from excitonic photoluminescence*, phys. stat. sol. (a) **118**, 225 (1990).

[Zim92] H. Zimmermann, R. Boyn, and K. Piel, *Thermal quenching of bound exciton emission due to phonon-induced non-radiative transitions: experimental data for CdTe and InP*, J. Phys.: Condens. Matter **4**, 859 (1992).